

POLITECNICO DI TORINO

Master's Degree in Mechanical Engineering

Master's Degree Thesis

**Design, assembly and commissioning
of DarkSide 20-k's prototype
"Proto-0" cryogenic system**



Supervisors

Prof. Maurizio SCHENONE
Prof.ssa Giuliana FIORILLO

Candidate

Gianfrancesco GRAUSO

DECEMBER 2021

ABSTRACT

The detection and study of the "dark matter" is one of the outstanding open questions in physics. Various projects world-wide aim at its direct detection by measuring the nuclear recoil signals left by dark matter particles scattering in sensitive detectors operated underground. Dual-phase TPC detectors are leading the field in terms of sensitivity since several years.

The object of my thesis work is the design, assembly and test of a cryogenic system that constantly purifies and liquefies Argon gas to be used in an experiment for the "dark matter" direct detection.

The project is called Proto-0 Stand Alone system, and it is a prototype of the DarkSide-20k experiment that is going to be the next step of the particle physics research using noble liquid detectors in the discovery and study of the dark matter.

The first chapter of the thesis is a brief introduction on the dark matter and on the current state of its research, with some details regarding the detection systems used. It also includes an overview of the DarkSide-20k experiment and then a description of the INFN's (National Institute of Nuclear Physics) Naples laboratory where the Proto-0 project has been assembled and tested.

The second chapter is dedicated to an overview of the Proto-0 stand alone system with its specifications and a description of its main components.

The third chapter is the analysis of the thermodynamic process, with a focus on one of the key components of the system: the "Universal Condenser" and its efficiency in the Ar liquefaction process.

The fourth chapter contains the mechanical resistance verification of the condenser according to the EN13445 – 3 standard of the unfired pressure vessels design and to the EN13458 – 2 standard of the cryogenic vessels design. This analysis is also validated by the Ansys Mechanical Finite Element Analysis (FEM) software simulation.

The last chapter describes the assembly operations and the commissioning of the system.

CONTENTS

1. Context.....	9
1.1. Dark matter research - Cryogenics.....	9
1.2. DarkSide-20k Project.....	11
1.2.1. Inner Detector.....	12
1.2.2. Photoelectronics.....	14
1.2.3. Cryostat.....	15
1.2.4. Cryogenics Systems.....	17
1.2.5. DAQ and Computing.....	20
1.2.6. Installation.....	21
1.3. Underground Argon Procurement and Purification.....	24
1.3.1. Urania.....	24
1.3.2. Aria.....	26
1.4. Cryolab at INFN - Napoli.....	28
2. The DarkSide Proto-0 system.....	30
2.1. System Overview.....	32
2.1.1. The Cryostat.....	32
2.1.2. The Universal Condenser.....	35
2.1.3. The Purification Getter.....	38
2.1.4. The Gas distribution Panel.....	39
2.1.5. Slow Control.....	43
2.1.6. Proto-0 TPC and DAQ.....	45
2.1.7. The Supply Tank.....	46
3. Proto-0 process analysis.....	50
3.1. Pre-cooling Plate heat exchangers.....	54
3.2. Tube and shell condenser.....	56

3.3. LN ₂ closed loop hypothetical setup	58
4. Mechanical assessment of the universal condenser	60
4.1. Universal condenser Design by Formulae verifications based on EN 13445	61
4.1.1. Shells Under Internal Pressure	64
4.1.2. Shells Under External Pressure	68
4.1.3. Heat exchanger tubesheet and channels	72
4.1.4. Expansion Bellow	76
4.2. Universal condenser FEA Analysis	79
5. Assembly and Commissioning	86
5.1. Proto-0 assembly	86
5.2. Leak tests	91
5.2.1. Universal condenser leak test	92
5.2.2. Assembled system leak test	93
5.3. Commissioning	94

LIST OF FIGURES

1.1.	Left: signal produced by a NR event. Right: signal of an ER event.....	10
1.2.	Principle of signal detection from nuclear recoil	11
1.3.	3D rendering of the TPC.....	12
1.4.	3D model of the DS-20k veto detector. Shown in blu are the Gd-loaded PMMA elements of the GdAS. The Faraday cage is represented in brown. The IAB is segmented into 8 inner sectors by green panels. The OAB is segmented into 8 sectors by yellow panels.	13
1.5.	Left: Single channel photodetector module (PDM). Right: The DS-20k PDU.....	14
1.6.	A view from inside of the ProtoDUNE cryostat operating at CERN.....	15
1.7.	Cross-sectional view of the DS-20k cryostat containing the passive and active veto detector and the LAr TPC	16
1.8.	DarkSide-20k cryogenics system P&ID.....	17
1.9.	DS-20k condenser box design, fabrication and assembly	19
1.10.	CAD rendering of the DarkSide 20k experiment in Hall C of LNGS.....	23
1.11.	Process Flow Diagram (PFD) of the Urania plant	25
1.12.	Seruci-0 distillation column, installed in the Seruci mine campus of CarboSulcis, Sardinia, Italy	27
1.13.	Pipes and Instrumentation Diagram (P&ID) of the external supply tanks 28	
1.14.	Layout of the Naples clean room	29
2.1.	Proto-0 system Pipe and Instrumentation Diagram (P&ID).....	31
2.2.	CF flanges standard	32

2.3. 3D model of the Proto-0 setup. (1)TPC field cage; (2) movable anode and diving bell; (3) PDU; (4) motion feedthrough adjusting gas pocket thickness; (5) motion feedthrough adjusting PDU position; (6) HV feedthroughs	33
2.4. Top flange layout	34
2.5. CAD drawing of the Universal COndenser	35
2.6. Kaori K50 Heat Exchangers	36
2.7. Johnston coupling elements	37
2.8. "Chicken feeder" CAD model	37
2.9. P&ID of the Universal Condenser	38
2.10. PS4-MT50-R SAES purification getter	39
2.11. Gas Distribution Panel 3D Model	40
2.12. The Gas Pump	41
2.13. Pump by-pass 3D model	41
2.14. P&ID of the gas distribution panel	42
2.15. VCR fitting components	43
2.16. CompactRIO controller	44
2.17. Slow control GUI	44
2.18. DAQ and Slow control system on the rack cabinet	45
2.19. LN ₂ and LAr supply tanks plant	47
2.20. Level and pressure indicator of the tank	48
2.21. Pipe and Instrumentation Diagram (P&ID) of the Supply Tanks	49
3.1. Proto-0 "loops" P&ID	51
3.2. Kaori plate heat exchanger working principle	54
3.3. "Tube and shell" 3D model section	56

3.4. "Tube and shell" exchange surface 3D model.....	57
3.5. LMTD in counterflow heat exchanger.....	58
3.6. Cryomech Gifford-McMahon AL600 cryocooler.....	59
4.1. N ₂ barrel and heat exchanger shell.....	65
4.2. Geometry of torispherical end.....	66
4.3. Parameter β for torispherical end - Design.....	67
4.4. Parameter β for torispherical end - Rating.....	68
4.5. Universal condenser's external vessel.....	69
4.6. Cylinder with heads.....	69
4.7. Values of ϵ	70
4.8. Values of $\frac{P_r}{P_y}$ versus $\frac{P_m}{P_y}$	71
4.9. Typical U-tube tubesheet heat exchanger.....	73
4.10. Unreinforced U-shaped bellow.....	76
4.11. Simplified model of the Universal condenser on SpaceClaim.....	80
4.12. Universal condenser mesh.....	81
4.13. Total deformation.....	82
4.14. Deformation along Y axis.....	82
4.15. Deformation along X axis.....	83
4.16. Deformation along Z axis.....	83
4.17. Equivalent Von-Mises stress result.....	84
4.18. First positive buckling mode.....	85
5.1. Proto-0 cryogenic system Solidworks model.....	86
5.2. Proto-0 cryogenic system in the clean room.....	87

5.3. PTFE thread tape application procedure	88
5.4. Indium wire sealing of the cryostat	88
5.5. Proto-0 cryogenic system in 2 nd level room	89
5.6. Safety valves calibration set-up	89
5.7. Proportional valve installation	90
5.8. Condenser leak test with vacuum method	92
5.9. Condenser leak test with overpressure method	93
5.10. Assembled system leak test.....	94
5.11. Manual vent line for the nitrogen in the N ₂ barrel	95
5.12. Proto-0 control panel - slow control.....	96
5.13. Temperature levels in the filling phase	96
5.14. tau vs. Ar gas inlet flow (MFM)	97
5.15. Condenser cooling power vs. Ar gas inlet flow (MFM).....	97
5.16. Condenser N ₂ side filing % vs. Ar gas inlet flow (MFM)	98
5.17. Condenser N ₂ side filing % vs. N ₂ outlet flow (MFC)	98

LIST OF TABLES

1. Ar and N ₂ thermal and physical properties.....	53
2. AISI 304L physical properties at 20°C.....	64
3. AISI 304L mechanical properties at 20°C.....	64

1 | CONTEXT

1.1 DARK MATTER RESEARCH – CRYOGENICS

The observations and studies of the Universe, distant galaxies, supernovae and cosmic background radiation led physicists to the idea that approximately 95% of the matter in the universe is not made of particles that emit or absorb electromagnetic radiation, therefore is invisible for us. This is called "dark matter", and a strongly supported hypothesis is that it consists of Weakly Interactive Massive Particles (WIMPs).

There is no clear definition of WIMPs. They are so massive and weakly interacting that they have yet to be observed in an experiment. The observation of WIMPs with masses in the 1 to $10^5 \text{GeV}/c^2$ range is a major objective of the particle physics experimental programmes.

Indeed, assuming that the dark matter is distributed all around the Milky Way, as the Sun moves around the galactic centre and the Earth around the Sun, an apparent "wind" of dark matter is expected to hit us. According to the theories these Weakly Interactive Massive Particles could be detected via elastic scattering from atomic nuclei in a suitable terrestrial target.

The energy depositions and interaction rates are extremely low, requiring that this type of experiment must be located deep underground for protection from cosmic rays, requiring the use of radio-pure materials for the detector and a shield against radioactivity in the environment.

Noble liquids are a particularly suited target for WIMP search: they have both high scintillation and ionization yields, which determine a high number of photons and electrons released after the WIMP scattering on the noble liquid nucleus; moreover, they are easy to purchase and to scale to larger volume. Liquid argon (LAr), in addition, offers a unique technique to discriminate the recoils due to a WIMP from the electrons/positrons and photons from local radioactivity, which are the most abundant background component.

There are 2 major sources of background that can interfere with the detection:

- *Electronic Recoil Background* (ERs) caused by electromagnetic interactions between atomic electrons and charged particles. Radioactivity in the shielding materials or nuclei produced by cosmic ray interactions with nucleons of the detector structure may produce β - and γ -backgrounds;
- *Nuclear Recoil Background* (NRs) induced by spontaneous fission reactions. Neutrons can cause single scatter recoils which create WIMP-like signals.

Therefore, dark matter direct detection experiments are provided with either significant event-by-event discrimination between electron recoils (from electro-

magnetic background sources) and nuclear recoils (from either WIMP or neutron interactions).

There are different strategies to lower the background level:

- *Selection and Purification of the detector's materials* The internal background level can be reduced by building the detector out of material with a low intrinsic radioactive contamination.

In some cases a constant purification during the experiment is needed, to remove elements like radon (Rn) that is continuously released from the materials.

- *Passive Shielding* High atomic number materials can be used to shield the detector from external γ -rays, while using dense materials or a water veto is possible to shield the detector from neutrons.
- *Active Rejection* During the experiment the previous precautions can be not sufficient and some background has to be rejected in a second moment. An example can be neutron-induced nuclear recoils that some detectors can distinguish from WIMPs recoils recording the scatter multiplicity of each event. Moreover, the dual-phase TPCs detectors can exploit pulse-shape analysis to distinguish also between ERs and NRs. This technique is based on the comparison of the scintillation (S1) and ionization (S2) signals.

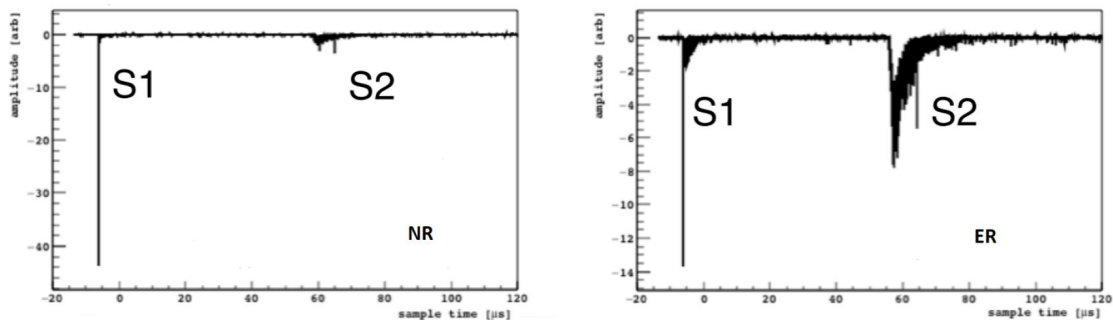


Figure 1.1: **Left:** signal produced by a NR event. **Right:** signal of an ER event

Scientists from all over the major groups currently using LAr to search for dark matter including ArDM, DarkSide-50, DEAP-3600, and MiniCLEAN, have joined to form the Global Argon Dark Matter Collaboration (GADMC) with the goal of building a series of future experiments that maximally exploit the advantages of LAr as a detector target.

The immediate objective of the GADMC is the construction of the DarkSide-20k detector, which will operate in Hall-C of the Gran Sasso National Laboratory (LNGS) in 2025.

1.2 DARKSIDE-20K PROJECT

The goal of the DarkSide-20k (DS-20k) project is to either detect WIMP dark matter or reach a 90% exclusion sensitivity to WIMP-nucleon cross sections of 7.410^{-48} cm^2 at the mass of $1 \text{ TeV}/c^2$.

Energy deposits in the LAr target result in the production of excited and ionized argon atoms, according to the underlying process for recoiling electrons or nuclei. Excited argon atoms, which can also be produced by recombining ionization charge, lead to an efficient formation of argon excimers decaying via the emission of scintillation light characterized by two decay time constants. Both components are combined to yield a prompt light signal, called **S₁**. Due to the deep UV nature (around 128 nm) of this scintillation light, which is absorbed by most materials, a thin layer of wavelength shifter, tetraphenylbutadiene (TPB), must cover all exposed surfaces to convert the photons to those of optical wavelengths for detection by photosensors. Ionization electrons escaping recombination are drifted to the top of the LAr by an applied electric field, where another electric field stronger than the field applied to drift the electrons, extracts the electrons into the gas pocket above the liquid. Here the strong field accelerates the electrons, enough for them to excite (but not ionize) the argon gas, producing a secondary (delayed) scintillation signal **S₂**, proportional to the ionization charge. Photosensors placed behind the wavelength shifter-coated windows at the top and bottom of the TPC, read out both scintillation signals (**S₁** and **S₂**) of each event. **S₁** is used for energy determination, as well as for pulse shape discrimination (PSD). **S₂** is used for energy and 3D position measurements of the event, the vertical coordinate is measured from the drift time between **S₁** and **S₂**, and the horizontal coordinates from the light pattern resulting in the top photosensors from **S₂**. This feature allows the identification and rejection of the events from surface backgrounds and multiple neutron scatters.

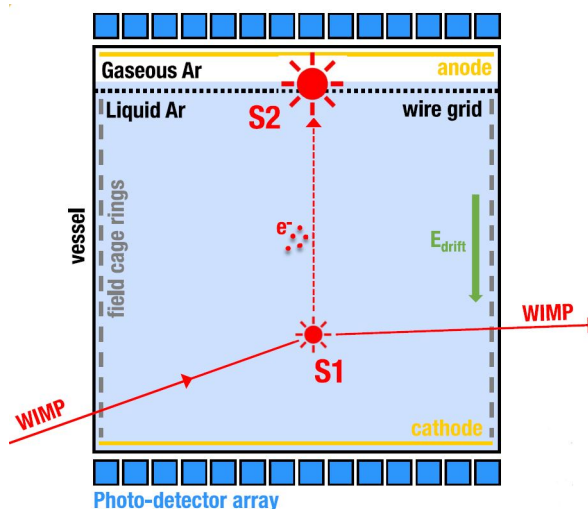


Figure 1.2: Principle of signal detection from nuclear recoil

1.2.1 Inner Detector

The DS-20k experiment will use a dual phase argon (50 t of low radioactive underground Argon – UAr) time projection chamber (TPC) as the target for WIMP detection, looking at both scintillation and ionization signals. An ultra-pure PMMA acrylic vessel is used to contain the liquid UAr. The TPC field cage system, an anode and a cathode are implemented on the inner surfaces of the acrylic vessel with a commercial conductive polymer coating, called Clevios™ and they form the TPC itself. The same pure acrylic material, in the form of 4 mm thick sheets, is used to hold the Enhanced Specular Reflector (ESR) reflector foils installed to maximize light collection. The use of these extremely radiopure materials to contain the UAr leads to a residual neutron background estimated to be $< 10^{-3}$ for the exposure of 200 t yr. The octagonal LAr TPC will have a height of 350 cm and a distance between parallel walls of 350 cm. Two octagonal structures called optical planes will be placed above the anode and below the cathode of the LAr TPC. They will be coated with photosensors.

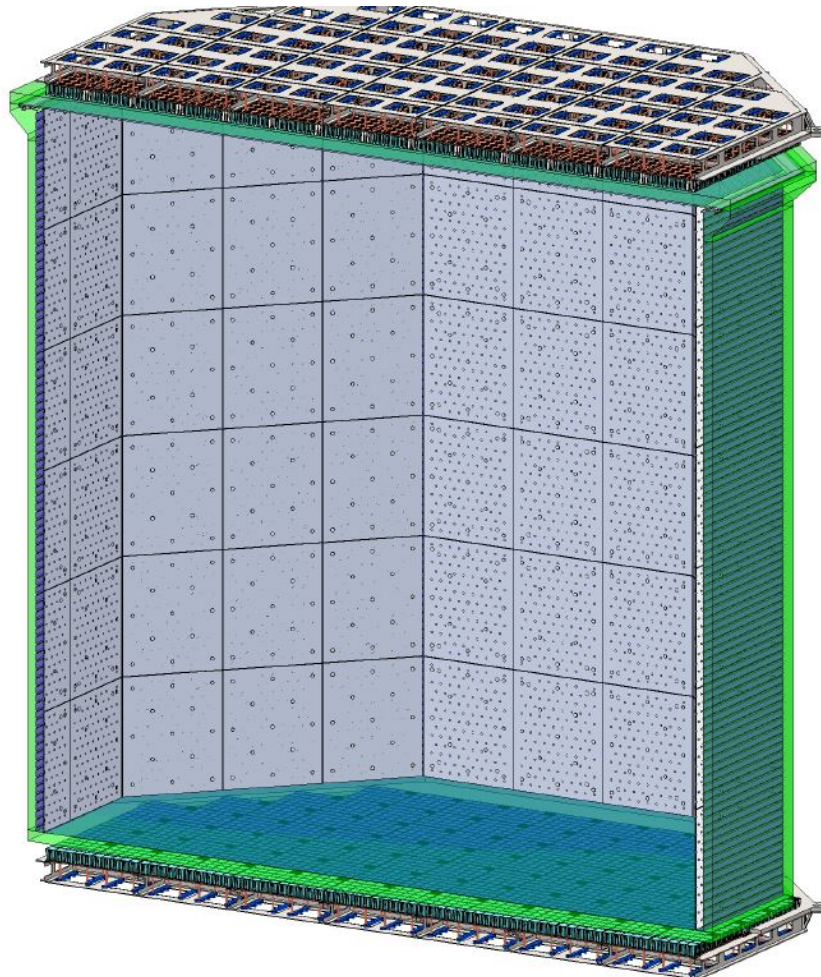


Figure 1.3: 3D rendering of the TPC

The inner detector is contained in a cryostat full of approximately 700 tons of atmospheric Argon (AAr) which also contains an outer detector acting as a **Veto** detector. The function of the veto is the passive shielding of the TPC from

neutrons coming from the surrounding environment and the active tagging of neutrons that produced WIMP-like signal events in the TPC and their rejection. The Veto detector is composed of three separate volumes:

- a 40 cm thick inner volume of active liquid AAr called the Inner Argon Buffer (IAB) surrounding the TPC vessel;
- a passive octagonal shell made of gadolinium (Gd) loaded PMMA acrylic called the "GdAS" and mounted around the IAB;
- a 40 cm thick outer active volume of AAr called the Outer Argon Buffer (OAB) contained between the GdAS and the outer copper Faraday Cage.

The Faraday Cage will contain the Veto and the TPC and optically and electrically isolate them from the remaining outermost AAr volume contained within the cryostat.

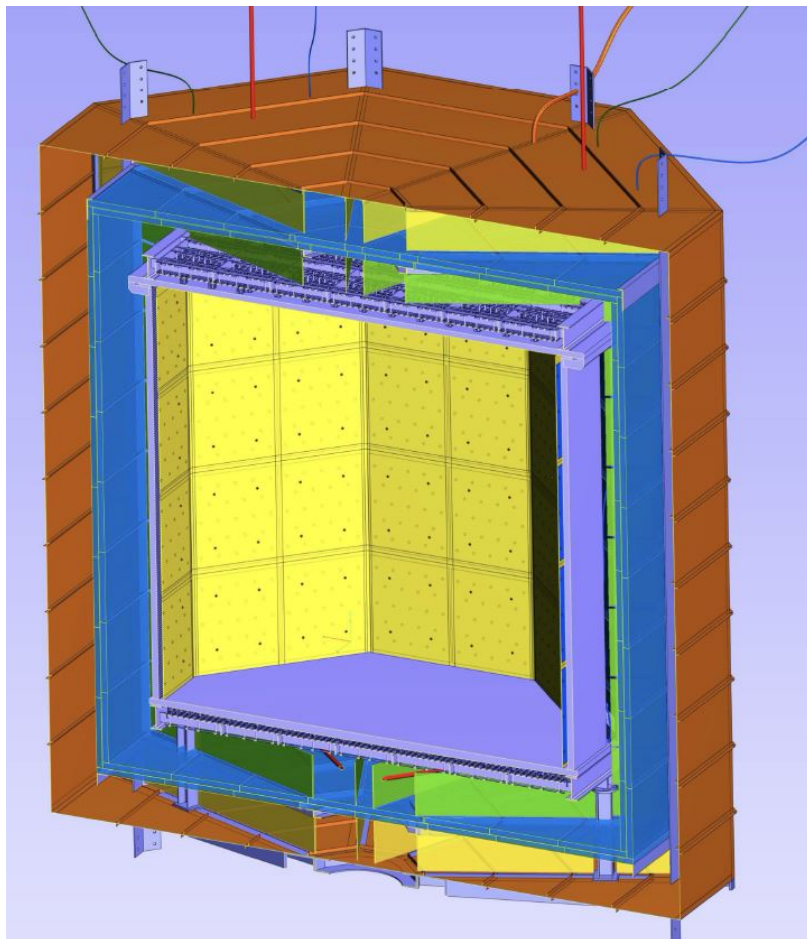


Figure 1.4: 3D model of the DS-20k veto detector. Shown in blu are the Gd-loaded PMMA elements of the GdAS. The Faraday cage is represented in brown. The IAB is segmented into 8 inner sectors by green panels. The OAB is segmented into 8 sectors by yellow panels.

The GdAS moderates neutrons emitted from all of the detector materials, particularly from the ones which make-up and surround the LAr TPC, while also enhancing the neutron capture probability with the inclusion of the Gd. The capture of the neutron on a Gd nucleus results in the emission of multiple γ

rays. The γ rays are detected by use of scintillation light emitted by the liquefied AAr in both the IAB and OAB during their interactions. The neutron detection efficiency of the veto depends on the GdAS thickness and Gd loading fraction, as well as the IAB and OAB thickness. To optimize light collection and reduce the instrumental background, the IAB and OAB are divided into 8 azimuthal segments by reflector and wavelength shifter-coated panels. On both sides of the GdAS will be mounted 3000 photosensors to collect scintillation light from both the IAB and OAB. The design concept is scalable, and can be the starting point for future bigger detectors.

Due to the complicated geometry, the veto detector will be built inside the cryostat following a detailed plan. The entire mounting procedure will take many weeks, and utmost care is needed to avoid contamination of its components.

1.2.2 Photoelectronics

In large-scale LAr-based dark matter experiments the key components that are used to read the scintillation signals are the **SiPMs** (silicon photomultipliers). In the Darkside-20k experiment the photosensing unit will be a PhotonDetector Module (PDM), consisting of a $50 \times 50 \text{ mm}^2$ tile of 24 SiPMs and a front-end board that operates as a single detector. Each module will also contain a cryogenic preamplifier board that will amplify the signal close to the sensor. In the DS-20k experiment the PhotonDetector Unit (PDU) is assembled with 25 PDMs (figure 1.5).

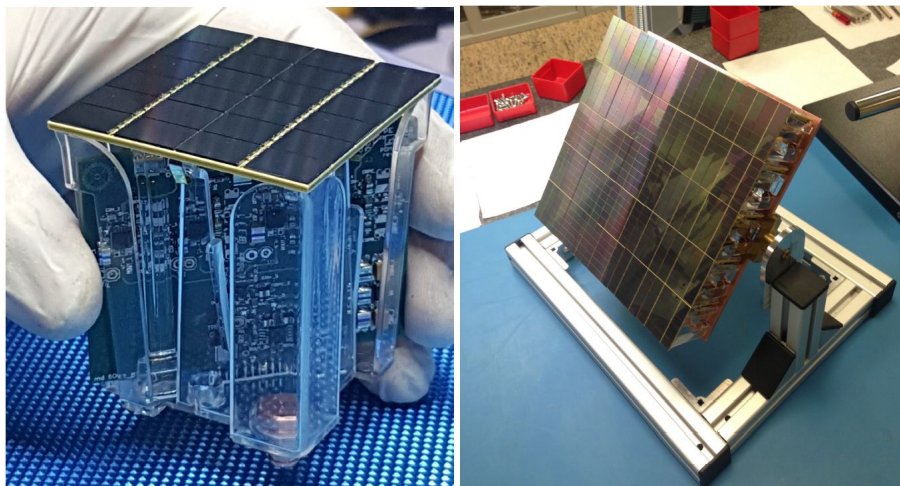


Figure 1.5: Left: Single channel photodetector module (PDM). **Right:** The DS-20k PDU

The signal transmission from the PDMs to the warm electronics is made with optical fibers to avoid the use of a large number of bulky cables and the inherent problems of radiopurity and heat load. The PDMs will be located above the anode and below the cathode, fully covering the top and bottom faces of the LAr TPC active volume, to detect both the S_1 and S_2 signals with high efficiency.

The SiPMs mass production for the DarkSide 20k detector is currently in progress by LFoundry (Avezzano, Italy), improving the first SiPM model made

by FBK (Fondazione Bruno Kessler, Trento). The DS-20k SiPM packaging foresees the production of more than 10000 PDMs in 2,5 years. This huge effort requires a large assembly facility, provided with specific equipment and trained personnel.

The GADMC selected for the NOA (Nuova Officina Assergi) DS-20k SiPM packaging facility a clean room to be built inside the LNGS surface laboratory with an area of 700 m².

Lastly, Naples Test Facility has been commissioned to test all the PDUs produced at NOA.

1.2.3 Cryostat

The DS-20k detector will be located inside a cryostat operating with an atmospheric argon fill refrigerated with the AAr cryogenic system.

Figure 1.7 shows the complete DarkSide-20k cryostat installation with a 3D cut-away view of the detector with the copper electromagnetic and light shield, the Veto detector, and the LAr TPC, all contained within the AAr outer cryostat.

The DS-20k outer cryostat and AAr cryogenics are based on the successful experience of the two large membrane cryostats deployed in the ProtoDUNE project at CERN (figure 1.6).

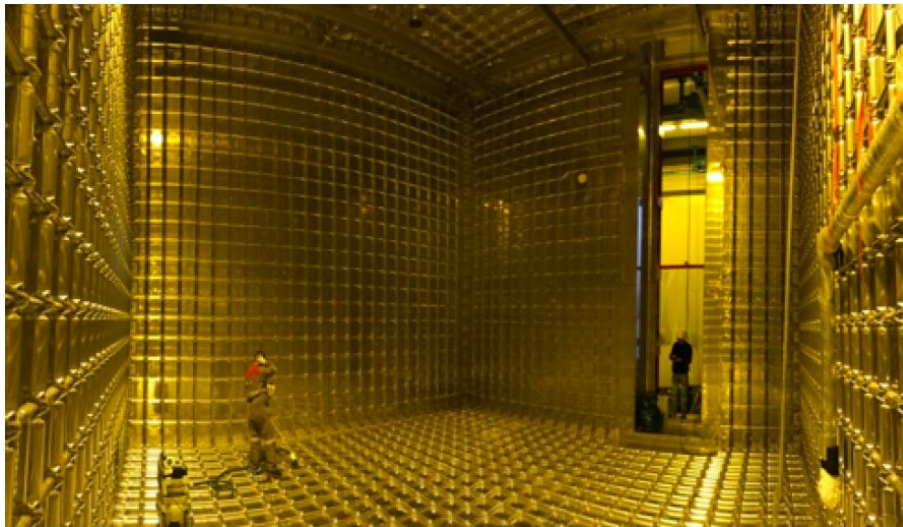


Figure 1.6: A view from inside of the ProtoDUNE cryostat operating at CERN

The membrane cryostat technology in use was initially developed for the overseas transport of liquefied natural gas (LNG).

The French engineering firm Gaztransport & Technigaz (GTT), leader of this international market, developed and adapted its MarkIII membrane cryostat technology for particle physics detectors.

The DS-20k cryostat will retain all major elements of the ProtoDUNE cryostats, including the stainless steel inner cold membrane that contains the cryogenic liquid, the foam insulation panels and a warm steel supporting outer structure. The cold primary membrane tank which contains the cryogenic liquid is made of stainless steel, and its liner has a special corrugation that allows it to expand

and contract in both transverse directions to provide mechanical relief to strains resulting from temperature changes.

A secondary barrier located between the polyurethane layers of insulation is a physical protection providing secondary containment for the cryogenic liquid in case of a failure of the first membrane.

The mechanical support is provided by a steel structure, consisting of large vertical beams alternated with a web of metal frames and a carbon steel tertiary membrane that surrounds the secondary barrier.

The warm structure of the AAr cryostat consists of two main elements: the lower vessel which will host the liquid, and the roof hosting all penetrations for cryogenics and services.

The roof structure is assembled from five pre-assembled modules called "Top Caps": four lateral top caps and one central top cap ($4.1 \times 4.1 \text{ m}^2$), that will enable the insertion of the TPC and of the large components of the veto detector.

The overall outer warm structure's dimensions are: width 11410 mm, length 11410 mm, height 10760 mm. This outer structure is designed to withstand the hydrostatic load of the liquid argon, the pressure of the gas volumes and all possible external constraints (e.g., gravitational, seismic, etc.). The structural beams are made of a special carbon steel alloy (S460ML 1.8838), able to maintain its mechanical properties down to 220 K.

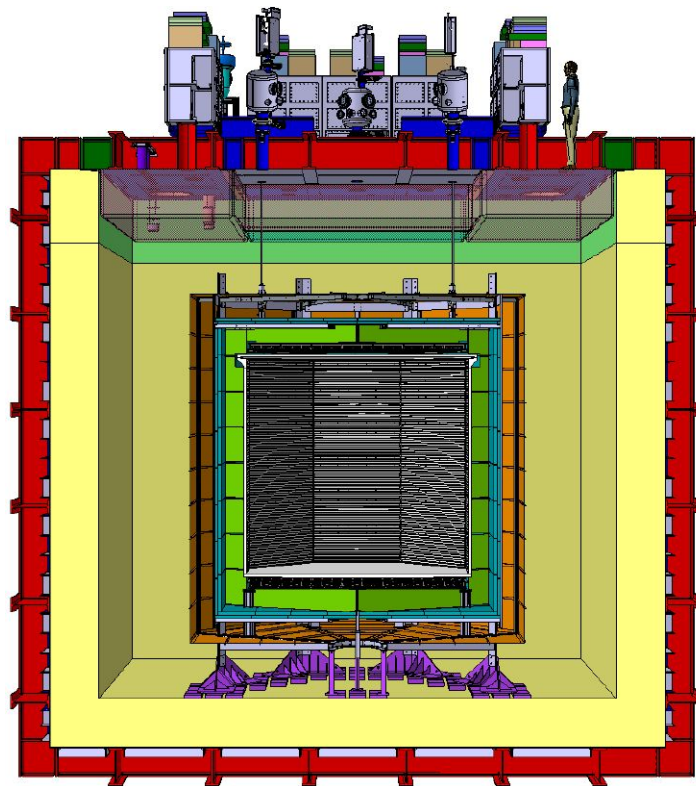


Figure 1.7: Cross-sectional view of the DS-20k cryostat containing the passive and active veto detector and the LAr TPC

1.2.4 Cryogenics Systems

DS-20k is equipped with two main **cryogenics systems**: one for the AAr in the Veto detector inside the ProtoDUNE cryostat and one for the UAr in the TPC, visible in the Pipes&InstrumentationDiagram of figure 1.8. Liquid nitrogen is the primary cooling source of the entire cryogenics system, whose key components are the LN₂/LAr heat exchangers. A minimum storage of liquid nitrogen is maintained such that the system will be protected during power failure mode. The two cryogenics systems share the same liquid nitrogen reserve loop, but have separate argon loops of UAr and AAr, respectively.

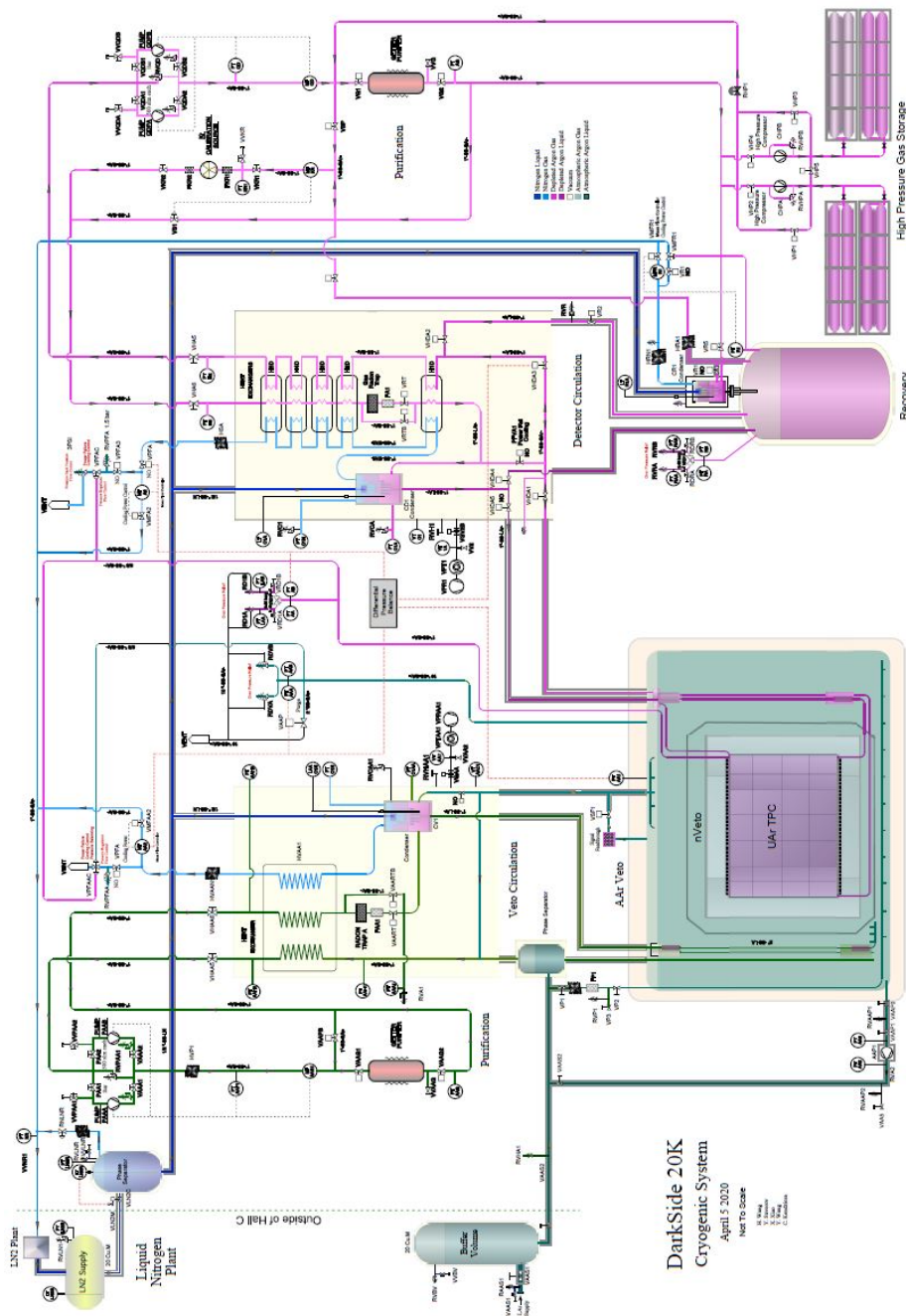


Figure 1.8: DarkSide-20k cryogenics system P&ID

The LN₂ reserve system is a closed loop with a LN₂ plant located outside of Hall C of the LNGS and a few local liquid nitrogen dewars. The system delivers liquid nitrogen as the cooling fluid to the condensers of the UAr cryogenics system in the inner detector, the AAr cryogenics system and recuperates the evaporated nitrogen gas to liquefy it back.

The AAr cryogenics system will be a liquid re-circulation system controlled by a pressure and vacuum relief valve and a warm purification system to assure an efficient impurity trapping in the gas phase of the ²²²Rn emanated from warm components. The continuous circulation of the argon along the purification system is allowed by a system of custom developed gas argon pumps with integrated heat exchangers.

The system can handle high circulation rates (equivalent mass flow of 10000 stdL/min AAr, and 1000 stdL/min UAr) drawing either, or both, liquid and gas phase argon to effectively remove electronegative impurities in a reasonable time. The designed system allows the use of a SAES hot getter to remove N₂, CO₂, and O₂. The total cooling power of the cryogenics system is designed to handle the total heat load from the power dissipated by the cold electronics operating inside the liquid argon volume. The AAr cryogenics system during normal operation conditions is estimated to need a cooling power of 10 kW, while in the available cooling capability including the LN₂ recovery system is of 10.3 kW.

A full-size prototype LAr condenser, the core component in the cryogenics system, has been already built and tested at UCLA, and a cooling power of 2.2 kW (latent heat only) has been achieved, nearly twice that needed for the DS-20k UAr cooling requirement.

The UAr cryogenics system is made up of several sub-systems: the liquid argon handling system, the UAr purification system, the cold box, the gas circulation pump, the integrated heat exchanger system and heat exchangers close to the TPC, and the UAr recovery and storage system.

The **LAr handling system** delivers the clean radon-free UAr, which is initially stored in the recovery storage system with two possible options at the moment: full liquid phase storage or gas phase high-pressure storage. Either solutions will include a gas handling system in order to pre-purify the UAr before filling the TPC volume. This system foresees the possibility to recuperate the UAr from the inner detector to the recovery system if an emergency occurs or at the end of the experiment.

The **UAr purification system** purifies the argon in gas phase during the circulation with a commercial Zr-based getter system.

The main components of DS-20k cryogenics system are contained in the "**cold box**" which is shown in figure 1.9. Together with the condenser, five heat exchanger modules are placed in it, to pre-cool the argon gas, by the circulation of cold nitrogen gas and the release of cold argon gas. Thanks to this pre-cooling system the efficiency of the liquefaction process significantly increases, and the necessary cooling power is dramatically reduced. Between the two coldest heat exchanger modules the radon trap is placed, as the optimal radon trapping is achieved when the argon is still in the gas phase and at its lowest temperature. To control and monitor the system eight cryogenics valves and temperature and

pressure sensors are placed. The stainless steel LAr condenser is a tube and shell model with 127 0.5" top sealed tubes welded on a plate as the thermal exchanging zone. The condenser is therefore separated into the nitrogen volume on the top and the argon volume on the bottom. The continuous LN₂ dropping in the nitrogen volume is granted by a so called *chicken feeder* welded at the bottom of the liquid nitrogen delivery tube. The amount of LAr produced by the condenser is controlled through the regulation of the evaporated nitrogen gas flow via a control valve, and monitored by a mass flow meter. The control valve uses the LAr TPC pressure from both UAr and AAr as feedback signal to automatically adjust the evaporated nitrogen gas flow rate, which is essentially the cooling power of the condenser, hence in return maintains the LAr TPC pressure at the desired set point and balanced with AAr system with an incredible stability. To connect these components 1" stainless steel tubes are chosen, in order to allow the argon circulation speed up to 1000 stdL/min.



Figure 1.9: DS-20k condenser box design, fabrication and assembly

In the activation phase of the system a circulation speed of 1000 stdL/min is required to achieve an acceptable UAr purity level in a reasonable time, and then the circulation speed can be decreased to only maintain the purity and stability. To have this kind of flexibility two individual **gas circulation pumps** will be placed in parallel, each providing a circulation rate up to 500 stdL/min. The key components of the pumps will be linear motors and reed valves. The linear motors, consisting of a piston and cylinder pair, can provide a continuously adjustable pumping power, and will be placed face to face to counteract the vibration produced during the motor activity. The reed valves guide the gas flow direction when the linear motors are going back and forth. The combination of the linear motors and the reed valve allows the pump to work in a friction-less condition, resulting in a long lifetime. A full-size prototype circulation pump has been fabricated at UCLA and Princeton. It was shipped to CERN, it has been

certified for the EU safety requirement and is part of the prototype cryogenics system of DS-20k that is being tested at CERN.

The **heat exchangers** close to the TPC are similar models to the condenser described before, but with an increased thermal exchanging surface area. A heat exchanger is placed above the LAr TPC to ensure that all outgoing argon will be in gas phase absorbing the heat of the incoming liquid-gas mixture of purified argon that comes in the TPC volume. Another set of near TPC heat exchangers are strategically placed close to bottom level of the UAr TPC for fast recovery during the draining stage, and is completely passive during normal operations.

The **underground argon storage and recovery system** is composed by a set of high pressure gas containers and of a vacuum insulated cryostat with a dedicated condenser for liquid phase recovery from the TPC. The recovery speed must be controlled in sync with the emptying of the AAr of the cryostat, to avoid a too high differential pressure across the vessel volume that would be dangerous for the TPC acrylic vessel.

At this stage the cryogenics system is under test at CERN as a part of the DS-Proto system to validate its functions. Two key goals have been achieved: The long term TPC pressure stability (an essential parameter for S2 resolution) and the immunity to total power failure that ensure the safety of the LAr TPC.

1.2.5 DAQ and Computing

The baseline scheme for both the TPC and Veto detector DAQ electronics foresees an optical signal receiver feeding a differential signal to a flash ADC (analog-to-digital converter) digitizer board that is connected to a large Field Programmable Gate Array (FPGA). The digital filtering capability within the digitizer board would allow the discrimination of single photoelectron signals and a first determination of the time and charge of the individual channel pulses.

The combination of the data processing in the digitizer board and in the first stage of the DAQ system CPU will provide the needed data reduction to allow trigger-less operation of the readout for the TPC and Veto detectors. The data from signal pulses from sectors of the TPC and Veto detectors will be transferred to front-end data processing units where further data reduction may be performed. The aggregate data from the entire TPC and Veto detectors will then be passed to a further processing stage that will reconstruct and select interesting events, thus realizing a software event builder and trigger for the experiment.

Single photo-electron signals detected in the TPC and Veto detectors will be stored with charge and time-of-arrival info only, signals like S2 characterized by an high density of photo-electrons will require partial waveform information for detailed analysis, whereas summed waveform for several readout channels will be saved for the Veto.

Each of the software trigger processors will consider all data of the TPC and Veto corresponding to a specified time interval of convenient length. Interesting events might be identified among these data using several algorithms that can run in parallel. In normal data-taking mode, an event could be identified by a

coincidence of hits in the TPC within a specified time window to select S_1 pulses for all energies.

Synchronization between the TPC and Veto DAQ is fundamental for the effectiveness of the design, and will be provided and maintained during the data taking.

The DAQ system will be located on top of penetrations on the roof of the AAr cryostat. This arrangement will allow personnel access while minimizing the length of the optical fibers used to transmit the data from the TPC and Veto to the signal receivers.

The basic readout element of the proposed DS-20k DAQ system is a multi-channel board hosting several flash ADCs (fADCs) linked to a large FPGA for digital signal processing. This will be connected to a host CPU for control, monitoring and data formatting using as an output channel through a 1 Gbit/s to 10 Gbit/s Ethernet connection to an external computer.

The development of this electronics board has been carried on in a partnership between CAEN of Viareggio, Italy, which was selected as the provider of the electronics by the INFN, and the GADM Collaboration.

The Maximum Integrated Data Acquisition System (MIDAS) has been chosen as a framework for developing the DAQ readout and related online control software for the DS-20k detector. The MIDAS DAQ package has been used extensively within the DEAP-3600 experiment, and together with the CAEN hardware provides a nice baseline for the digitization and recording of the raw data.

The data storage and offline processing system must support transfer, storage, and analysis of the data recorded by the DAQ system, for the entire lifespan of the experiment. It must provide for production and distribution of simulated data, access to conditions and calibration information and other non-event data, and provide resources for the physics analysis activities of the collaboration.

The total storage inventory required for the experiment is expected to be more than 20 PB, including the storage needed for simulated and reconstructed events.

DS-20k will adopt an object-oriented approach to software, based primarily on the C++ programming language, with some components implemented using other high level languages (Python etc.).

1.2.6 Installation

The DarkSide 20-k system will operate in Hall-C of the Gran Sasso National Laboratory (LNGS). The dimensions of the cryostat and of the system's components combined with the uneasy underground position of the installation site forced the collaboration to design an assemblable on site system represented in the 3D model of figure 1.10.

The first element to consider is the main and largest element of the DS-20k apparatus: **the cryostat**. The cryostat, as mentioned in section-1.2.3, will be built by GTT under the direction of CERN. The thermal insulation and inner membrane are based on the LNG technology developed by the GTT. GTT does not construct the LNG carriers, but has defined a network of firms with permission to use their technology and IP.

As described in section-1.2.3 the roof of the cryostat will be composed of 5 modules, four side modules and a central module. These modules will host all the penetrations necessary to support the active detector, all electrical and signal feedthroughs and all cryogenic services. The modules will arrive at LNGS pre-assembled and already including the beams frame, the warm skin, the insulation and the cold membrane. With the side modules in place, a square opening on the roof of the cryostat with dimensions of $4122 \times 4122 \text{ mm}^2$ will be used for detector installation and the central top cap module will close this opening once the inner detectors (TPC, Veto) have been installed in their final position. Four large penetrations will be placed on the four corners of the roof of the cryostat with the purpose of allowing access to the inside, to bring clean air inside the vessel during installation and particular attention will be given in all steps of the construction work to avoid radionuclide contamination of the materials, in particular for the primary membrane closer to the detector.

Regarding the **TPC** and **Veto**, their assembly and preparations will start in the NOA Rn-suppressed clean room above ground. A test of the fully assembled TPC is considered necessary prior to inserting it in the experiment cryostat. This test will be performed in an auxiliary cryostat designed to serve as the UAr recovery cryostat in case the experiment cryostat needs to be emptied during operation phase. A large Rn-suppressed clean room, located inside the underground Hall C, in the immediate proximity of the main cryostat, allowing it to be served by the UAr cryogenic system to be used for the experiment, and operated at a Rn level of 1 Bq/m^3 or better, is required in order to perform the final assembly and cryogenic test of the TPC PMMA sealed vessel. The clean room roof will be openable to allow the use of the main Hall C crane for the transfer of the TPC into and out of the test cryostat, and eventually into its final position inside the experiment cryostat.

Upon completion of the experiment cryostat, the Veto detector acrylic panel assembly and positioning inside the cryostat will start. The cryostat will be transformed into a Rn-suppressed environment with a light temporary cover structure on the cryostat roof opening. After the deployment of the Veto detector bottom part and of the Veto detector support structure, the TPC will be transferred from the underground Rn-suppressed clean room and installed at the center of the Veto detector support structure. Once the TPC is in its final position, the assembly of the lateral walls and top portion of the Veto can proceed. At this point the outer Faraday cage will be installed. The fully assembled and nested TPC, Veto detector, and outer Faraday cage will be attached to the cryostat top cap through the Detector Support System (DSS).

The **AAr cryogenic system** serving the experiment will be installed in LNGS Hall C once the cryostat and the DS-20k metallic structure construction are complete. It will include several subsystems: the liquid argon storage, the liquid nitrogen reserve, the purification system, the condenser box, the liquid circulation pump, the gas circulation pump, and the pressure relief valve assembly. The tanks of the liquid nitrogen reserve system and the liquid argon buffer storage tank will be located in the LNGS truck tunnel close to the entrance to Hall C.

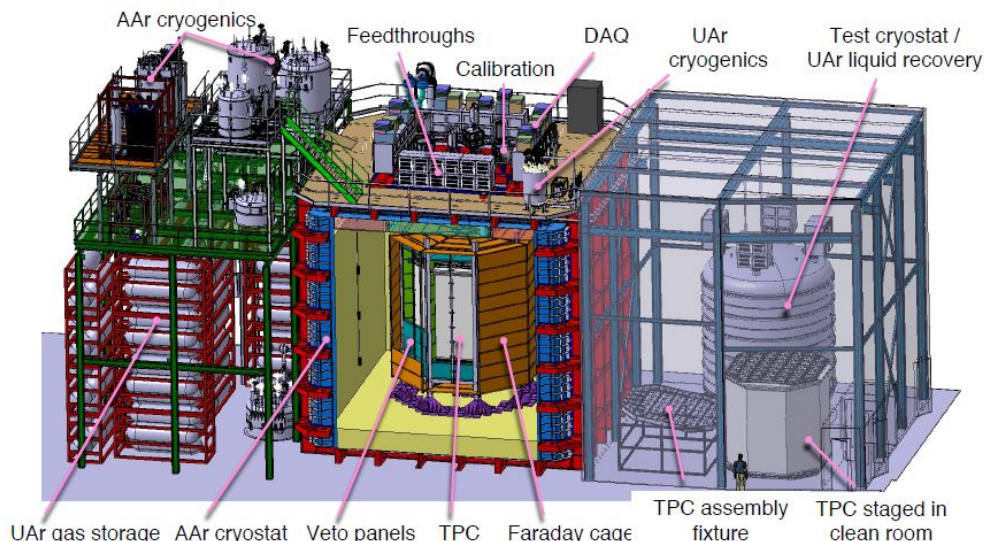


Figure 1.10: CAD rendering of the DarkSide 20k experiment in Hall C of LNGS

The total available surface in Hall C is $14\text{ m} \times 28\text{ m}$ (or $2 \times 14\text{ m} \times 14\text{ m}$). The surface needed for cryostat installation is $14\text{ m} \times 14\text{ m}$, and additional $14\text{ m} \times 14\text{ m}$ for cryostat parts pre-assembly.

It is estimated that DS-20k will need a total electrical power of 222 kW:

- Cryostat: 27 kW
- DAQ: 45 kW
- Ancillaries (Water Plant, Exhaust, Radon Abatement System, Lighting): 50 kW
- Nitrogen Recovery System: 100 kW

In addition, a powerful UPS line is needed with a total capability of delivering 85 kW for the time needed to put in safe conditions all the delicate equipment:

- Cryostat and external AAr cryogenics: 10 kW
- DAQ: 45 kW
- Gas Panel: 25 kW
- Control System: 5 kW

The current DS-20k detector and cryogenic services layout implies the use of the truck gallery for the storage of depleted underground argon UAr arriving from the ARIA plant in Sardinia. The UAr transportation system and containers may also play the role of a UAr storage system.

1.3 UNDERGROUND ARGON PROCUREMENT AND PURIFICATION

Atmospheric argon suffers from the fact that it is intrinsically radioactive at a rate of 1 Bq/kg, and the exploitation of the DS-20k's features mentioned in the previous paragraph is only possible because of the discovery of low radioactivity argon in underground CO₂ wells (UAr) with an activity 1400 times lower than atmospheric argon. This particular quality of argon gas is extracted from underground caves located at the Kinder Morgan Dow Canyon Facility in Cortez, Colorado (USA) in the **URANIA** project with a grade of purity of 99.9% and a rate of 330 kg/day. Then it's purified via isotopic separation with cryogenic distillation in a plant located in Seruci (Sardegna) in the **ARIA** project, in order to exclude the radioactive isotope Ar³⁹.

1.3.1 Urania

The goal of the Urania project is to be capable of extracting and purifying UAr at a maximum rate of 330 kg/day to be the source of UAr also for future, larger argon-based detectors such as Argo. The strong relationship between the DarkSide Collaboration and the Kinder Morgan Corporation led to the construction of Urania. During the extraction of the DarkSide-50 UAr the DarkSide Collaboration provided to Kinder Morgan an analysis of the gas stream that brought to a major industrial partnership between Kinder Morgan and a third party for helium extraction from the CO₂ at Kinder Morgan's Doe Canyon facility. This plant makes up 15% of the production rate of helium in the United States.

The DarkSide Collaboration reached an agreement with Kinder Morgan to feed the Urania plant with a small fraction (~ 15%) of the gas stream returned to Kinder Morgan after argon extraction. Argon from the active CO₂ wells in southwestern Colorado has been found to contain very low levels of the radioactive isotope ³⁹Ar, with the concentration shown to be a factor of $(1.4 \pm 0.2) \times 10^3$ below that of argon derived from the atmosphere.

The Urania feed gas stream is ~ 95% CO₂, plus a few percent of N₂, one percent CH₄, 430 ppm of UAr, and traces of higher hydrocarbons. The processing scheme of the UAr extraction plant visible in figure 1.11 is optimized to achieve an UAr purity of better than 99,99%. The UAr extraction plant consists of three gas-processing units followed by a cryogenic distillation unit. The gas-processing units are two CO₂ liquefier/strippers followed by a pressure swing adsorption unit (PSA).

The gas at (49 ± 1) bar with a flow rate of 20 000 stdm³/h and a temperature of 5°C runs through the **first liquefier**. At these conditions, the CO₂ partially condenses and the stream is separated into 2-phases (gas/liquid) as it goes to the first stripper. Here a controlled quantity of heat is given by a hot fluid working between the chiller condenser and the column reboilers. In this process are generated light products, that are vaporized and recovered from the top of the column in gas phase, and heavy products (mainly CO₂) that are collected

from the bottom, compressed to 50 bar and returned to Kinder Morgan as a gas. The light products coming from the column head are cooled down in the second step to approximately $-50\text{ }^{\circ}\text{C}$ and sent to the second stripper.

The second liquefaction and stripping unit, with a similar process as the first unit, further reduces the CO_2 content. The product gas from the second stripper is re-heated in a heat exchanger and delivered to the PSA unit, which separates the light fractions, including the argon, from the remaining CO_2 . **The PSA** is composed of four adsorption beds to allow continuous operation with short time adsorption cycles. The desorption of CO_2 is made by decreasing the pressure on the bed. The PSA is a critical unit of the entire process since the dynamic adsorption conditions are the most difficult to simulate and predict. Optimization of the sorbent and other operational parameters has been done at Università degli Studi di Napoli "Federico II" via a small scale lab setup in which breakthrough tests are performed for a variety of gas species.

The final unit of the UAr extraction plant consists of three cryogenic distillation columns. The first column works at a lower temperature and pressure ($\sim 9\text{ barg}$) to remove the CH_4 from the CO_2 -free gas coming from the PSA. Then the second column is used to remove the remaining light fractions from the N_2 stream, and in the third column will be performed the final purification of the UAr.

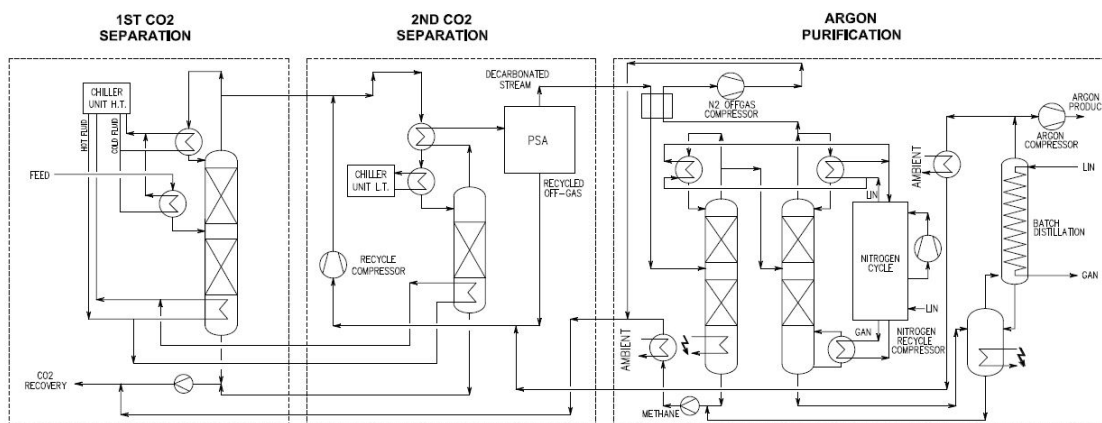


Figure 1.11: Process Flow Diagram (PFD) of the Urania plant

All the wastes are returned to Kinder Morgan along with the CO_2 . The UAr argon extracted and purified is sent to Sardinia, where it is further chemically purified by the Seruci-I column (see below).

The shipment from Colorado to Sardinia will be done by boat in order to minimize the cosmic activation of the argon. Currently the program is to ship the UAr in high-pressure gas cylinders mounted in skids that will operate at 400 bar. The benefit of this idea is that the gas can be maintained in the cylinders for years eliminating the risk of losing any of the UAr during the transport and storage, other than potential loss of the shipment.

The commissioning of the Urania plant is foreseen in 2022.

1.3.2 Aria

The Aria plant goal is to perform the final chemical purification of the UAr extracted by Urania, and to test a method for the active removal of ^{39}Ar from the UAr.

Aria consists of a 350 m tall distillation column, Seruci-I, capable of separating isotopes by cryogenic distillation. The plant is being installed in a vertical shaft of 5 m diameter and 350 m depth, located at the Seruci mine campus of CarboSulcis, a mining company owned by the Regione Autonoma della Sardegna (RAS).

The unit is composed of a series of prefabricated modules, that shall be positioned and reassembled after transportation to Seruci facility, with the intention of reducing the site activities as possible to have a better quality and cost control and a limited construction time and issues. Seruci-I will be composed by 28 modules of 12 m height, plus a top module (condenser and heat exchangers) and a bottom module (reboiler). The column, the cryogenic tanks and heat exchangers are enclosed in a cold box of 711 mm (diameter) \times 348 m (height), to reduce heat losses. The structure of the cold box, the internal equipment and piping are fully welded to reduce the risk of leaks. To account for the cold-box structure thermal contraction, an axial bellow is supplied on each module. Due to the presence of bellows, the loading of each module is independent. Each module is equipped with anchor points supported with external beams to be fixed on the lateral structure of the well. This layout allows to distribute the loading laterally to the shaft walls.

At the top of the column the condenser is fed with liquid nitrogen under liquid level control. The condensed liquid is used as reflux liquid in the distillation column. The reboiler is fed with nitrogen compressed by a nitrogen recycle compressor under temperature control. From the bottom of the column the heavy Argon isotopes mixture is spilled in liquid phase, heated in the heat exchanger and then delivered to the product storage facilities. From the top of the column the light Argon isotopes mixture is heated in the heat exchanger and delivered to the product storage facilities. The products are compressed by compressors and sent to cylinders or tube trailers. Based on technical and economic considerations the selected heat transfer fluid is nitrogen. In a dedicated closed loop circuit the compressed nitrogen is cooled in the heat exchanger and liquefied in the reboiler. Two parallel pumps (one operating, one in standby) are provided in order to deliver the liquid nitrogen from the lower part of the cold box to the upper part. The liquid nitrogen is used then as cooling fluid in the column condenser.

All the modules have already been built and individually checked. The design technical calculations indicates that the plant will be able to provide purified UAr at a rate of 1 ton/day.

During July/August 2019 Seruci-0, a test column composed by the top (condenser) and bottom (reboiler) modules and a single central module has been assembled in the mine site and activated (figure 1.12). The test was performed

with nitrogen both as refrigerant and liquid to be distilled (^{14}N and ^{15}N) and stable distillation conditions were achieved for several days.

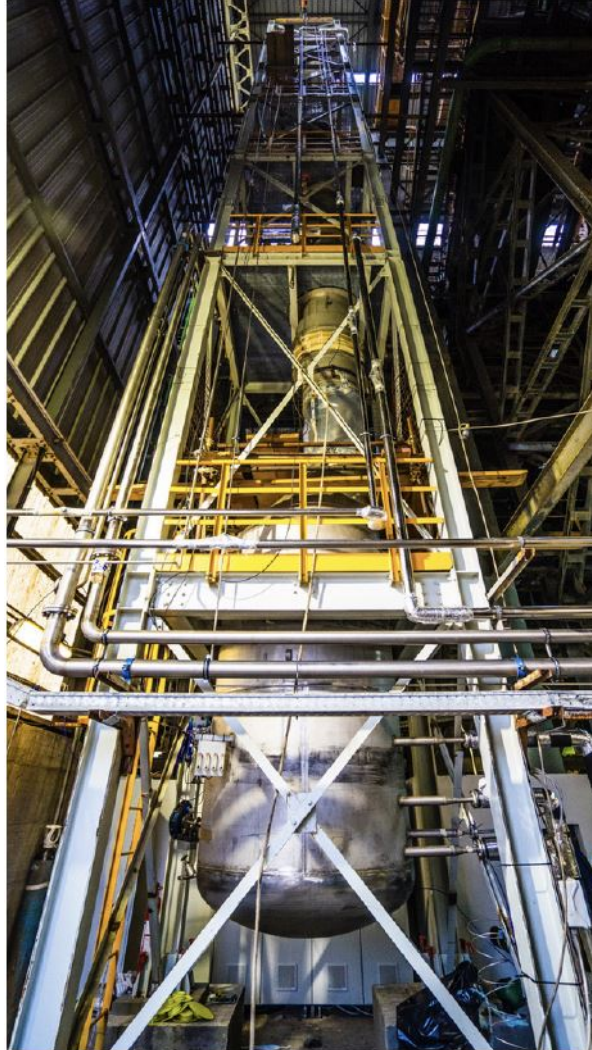


Figure 1.12: Seruci-0 distillation column, installed in the Seruci mine campus of Carbo-Sulcis, Sardinia, Italy

1.4 CRYOLAB AT INFN - NAPOLI

During my thesis experience I have worked for the INFN (National Institute of Nuclear Physics) in its Naples laboratory, under the supervision of Professor Giuliana Fiorillo, Deputy Spokesperson, National PI for INFN, Napoli group leader in the DarkSide experiment at LNGS and nuclear and sub-nuclear physics full professor at Federico II University of Naples. Professor Fiorillo runs the Naples INFN laboratory located in the Physics Department of the Federico II University in the Monte Sant'Angelo campus.

The laboratory is equipped with a “clean room”, a special facility where provisions are made to reduce particulate contamination and control other environmental parameters such as temperature, humidity and pressure. All of the air delivered to a cleanroom passes through HEPA filters (High Efficiency Particulate Air) to trap particles that are 0.3 micron and larger in size, and employs laminar or turbulent air flow principles.

Personnel that works in cleanrooms enter and exit the cleanroom through airlocks, air showers and/or gowning rooms, and they must wear special clothing designed to trap contaminants that are naturally generated by skin and the body.

This particular environment and care is mandatory in the particle physics experiments that take place in this facility.

Another key feature of the laboratory is the presence of an external area dedicated to the storage of the liquefied argon and nitrogen needed in the cryogenic systems. This plant is composed of 2 tanks installed and maintained by the Linde company (figure 2.21).

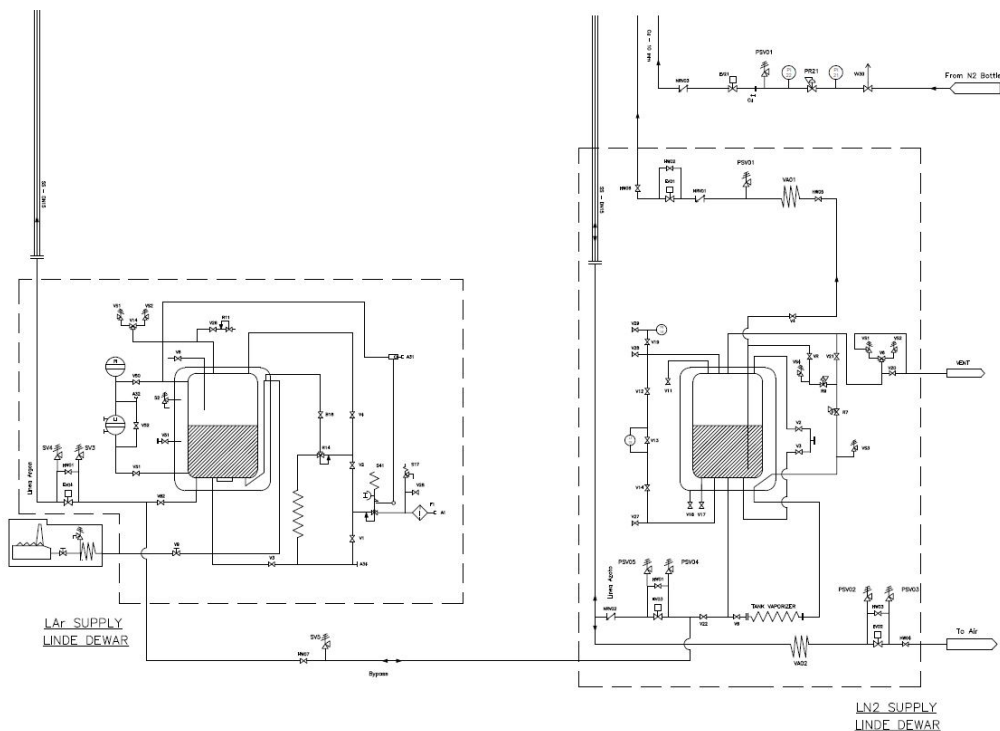


Figure 1.13: Pipes and Instrumentation Diagram (P&ID) of the external supply tanks

Through dedicated super insulated double wall pipelines it is possible to have a constant supply of liquid nitrogen and argon directly in the clean room. This storage and supply plant is equipped with pressure transducers and safety valves, and can be remotely controlled by electric valves. The laboratory has the two double wall transferlines, connected to the external liquid Ar and N₂ tanks, coming through the ceiling on the opposite sides of the room, providing two access points to the cryogenic fluids for multiple simultaneous systems. Due to a recent upgrade of the supply plant a by-pass line with a manual valve (HW07) and a safety valve has been installed, which allows the connection of each of the tanks with both the transferlines.

Indeed, during this period, the laboratory has been the setting of two experimental systems related to the DarkSide collaboration project at the same time. From the layout of figure 1.14 you can see that one section of the laboratory is dedicated to a small scale prototype of DarkSide-20k: the Proto-0 stand alone system; while another area of the clean room is dedicated to the "**PDU Test Facility**": an installation designed specifically for the serial test and characterization in a cryogenic environment of all the PDUs that are going to be part of the DarkSide-20k experiment. All the 350 PDUs that are going to be used in the TPC of DS-20k must be tested and characterized in liquid nitrogen (LN), with an estimated rate of 12 PDUs a week.

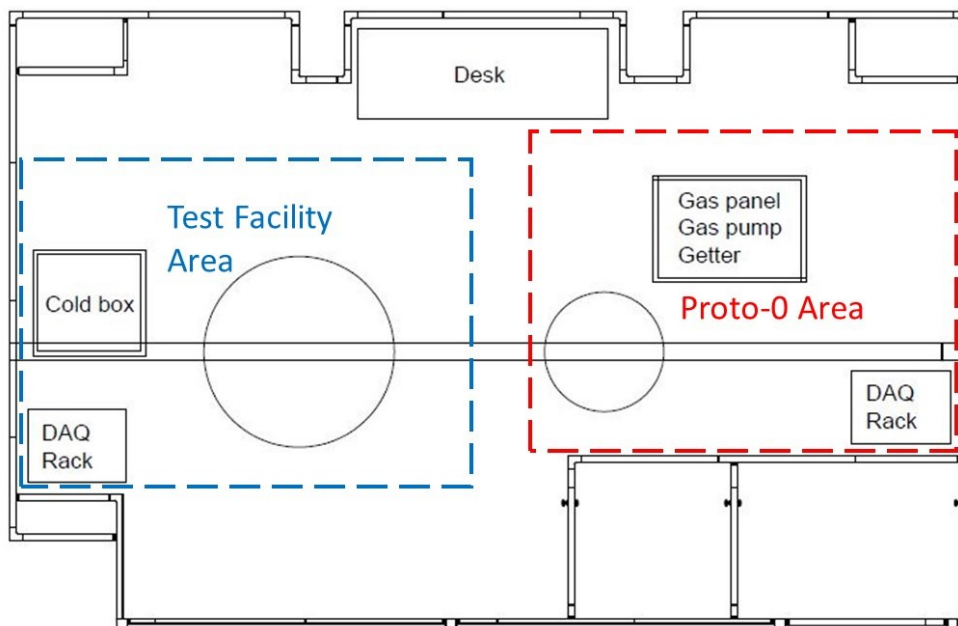


Figure 1.14: Layout of the Naples clean room

2

THE DARKSIDE PROTO-0 SYSTEM

The purpose of the DarkSide Proto-0 experiment in this thesis is the construction and commissioning of a smaller size prototype of the DarkSide 20k system to validate and test mechanical and functional aspects of the new technologies that will be used in final experiment at the LNGS. Proto-0 is not intended to replace the tests made in the laboratories on the single components, but rather complement them with the integration of the rest of the system, moreover not all its features are exactly the same of the final DS-20k experiment to keep up with the project's schedule.

The Proto-0 system goal is to test the DS-20k TPC prototype in a double wall, vacuum insulated **cryostat** filled with 200 liters of liquid argon. The 6.0 Ar needed in the experiment is stored in a pressurized tank in gas phase. The 99.9999% purity granted by the 6.0 Ar gas is mandatory to simulate the closest conditions to DS-20k.

A **condenser** is used to liquefy the Ar and fill the cryostat. The heat exchange is made with a constant supply of liquid nitrogen from an external storage tank.

Before the liquefaction process the Ar gas flows through a **gas recirculation panel** and gets purified by a SAES rare gas purifier getter.

The system can be separated in two loops: the N₂ loop and the Ar loop (figure 2.1).

By opening the bypass valve (HW07) (1.4) and the electric valve (EV04), the liquid nitrogen flows to the condenser through a double wall, vacuum insulated transfer line. The flow rate of the incoming LN₂ is regulated by a proportional pneumatic Siemens valve (PV10). After the heat exchange the nitrogen gas is expelled with a controlled flow rate into the vent line by a Mass Flow Controller (MFC).

During the first activation of the system the argon gas coming from the bottle is recirculated into the gas panel and the getter to be additionally purified. Then it is liquefied in the condenser and flows into the cryostat. Here, the heat produced by the electronics and the PDU (1.2.2) in addition to the heat coming through the top flange, begins the evaporation process of the argon. The argon gas forms a gas pocket between the LAr surface and the top flange of the cryostat. The evaporated argon gets pumped into the getter, purified and sent to the condenser to be liquefied again.

The Ar loop is a closed loop.

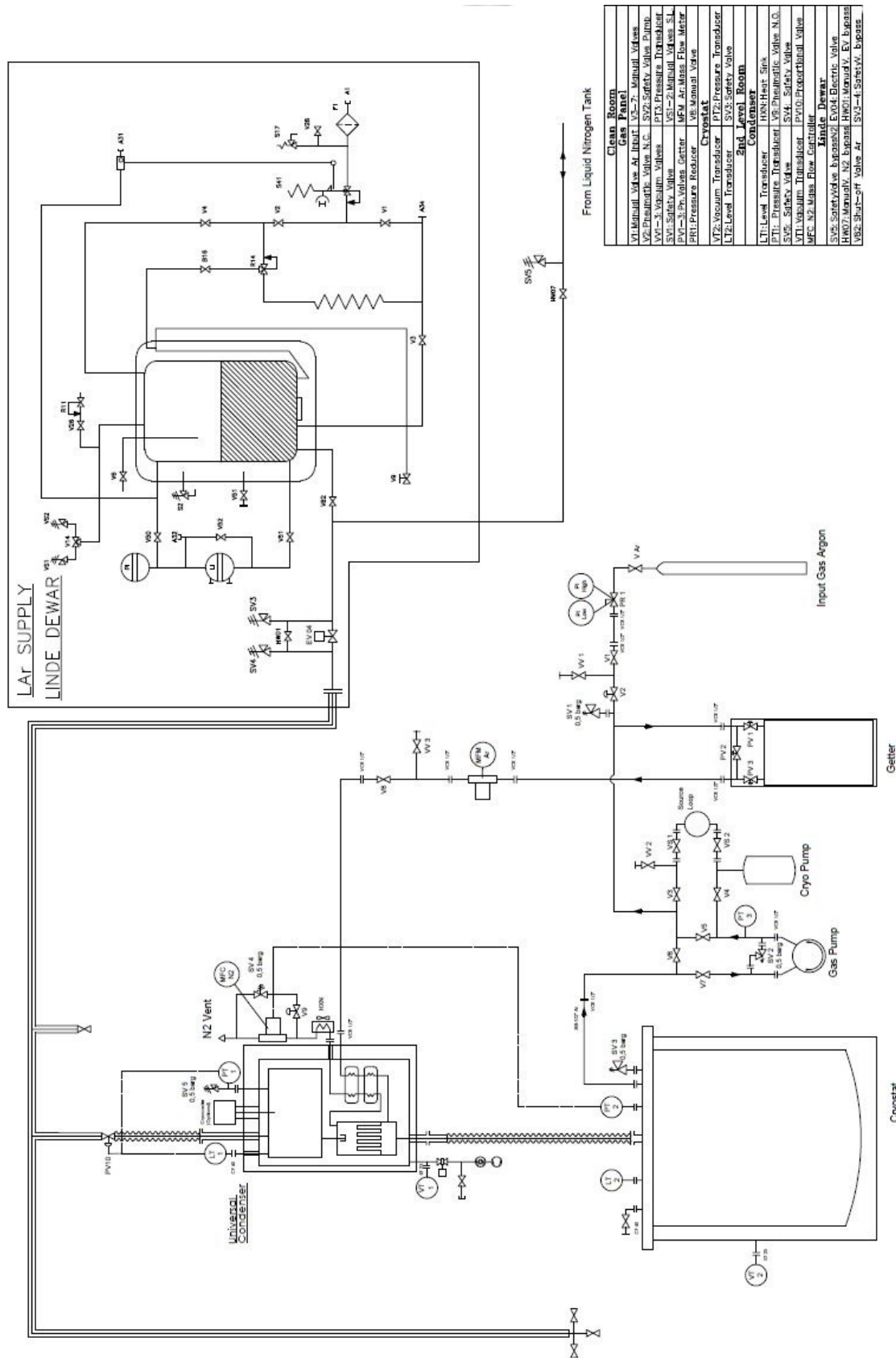


Figure 2.1: Proto-0 system Pipe and Instrumentation Diagram (P&ID)

2.1 SYSTEM OVERVIEW

The Proto-0 system can be schematically subdivided in 6 main elements:

- The cryostat,
- The “ Universal Condenser”,
- The purification Getter,
- The “Gas Distribution Panel”,
- Slow Control,
- The supply tank.

2.1.1 The Cryostat

The cryostat is a dewar with a capacity of up to 300 liters of LAr, where the TPC with a single motherboard is placed for the experiment (figure 2.3). The dewar is sealed with a top flange that has 8 openings of different dimensions.

These openings are all equipped with CF flanges. CF-style vacuum flanges and fittings are the standard for ultrahigh vacuum (UHV) applications. Also known as ConFlat flanges, they use a copper flat gasket placed between two knife edges to provide an extremely leak-tight vacuum seal (up to 1.0×10^{-6} mbar). Mating flanges have identical profiles, i.e. they are sexless, eliminating the need to store two types or worry about compatibility.

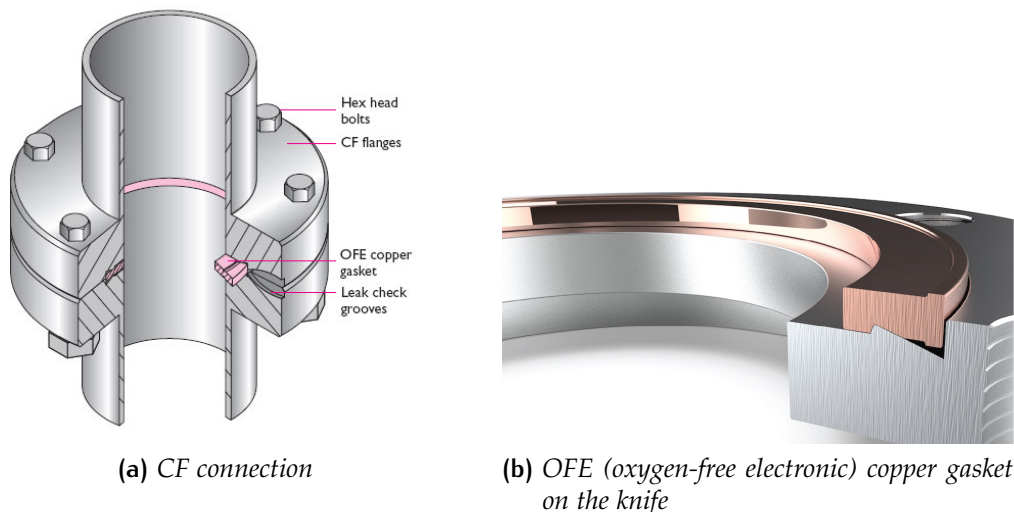


Figure 2.2: CF flanges standard

Made with very high purity stainless steel and meticulous cleaning procedures, the flanges, seals, screws, and nuts are suitable for use in the ultrahigh vacuum applications and in a wide temperature range from -200 C to 500 C.

These flanges with the appropriate adapters allows to install the needed sensors and connections with the other components of the system:

- 1 flange CF63 for the PDM signal and power supply cables;

- 6 **flanges CF40** for the liquid Ar inlet, the gas Ar outlet, the pressure and level sensors, the safety valve, the motion feedthrough, the High Voltage feedthroughs;
- 1 **flange CF16** for the optical feedthrough.

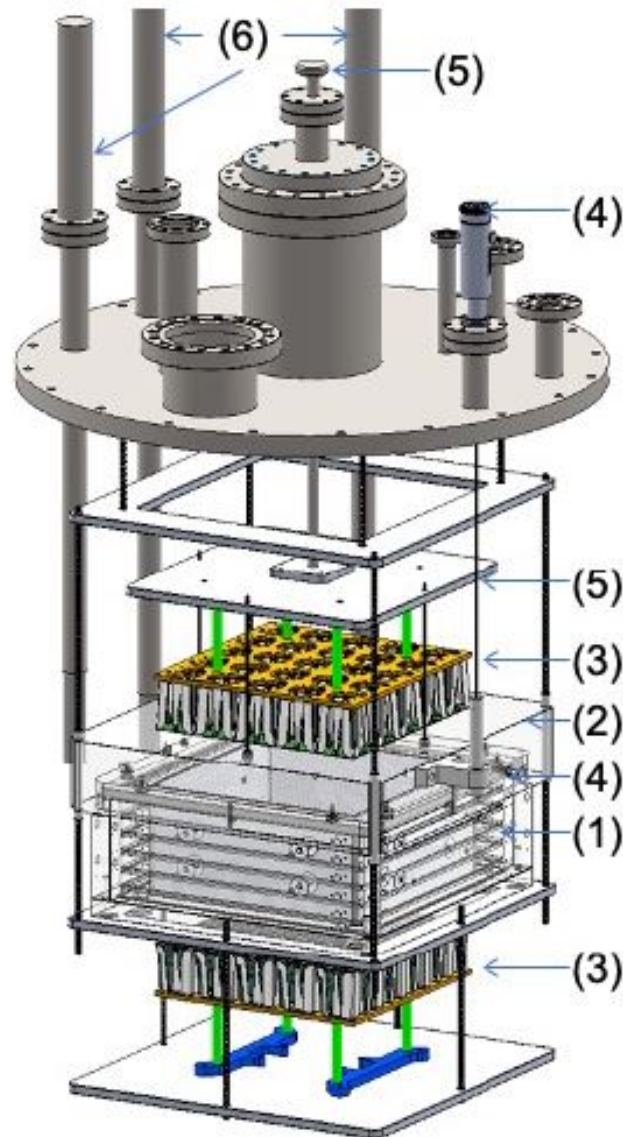


Figure 2.3: 3D model of the Proto-0 setup. (1)TPC field cage; (2) movable anode and diving bell; (3) PDU; (4) motion feedthrough adjusting gas pocket thickness; (5) motion feedthrough adjusting PDU position; (6) HV feedthroughs

The **level sensor** is made of 5 PT100 RTD (Resistance Temperature Detectors) sensors connected to a vertical bar that measure the temperature in the cryostat at different heights. These elements are made from a pure material whose resistance at various temperatures has been documented. The material has a predictable change in resistance as the temperature changes; it is this predictable change that is used to determine temperature. The value of the temperature

measured by every sensor allows to determine the level of the LAr in the dewar with a reasonable accuracy.

The **pressure sensor** is a Wika S-20 model. It is a pressure transmitter for general industrial applications that features a very good accuracy and a robust design. It's capable to operate effectively also with cryogenic temperatures. The model S-20 offers continuous measuring ranges between 0...0.4 and 0...1,600 bar in all the major units. This pressure sensor is essential to keep under control the pressure in the cryostat, and to adjust the LAr flow inlet coming from the condenser.

Since the dewar is not PED (Pressure Equipment Directive) certified the pressure inside the cryostat has to remain under 1.49 bar. To avoid the raise of the pressure due to a failure of the regulation system, a **safety valve** is installed. The safety valve is calibrated to release the Ar gas if the internal pressure goes over the chosen value of 1.5 bar.

One of the key factors of the experiment is to have the motherboard always submerged in the LAr. It is crucial to manage the progressive evaporation of the liquid argon due to the heat released by the PDU and all the electronics by replacing the evaporated liquid with fresh purified liquefied gas.

Therefore is essential to preserve the balance between the evaporation rate of the LAr and the refill flux coming from the condenser.

The **LAr inlet line** is a double wall vacuum insulated transfer line. The line is connected to the top flange of the cryostat with a bayonet CF40 flange. This connection system has a double purpose: the flange is thermally insulated and the bayonet has a specific length that allows to smoothly direct the LAr flux on the dewar's wall.

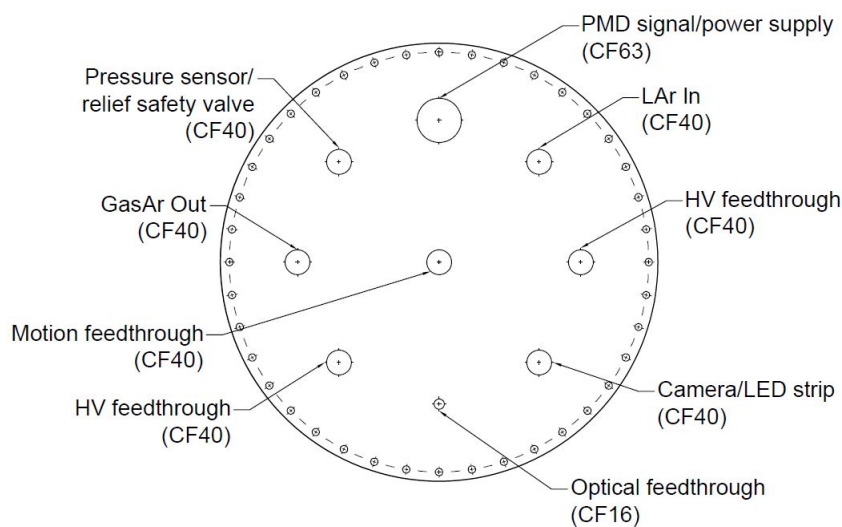


Figure 2.4: Top flange layout

2.1.2 The Universal Condenser

The **Universal Condenser** (fig. 2.5) is the key component that allows the system to work in a closed loop. The condenser is called “Universal” due to the multiple possible operating modes and to the wide power range it can provide. This condenser can be used in all situations where liquefaction of argon gas is required. It can perform with a constant supply of cooling fluid, or in a completely closed loop with a cryocooler that liquefies the cooling fluid evaporating in the heat exchange process. This flexibility is the reason why this component could be used in completely different systems and conditions. The condenser was designed by UCLA professor Hanguo Wang and his team at CERN as an upgrade of the condenser used in the DarkSide-50 system, and produced by DEMACO. All the component’s parts are made of stainless steel AISI 304L.

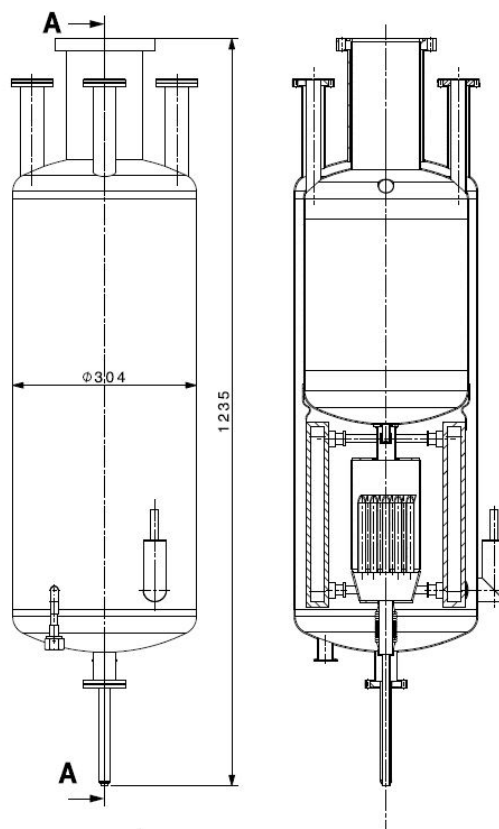


Figure 2.5: CAD drawing of the Universal CONDenser

The Universal Condenser is equipped with 2 Kaori K50 brazed plate heat exchangers to pre-cool the Ar gas (fig. 2.6). The selected model is made of 10 corrugated chevron plates of copper/nickel as brazing materials.

These two heat exchangers purpose is to bring the gas Ar as close as possible to the liquefaction temperature. The purified Ar gas coming from the getter flows into the condenser through a stainless steel single wall 1/2" flexible line connected with a VCR coupling (see subsection 2.1.4), and passes through the heat exchangers.

The liquefaction process takes place in a tube and shell heat exchanger made of 19 tubes welded on a tubesheet that separates the LN₂ chamber from the Ar

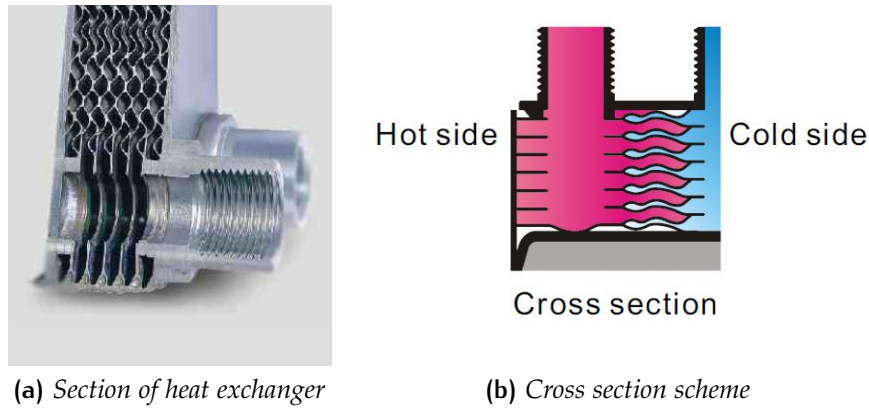


Figure 2.6: Kaori K50 Heat Exchangers

chamber. Here the Ar gas liquefies and flows through a metal bellow line that can adapt to the relative displacements of the previously mentioned components caused by material's thermal expansions and contractions. The condenser is connected to the cryostat via a vacuum insulated flexible transfer line.

The transfer line connection with the condenser outlet is a CF40 bayonet coupling.

The upper part of the condenser is dedicated to the cooling fluid. There are five openings in the top dome of the LN₂ barrel. On the perimeter there are 4 CF40 flanges dedicated to the level meter, the pressure sensor, the relief valve and to the LN₂ inlet transfer line. In the center there is a bigger flange dedicated to the optional installation of the Cryocooler.

The LN₂ barrel is designed to store up to 20 liters of liquid nitrogen and works as a phase separator. The phase separator ensures the supply of 100% liquid at a stable, predefined pressure. The phase separator working principle is to temporarily bring the liquid gas to a standstill in the buffer dewar. Then, because gas is lighter than liquid, any gas bubbles naturally rise at a standstill (or at very low flow rates). At a preset pressure level, a relief valve opens at the dewar's top, releasing the gaseous portion. At the bottom of the dewar, the pure liquid gas can then be extracted at the required output pressure. The LN₂ supply from the external tank is regulated by a Siemens proportional pneumatic valve (PV10) controlled by the level sensor and pressure sensor with a proportional-integral-derivative controller (PID controller). The correct control of the filling valve is essential for the phase separator to operate correctly and open precisely at the right moment, maintaining the liquid level in the barrel in the predefined range and releasing the gas to keep the required pressure.

The liquid nitrogen inlet transfer line is connected with one of the CF40 top flanges of the condenser, while the connection with the Siemens filling valve is a Johnston coupling.

The Johnston coupling consists of a male and female connector (bayonet) that can easily be installed without welding or special knowledge. The coupling is secured by KF50 hinged clamp and the sealing is granted by an O-ring and

a teflon cylinder that ensures the contact between the tip of the male and the female.

The crucial feature of the Johnston coupling is the presence of a vacuum space between male and female connectors. The potential LN₂ leak would evaporate and remain confined there, creating a gas pocket. This gas would act as a stopper making further LN₂ leaks impossible.

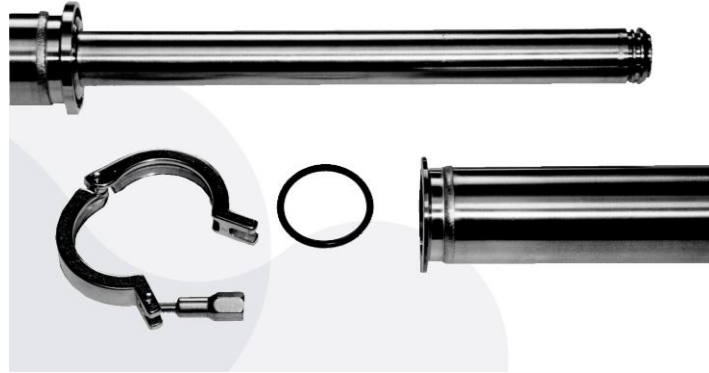


Figure 2.7: Johnston coupling elements

The liquid N₂ flows from the buffer to the heat exchanger through a siphon like pipe called "Chicken Feeder" (fig.2.8).

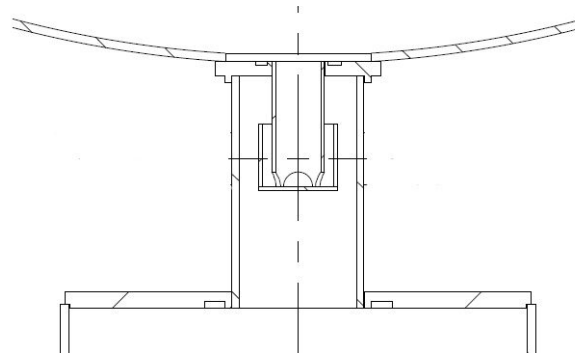


Figure 2.8: "Chicken feeder" CAD model

The cooling power adjustment of the condenser is done by a mass flow controller (MFC) that regulates the exhaust N₂ flux rate from the last heat exchanger. In this way the chicken feeder enables the income of a corresponding amount of liquid N₂. As a result this process regulates the amount of Ar gas liquefied, and, therefore, needs to be controlled by the cryostat's level sensor and pressure sensor. The nitrogen expelled from the condenser is additionally heated by a "heat sink" to prevent the freezing of the line and of the mass flow controller. This line is also equipped with a safety by-pass. In case of power failure a normally open pneumatic valve (V9) allows the nitrogen flux to by-pass the MFC (fig. 2.9), that will act as a normally closed valve, passing through a relief valve calibrated on a predefined pressure (1,49 bar).

All of the previously mentioned components of the condenser are contained in an external vessel to provide a vacuum thermal insulation with a dedicated vacuum pump and sensor (VT1 see fig. 2.9).

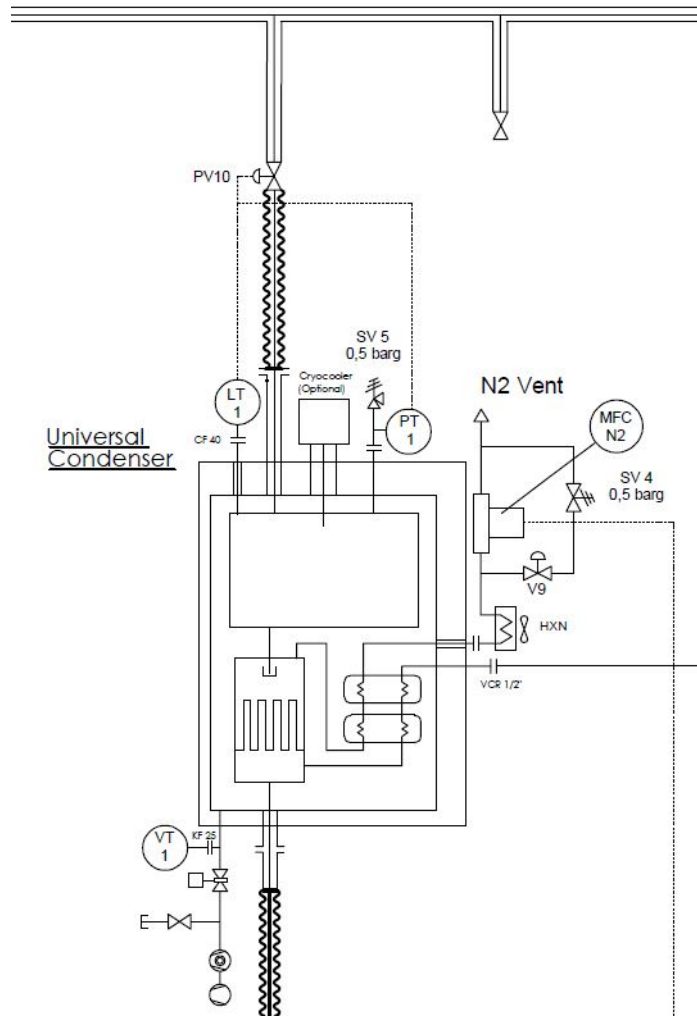


Figure 2.9: P&ID of the Universal Condenser

2.1.3 The Purification Getter

The **purification getter** selected for the system is a PS4-MT50-R SAES rare gas purifier.

The MonoTorr Rare Gas Purifier is a getter-based purifier designed specifically to provide ultra-high purity gas for semiconductor applications. Outlet impurity levels for O_2 , H_2O , CO , CO_2 , H_2 , N_2 and CH_4 are reduced to low parts per billion (ppb) levels or below.

The patented getter alloy operated at elevated temperatures, removes impurities by forming irreversible chemical bonds. Impurities will not be released under any circumstances when the purifier is operated within specification.

The purifier will continuously supply ultra pure gas at rated flows provided that inlet impurities are within specified levels, until getter cartridge replacement is necessary.

The SAES PS4-MT50-R features a Fully Automated Microprocessor Controller that continually monitors system operation providing fault detection, temperature control and valve sequencing ensuring purifier reliability while minimizing operator involvement.



Figure 2.10: PS4-MT50-R SAES purification getter

All purifier operations (except the manual by-pass valve) are controlled from the purifier Human Machine Interface (HMI), which is installed in the electrical access door (fig. 2.10). The HMI is comprised of a two line LCD display and ten touch-sensitive buttons which are used to navigate through operation menus and acknowledge and clear alarms or warnings.

The getter is connected to the rest of the system via 2 VCR 1/2" couplings, that link the inlet and outlet lines to the getter's pneumatic valves. The maximum flow rate of the delivered purified gas is 100 slpm, the inlet pressure acceptable range is between 2.8 bar and 10.3 bar. The inlet gas temperature range is 0 C - 35 C, while the maximum outlet gas temperature is 55 C. If all of the above requirements are met, the purifier grants an impurity level below 1.0 ppb (parts per billion).

2.1.4 The Gas distribution Panel

The **gas distribution panel** is the set of tubes, sensors and valves that connect the input Ar gas bottle, the purification getter, the condenser and the cryostat.

All the tubes and fittings are made of AISI 316L stainless steel. The system's valves are Swagelok BN series bellows-sealed high purity valves, with VCR 1/2" connections.

The Ar gas is stored into a pressurized bottle at 200 bar, therefore a pressure reducer is needed to obtain the allowed pressure. The bottle is connected to the

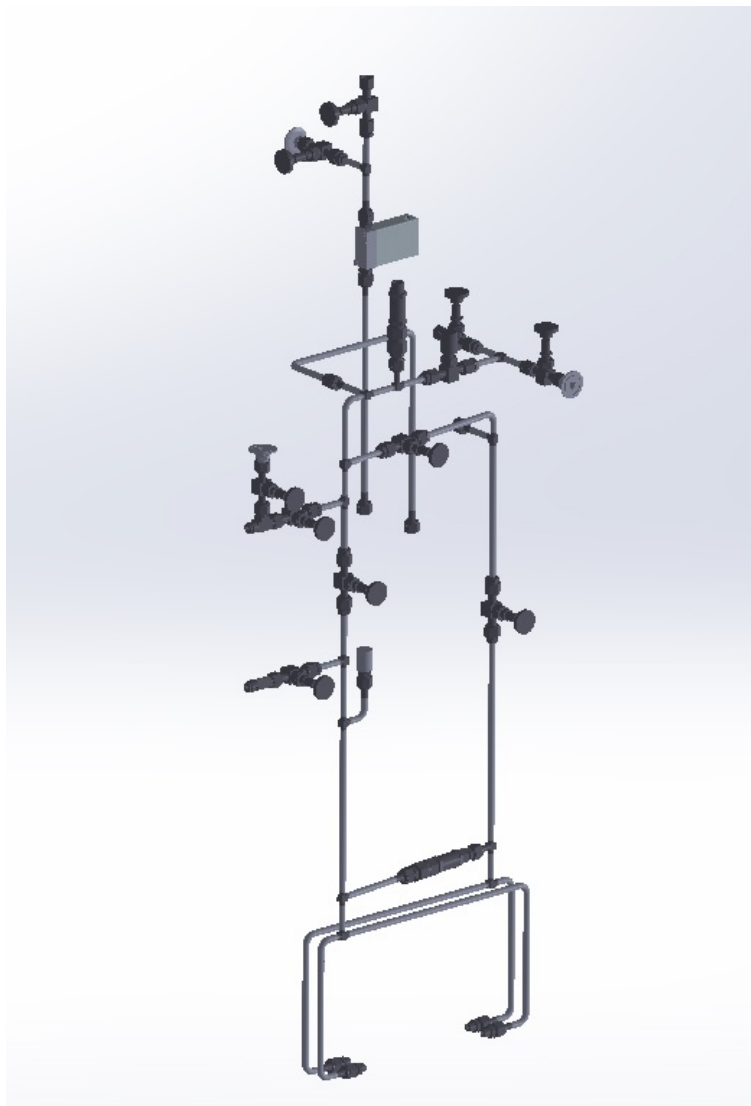


Figure 2.11: Gas Distribution Panel 3D Model

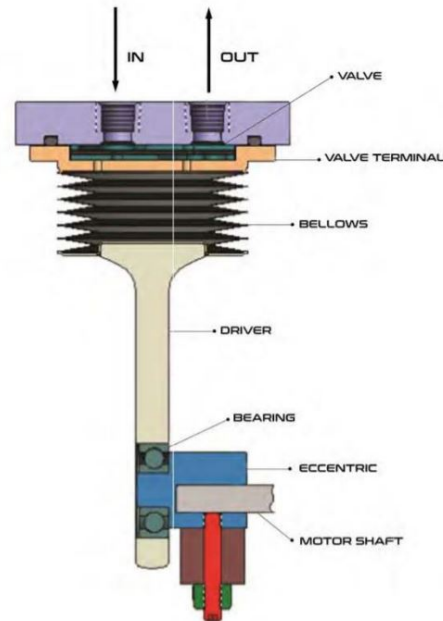
V1 manual valve of the gas panel with an adapter to match the 1/4" flexible tube to the 1/2" female VCR port. For the Ar gas filling of the system, when both the manual valve V1 and the pneumatic normally closed valve V2 are open, the Ar gas can flow into the system. The Ar flow first needs to pass through the purification getter, then it goes to the condenser to be liquefied. On this line is installed a mass flow meter (MFM Ar) to measure the Ar flow rate entering in the condenser. The filling process goes on until the cryostat is filled with LAr to the desired level.

Once the normal operating conditions are reached, the Ar gas bottle can be disconnected and the recirculation begins. The evaporated argon coming from the cryostat gets pumped into the getter to be purified and is sent to the condenser to be liquefied again. The gas pump used is a Senior Aerospace Metal Bellows model MB-602. The pump has 4 3/8" NPT ports that are connected via 3/8" NPT to 1/2" VCR custom adapters designed by Criotec Impianti S.p.A. to the gas distribution panel. A Positive Displacement Pump like this one is a "chamber that can be expanded or contracted by an external force", and generates the same

flow at a set speed whatever the discharge pressure. This particular company uses an unique welded metal bellows technology as the pumping chamber, that can ensure zero leakage, zero contamination, high reliability, and long life. The engine is a 1/2 HP single phase Open Drip Proof motor supplied with 220 V. Its operating speed at 60 Hz is of 3450 rpm.



(a) Gas Pump with anti-vibration support



(b) Gas Pump working principle

Figure 2.12: The Gas Pump

The gas pump is protected from a high counterpressure by a safety bypass line. A tube with an inline check-valve links the inlet and outlet lines of the pump. If the outlet pressure exceeds the safety value (1,49 bar), the check-valve opens and creates a loop between the inlet and the outlet.

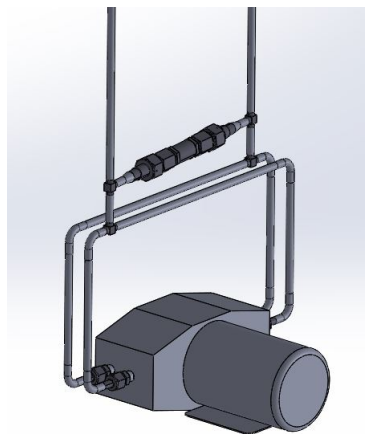


Figure 2.13: Pump by-pass 3D model

The 3 valves (VV1 – 3) purpose is to allow the connection of a vacuum pump to generate vacuum in each section of the gas panel individually and remove the air before pure Ar input.

An interesting feature is the possibility to install a "source loop" for the detector calibration.

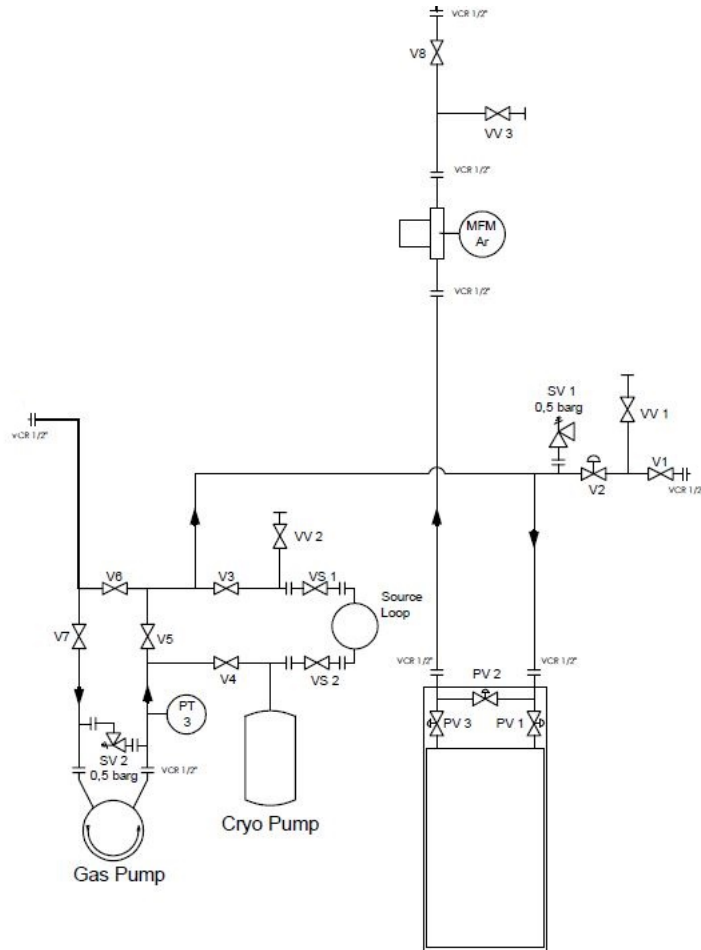


Figure 2.14: P&ID of the gas distribution panel

The source loop is a small tank containing a radioactive source to test the detector response to nuclear recoils with given deposited energy. The chosen calibration element is ^{83m}Kr gas. The source loop calibration provides different advantages such as a background free estimation of scintillation light yield and resolution at low energies combined with the effectiveness of the recirculation system study.

Particular attention should be given to the V8 manual valve (fig. 2.14). This valve is installed at the condenser inlet line and its purpose is to adjust the Ar gas flow rate entering in the heat exchanger.

All the valves and the connections between the lines are VCR 1/2" standard couplings. VCR means vacuum coupling radiation, this fitting's standard provides leak-tight service from vacuum to positive pressure. The VCR product lines have a zero clearance capability, which means they can be disassembled in line with no clearance requirements. VCRs serve as a make and break point,

a spot to access the system for repair and upgrades without having to remove multiple parts.

The VCR connections are composed by a gland with a female nut that couples with another gland with a male nut, and a sealing gasket between them (fig. 2.15).

The glands are orbital-welded to the 1/2" pipes, ensuring no leaks or the release of gasses trapped during the welding process.

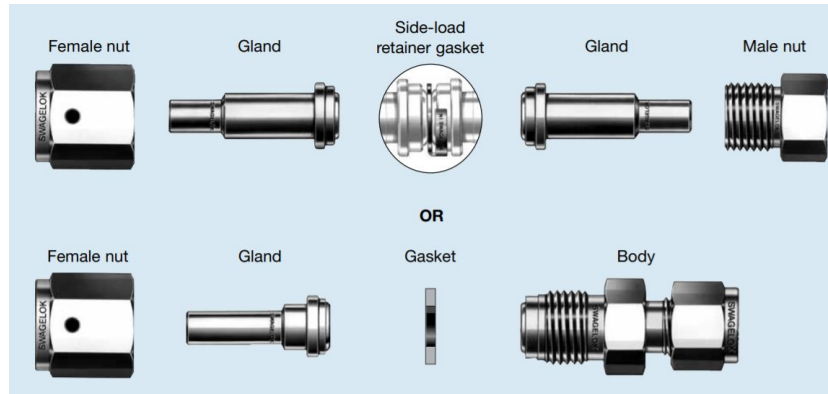


Figure 2.15: VCR fitting components

The gas distribution panel is also equipped with a pressure transducer Wika S-20 and a safety valve.

2.1.5 Slow Control

The Proto-0 system has been designed to be remotely controlled and mostly automatic during its activity period. After the activation phase, once the cryogenic recirculation system is at regimen, the key components are automatically controlled on the basis of the pressure and level sensors data of the cryostat and of the LN₂ barrel in the condenser.

This is performed by a "Slow Control" system. Slow Control Systems are used for setup and monitoring of hardware that is not time-critical, and can be run at a low priority. The Proto-0 slow control system is responsible for the control of all the electrical devices (valves, gas pump, getter, heat sink) and the readout of the temperature, level and pressure sensors as well as the data acquisition from the TPC installed in the cryostat that is the core of the experiment.

Every electrical component is connected to the CompactRIO controller. CompactRIO (or cRIO) is a real-time embedded industrial controller made by National Instruments for industrial control systems. The CompactRIO is composed by a real-time controller chassis, reconfigurable I/O Modules (RIO), FPGA (field-programmable gate array) module and an Ethernet expansion chassis to connect the CompactRIO controller to a PC. The NI-produced chassis controllers are generally compatible with third-party modules.

CompactRIO is optimized for programming with LabVIEW, National Instruments graphical programming language, as LabVIEW can be used to write code deployed onto both the real-time operating system and directly onto the FPGA.



Figure 2.16: CompactRIO controller

The cRIO is connected to a PC to host a GUI that can display all the sensors values and manage all the configurations of the system (fig. 2.17).

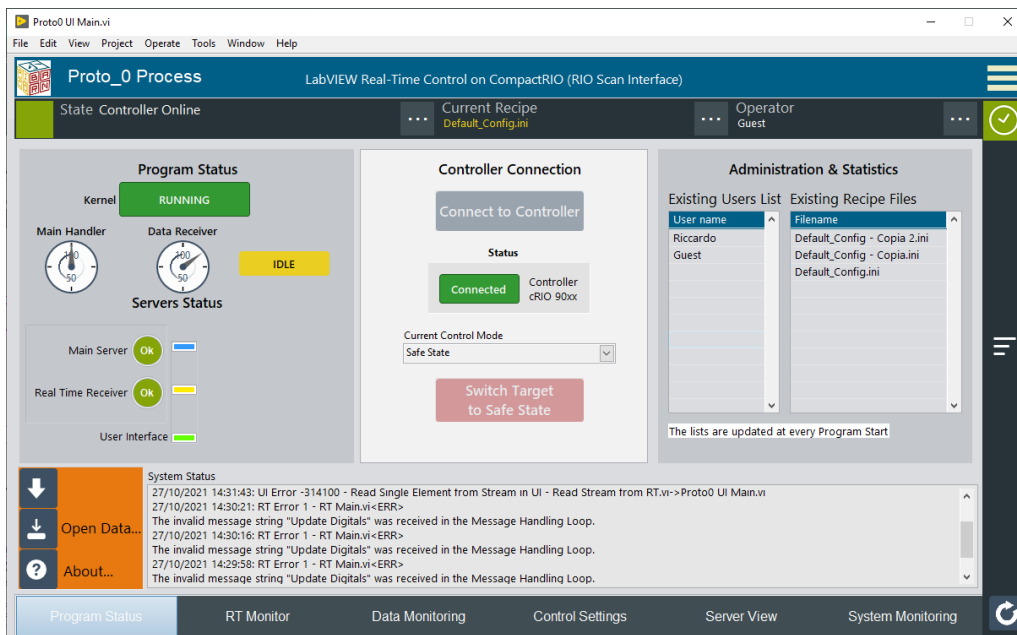


Figure 2.17: Slow control GUI

Regarding the cryogenic system, the slow control software foresees a "start-up verifications" subroutine, to check that all the temperature, pressure and vacuum sensors are properly working.

Then there is a "filling phase" subroutine dedicated to the filling of the argon side of the system with the activation of the N.C. pneumatic valve, gas pump and getter of the gas distribution panel. At the same time also the electric valve of the supply tank, the proportional pneumatic valve and the mass flow controller of the N_2 loop needs to be activated, to begin the liquefaction process of the Ar gas in the condenser.

During the "normal operating phase" the slow control is monitoring the values of the sensors of the cryostat and condenser. The condenser is constantly refilled

with LN₂ via the proportional valve rate opening adjustment, made through a PID (proportional–integral–derivative) control related to the level indicator and pressure sensor signals of the LN₂ barrel. Another key activity managed by the slow control during the normal operating phase is the condenser's cooling power regulation. The LAr flow rate produced by the condenser is adjusted via the variation of the flow rate of the exhaust evaporated nitrogen expelled through the mass flow controller. The MFC opening grade is set by the pressure sensor signal coming from the cryostat.

The software is also designed for a "switch off" phase and for an "emergency shut down" phase.

2.1.6 Proto-0 TPC and DAQ

The Data Acquisition System is equipped with 4 CAEN V1725B digitizers (250 MS/s, 14-bit, 16 channels). The DAQ and Slow control hardware elements are installed on a rack cabinet located close to the cryostat and to the gas panel (fig.2.18).

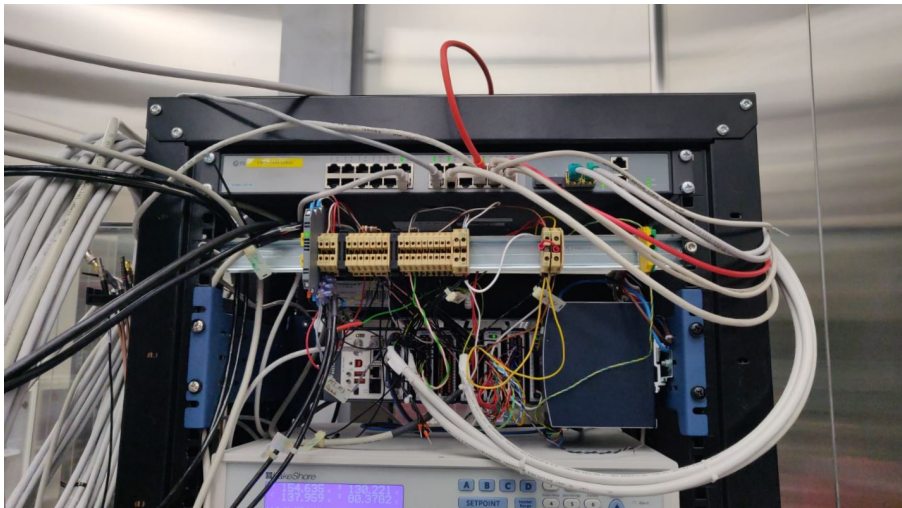


Figure 2.18: DAQ and Slow control system on the rack cabinet

Most of the electronic components needed in the experiment have been delivered from CERN, including the Low Voltage/ High Voltage filter box, the adapter box with steering module and its driver, the differential to single-ended converter board and the TPC itself.

The set-up of a single test involves different configuration steps on many items such as:

- Digitizers (25 channels/PDU, trigger, thresholds,...)
- High Voltage (power on/off, ramp rate,...)
- Low Voltage Power Supply (power on/off, voltage control)
- Laser (power on/off, frequency,...)

Using different tools for each item would be a time consuming task prone to errors. Therefore a web interface for DAQ and slow control has been created.

This Graphical User Interface (GUI) provides to the user a single-point management for DAQ and slow control settings in order to simplify the handling of testing tasks.

The GUI has an interface with LabVIEW for the slow control and an interface with the Maximum Integrated Data Acquisition System Online Data Base (MIDAS ODB) for the CAEN digitizers of DAQ system.

MIDAS is a modern data acquisition system developed at Paul Scherrer Institut (PSI) and at Canada's particle accelerator center TRIUMF. Midas provides by default a complete DAQ system, the main features of which comprise: front-end template for acquiring your hardware information, data transfer mechanism to local/remote computer, data logging capability, data analysis framework, data monitoring, full run control, and web interface for experiment control/monitoring.

The Computing system consists of:

- **darkside-daq**: the main DAQ machine with ROOT online server for online and offline analysis;
- **darkside-ui**: a gateway for user analysis;
- **darkside-stor**: the DAQ storage server.

2.1.7 The Supply Tank

Outside of the Physics Department is located a supply plant that features two tanks dedicated to the storage of LN₂ and LAr.

The producer and maintainer of the tanks is Linde. Linde is a global multinational chemical company whose primary business is the manufacturing and distribution of atmospheric gases, including oxygen, nitrogen, argon, rare gases, and process gases, including carbon dioxide, helium, hydrogen, ammonia, electronic gases, specialty gases, and acetylene. Therefore, they also are the laboratory N₂ and Ar providers.

The vacuum-insulated double wall tanks consist of two concentric vessels, an austenitic steel inner tank and an outer jacket in carbon steel with an anti-corrosion primer. An adsorbent is added to maintain the vacuum in the insulation interspace.

The tanks have a gross nominal water capacity of 3,300 liters and a maximum allowable working pressure for the inner vessel of 18 bar. The working temperature range of the inner vessel is between +20 and -196° C.

The pressure vessels are manufactured and tested in accordance with the Pressure Equipment Directive EU 97/23/EC and EN 13458.

At the moment the systems assembled in the laboratory only need liquid nitrogen. Proto-0, as mentioned before, works with Ar gas that gets liquefied with liquid nitrogen.

The working pressure in the LN₂ tank is of 2,9 bar. An indicator placed on the side of the tank indicates the percentage level of liquid nitrogen in the inner vessel and its pressure. This information is live shared with Linde to allow the automatic delivery of LN₂ for the periodic refill.



(a) Supply tanks top view



(b) Supply tanks frontal view

Figure 2.19: LN₂ and LAr supply tanks plant

These tanks are equipped with a complex system of safety valves and control valves. Each of the two tanks has a dedicated electric valve and is connected to the laboratory systems via a dedicated double wall vacuum insulated line. In this way it is possible to remotely open the valves and get the liquid gases to the systems. This year a custom modification to the lines has been done. Thanks to the installation of a 2-way by-pass between the transfer lines connected to the tanks, it is possible to have either LN₂ or LAr flow in each line. This by-pass line is located immediately before the electric valves of each line and is equipped



Figure 2.20: Level and pressure indicator of the tank

with a safety valve and a manual valve to close the by-pass returning to the original situation.

To underline the by-pass importance let's consider the laboratory as virtually divided in two areas. On one side there is the end point of the LN₂ transfer line, on the other side there is the end point of the LAr line. The Proto-0 cryogenics system is installed on the LAr side, therefore before this by-pass upgrade it would have been impossible to supply the condenser with liquid nitrogen. After this crucial modification of the delivery system it is now possible to have a simultaneous supply of LN₂ on both the transfer lines, and have all the systems running at the same moment.

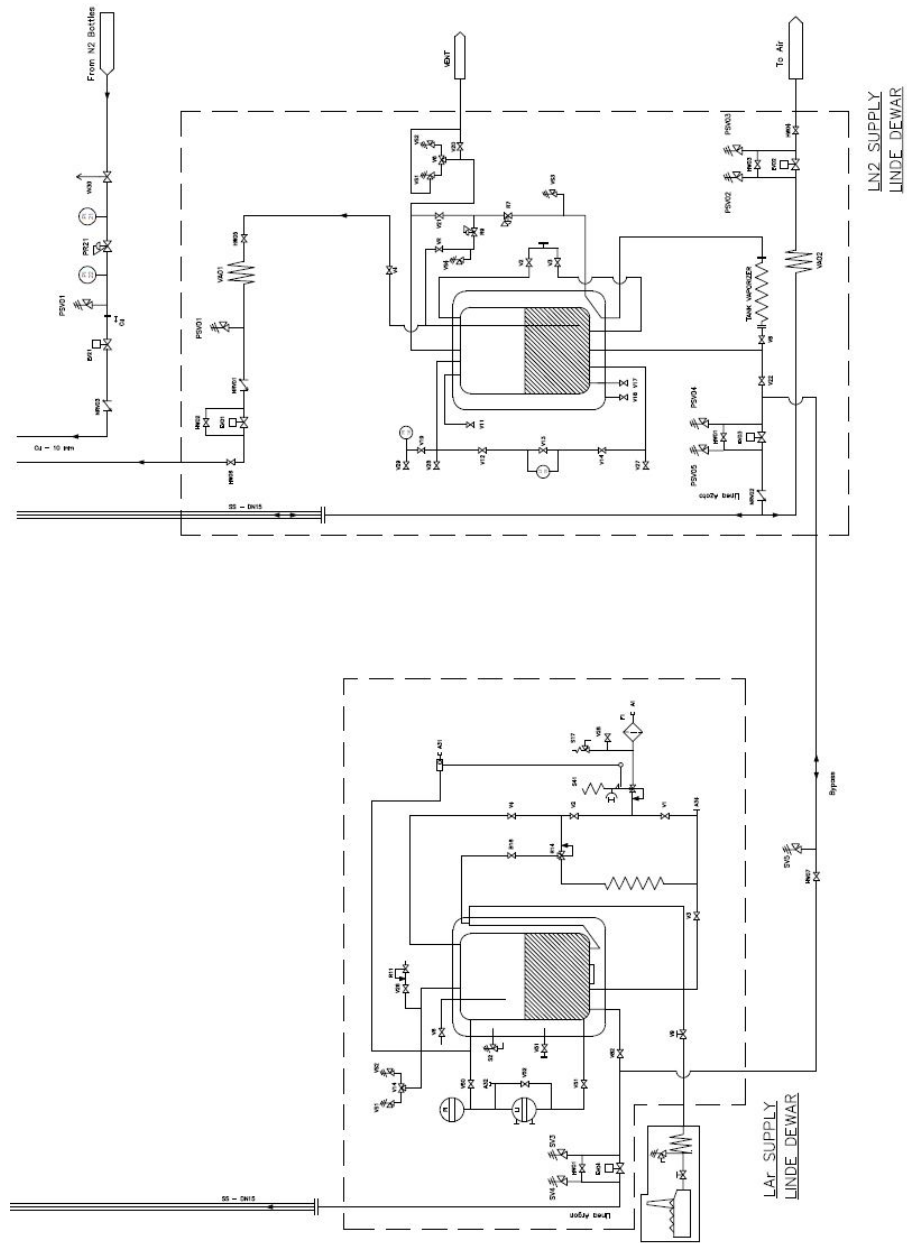


Figure 2.21: Pipe and Instrumentation Diagram (P&ID) of the Supply Tanks

3

PROTO-0 PROCESS ANALYSIS

In this chapter the process of the cryogenic system is shown and the analysis of the Ar liquefaction process in the condenser is performed both numerically and with a virtual simulation with the chemical process simulator software Aspen HYSYS.

The Proto-0 cryogenic system has the purpose to obtain liquid Ar to fill the cryostat where the TPC is installed. In addition the system has to maintain the LAr level constant liquefying the evaporated Ar due to the heat transfer through the non-insulated flange of the cryostat and the heat produced by the electronics components. During this process the Purification Getter filters the Ar gas to remove the impurities released by the elements in contact with the Ar. The key component of this system is the "Universal Condenser". The condenser, as discussed in subsection 2.1.2, is composed by two plate heat exchangers and a tube and shell heat exchanger.

The system can be splitted into the "Ar side" and the "N₂ side".

The Ar gas comes from a pressurized bottle connected to the gas panel. During the filling phase of the argon loop, the 6.0 Ar gas is injected in the system at room temperature until the pressure in the cryostat (PT2 fig.3.1) reaches a value of 1.4 bar. At this point the liquefaction process can start. The gas pump allows the gas to recirculate into the system, flowing through the getter, then in the condenser the liquefaction process takes place. The LAr flows directly into the cryostat through a double wall vacuum insulated transferline. During the cryostat filling phase the reduction of volume caused by the transformation of argon from gas state to liquid state requires the refill of Ar gas from the bottle in order to maintain a constant value of pressure into the Ar side of the system. Once the LAr desired level in the cryostat is reached, the system constantly recirculate the evaporated Ar, purifies it and liquefies it back, to ensure liquid level, Ar purity and pressure in the required ranges.

The N₂ path starts from the LN₂ supply tank, where up to 3300 liters of liquid nitrogen are stored. After the opening of the electric valve EV04 (fig.3.1) and of the by-pass valve HW07, the LN₂ flows into the condenser with a regulated flow rate due to the proportional inlet valve PV10. The LN₂ barrel gets constantly refilled during the normal operation state. At the bottom end of the LN₂ barrel there is the key component of the condenser: the "chicken feeder". The chicken feeder allows the passage of the liquid nitrogen from the N₂ barrel to the tube and shell heat exchanger. The flow rate is regulated by the variation of the evaporated nitrogen flow rate operated by the MFC. The Mass Flow Controller is the crucial component that allows us to regulate the amount of LN₂ that flows in the heat exchangers, and in this way sets the cooling power of the universal condenser.

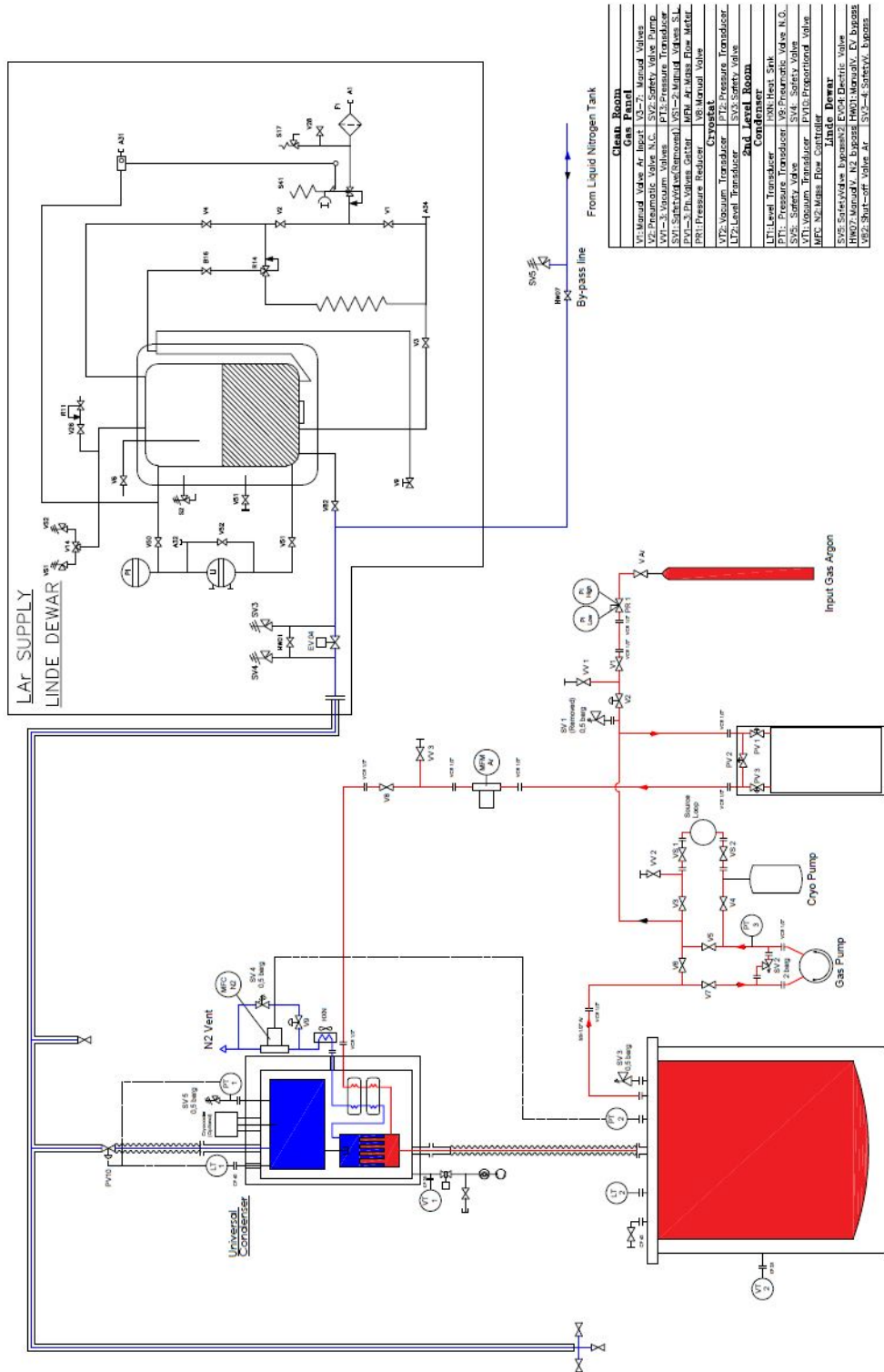


Figure 3.1: Proto-0 "loops" P&ID

This chapter is focused on the heat exchange process that takes place in the condenser. We can subdivide the heat exchange process in a "pre-cooling phase" and in the "liquefaction phase".

The **pre-cooling phase** takes place in the two commercial Kaori K50 plate heat exchangers. In these components the hot Ar gas gets pre-cooled exploiting

the remaining cooling power of the nitrogen coming from the tube and shell exchanger. The Ar gas gets cooled down as close as possible to the phase passage temperature of 88.9 K, ready to become liquid in the main heat exchanger.

The **liquefaction phase** takes place in the tube and shell heat exchanger where the liquid nitrogen, directly coming from the LN₂ barrel, fills the shell side, while the Ar gas coming from the plate heat exchangers flows in the tubes side. Here the argon liquefies exchanging the remaining sensible heat and the latent heat with the LN₂.

For the thermodynamic analyses performed in this chapter the following generic assumptions have been made:

1. One-dimensional flux regimen;
2. Steady-state regimen;
3. Negligible kinetic terms of the energy and exergy balances;
4. Negligible potential terms of the energy and exergy balances;
5. Thermodynamic equilibrium in the inlet and outlet sections of the heat exchanger;
6. Negligible thermal power released in the external environment;
7. No mechanical work in the heat exchanger;
8. Single inlet and single outlet systems (either hot fluid and cold fluid);
9. Internally reversible transformations (negligible internal friction, uniform pressure for both hot and cold fluids);
10. The enthalpy of the evolving fluids is a linear function only of the temperature, that is acceptable for:
 - Ideal gasses with constant specific heat coefficients ($c = c_p$);
 - Liquids with incompressible flux ($v = \text{const.}$), that means ($c = c_p = c_v$);
11. Constant specific heat coefficients;
12. Constant global heat exchange coefficient ($U = \text{const.}$)

In addition, the argon and nitrogen thermal and physical properties needed for the thermodynamic analyses are specified in the following table (tab.1).

The following numerical analysis is focused on the cryostat filling phase. We have assumed a system setting such that the Ar flow rate is 80 sL/m, that is compatible with the getter's maximum manageable flow rate (100 sL/m), and can result in an acceptable filling time. Starting from this assumption, the required N₂ flow rate is obtainable from a thermal balance restricted to the Ar. This way it is possible to evaluate the required cooling power to liquefy the previously established Ar flow rate. In an hypothetical simplified heat exchanger the heat that has to be transferred from the Ar to have the phase transition it is given by the following equation:

$$\dot{Q}_{Ar} = \dot{m}_{Ar}c_{p,Ar} (T_{Ar,amb} - T_{LAr}) + \dot{m}_{Ar}\lambda_{Ar} \quad (3.1)$$

Latent Heat N₂ [λ_{N_2}] (J/kg)	199000
Latent Heat Ar [λ_{Ar}] (J/kg)	161000
Specific heat at constant pressure [c_{p,N_2}] N₂ (J/kg · K)	1040
Specific heat at constant pressure [$c_{p,Ar}$] Ar (J/kg · K)	522
Density N₂ [ρ_{N_2}] (kg/m ³)	1.25
Density Ar [ρ_{Ar}] (kg/m ³)	1.78
Saturation liquid temperature N₂ (K)	77
Saturation liquid temperature Ar (K)	88.9
Viscosity N₂ (Pa · s)	0,0000165
Viscosity Ar (Pa · s)	0,0000229
Thermal conductivity N₂ (W/m · K)	0,02598
Thermal conductivity Ar (W/m · K)	0,0168

Table 1: Ar and N₂ thermal and physical properties

The first term of the sum is the sensible heat that is going to be transferred in the plate heat exchangers and in the tube and shell heat exchanger, while the second term is the latent heat that is going to be transferred during the phase change in the tube and shell heat exchanger.

Since we know that:

$$\dot{Q}_{Ar} = \dot{Q}_{N_2} = \dot{m}_{N_2} \lambda_{N_2} \quad (3.2)$$

we can calculate the required N₂ flow rate as it follow:

$$\dot{m}_{N_2} = \frac{\dot{Q}_{Ar}}{\lambda_{N_2}} = 0.0026 \text{ kg/s} = 125 \text{ sL/m} \quad (3.3)$$

3.1 PRE-COOLING PLATE HEAT EXCHANGERS

Kaori K50 brazed plate heat exchangers consists of 10 corrugated chevron plates. The plates produce an extremely large surface area, which greatly increases the speed of the temperature change. The reduced thickness of each chamber ensures that the majority of the volume of the fluid is in contact with the plate, aiding again the exchange. The grooves have also the purpose to create and maintain a turbulent flow in the fluid that maximizes the heat transfer. The plate heat exchangers are extremely effective when both hot and cold fluids are in gas phase. In fact, in that case the high exchange surfaces compensate for the low thermal exchange coefficients of the gasses.

In the analysis of the pre-cooling phase we have considered the two Kaori K-50 plate heat exchangers as a single counterflow heat exchanger with the same features but with an exchange surface equal to the sum of the two.

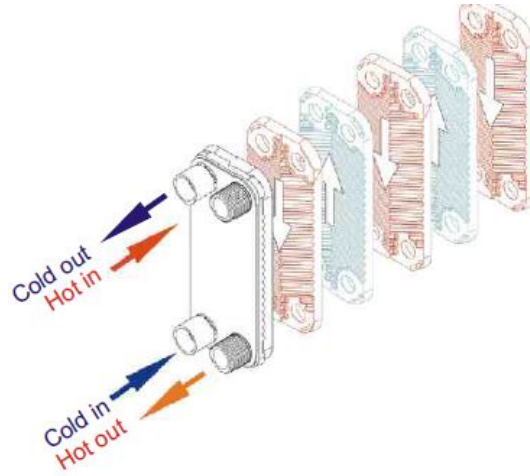


Figure 3.2: Kaori plate heat exchanger working principle

In the heat exchangers design and verification two main numerical methods are used: the **logarithmic mean temperature difference (LMTD)** and the **ϵ -NTU method**.

In this specific case, the missing information regarding the outlet temperature of both argon and nitrogen would have requested an iterative calculation with the LMTD method. Instead the **ϵ -NTU method** proves to be more convenient.

The efficiency (ϵ) - Number of Thermal Units (NTU) method is based on the dimensionless parameter ($0 < \epsilon < 1$) defined as the **heat exchanger efficiency** :

$$\epsilon = \frac{\dot{Q}}{\dot{Q}_{\max}} \quad (3.4)$$

Where \dot{Q} is the actual heat transfer rate and \dot{Q}_{\max} is the maximum possible heat transfer rate.

The actual heat transfer rate can be determined with an energy balance on either the cold or the hot fluid:

$$\dot{Q} = C_c (T_{c,o} - T_{c,i}) = C_h (T_{h,i} - T_{h,o}) \quad (3.5)$$

Where $C_c = \dot{m}_c c_{p,c}$ and $C_h = \dot{m}_h c_{p,h}$ are the heat capacity rates (mass flow rate multiplied by specific heat) for the cold and hot fluids respectively.

The maximum possible heat transfer rate is the value obtained by the fluid with the lowest heat capacity rate, that would undergo the maximum possible temperature change in this hypothetical infinite long exchanger (ΔT_{\max}).

$$\dot{Q}_{\max} = C_{\min} (T_{h,i} - T_{c,i}) = 276.9 \text{ W} \quad (3.6)$$

where C_{\min} is the smaller value between the heat capacity rates of the two fluids.

For any heat exchanger it can be shown that:

$$\epsilon = f \left(\text{NTU}, \frac{C_{\min}}{C_{\max}} \right) \quad (3.7)$$

The Number of Thermal Units (NTU) can be calculated with the following equation:

$$\text{NTU} = \frac{UA}{C_{\min}} \quad (3.8)$$

Where U is the overall heat transfer coefficient and A is the heat transfer area.

For thin wall pipes of high thermal conductivity, like in this case, the overall heat transfer coefficient can be calculated by:

$$\frac{1}{U} = \frac{1}{h_i} + \frac{1}{h_e} \quad (3.9)$$

where h_i and h_e are the internal and external convective heat transfer coefficients calculated with the following equation in both hot (Ar) and cold (N_2) fluid conditions:

$$h = \frac{\text{Nu} \cdot k}{L} \quad (3.10)$$

In the previous equation Nu is the Nusselt number, that is function of the Reynolds Re and Prandl Pr numbers.

The overall heat transfer coefficient for this plate heat exchanger is $U = 1.8 \frac{\text{W}}{\text{m}^2\text{K}}$.

The NTU is equal to $\text{NTU} = 0.66$.

Considering the exchanger as a counterflow heat exchanger, the efficiency can be calculated with:

$$\epsilon = \frac{1 - \exp(\text{NTU}(1 - c))}{1 - c \cdot \exp(-\text{NTU}(1 - c))} = 0.44 \quad (3.11)$$

where $c = \frac{C_{\min}}{C_{\max}}$.

At this point, with the already known maximum possible heat transfer rate, is possible to calculate the actual heat transfer rate:

$$\dot{Q} = \epsilon \cdot \dot{Q}_{\max} = 123.1 \text{ W} \quad (3.12)$$

By executing an energy balance limited to the argon side of the heat exchanger it is possible to obtain the Ar outlet temperature:

$$T_{\text{Ar,o}} = T_{\text{Ar,i}} - \frac{\dot{Q}}{m_{\text{Ar}}c_{p,\text{Ar}}} = 200.8 \text{ K} \quad (3.13)$$

3.2 TUBE AND SHELL CONDENSER

The next step is the analysis of the liquefaction process. This process takes place in the "tube and shell" heat exchanger. This is not a typical tube and shell heat exchanger, but for this analysis it has been treated if it was.

This heat exchanger is composed by a top "shell" side, where the liquid nitrogen flows through the chicken feeder and a bottom "tubes" side where the pre-heated gas argon flows to be liquefied (fig.3.3).



Figure 3.3: "Tube and shell" 3D model section

The shell side can be filled with a certain amount of LN_2 to have the desired cooling power. This is controlled by the MFC installed on the Universal Condenser's outlet line. The MFC can adjust the flow rate of the evaporated nitrogen that flows through all the heat exchangers and gets expelled. According to this flow rate, the pressure reduction in the N_2 side of the condenser allows the admission of a proportional amount of liquid nitrogen in the shell side.

At the same time the Ar gas flows into the exchangers with the selected flow rate.

The requested power to liquefy the selected Ar flow rate in the tube and shell heat exchanger can be obtained from the following equation, that is part of the

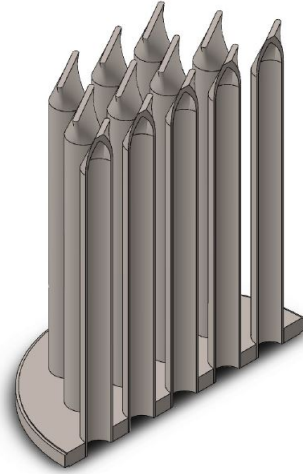


Figure 3.4: "Tube and shell" exchange surface 3D model

first thermal balance used to calculate the N_2 flow rate. This equation requires the knowledge of the Ar inlet temperature in the tube and shell exchanger $T_{Ar,i} = 200.8 \text{ K}$, that we achieved in the plate heat exchangers analysis performed in the previous section.

$$\dot{Q}_{req,Ar} = \dot{m}_{Ar} c_{p,Ar} (T_{Ar,i} - T_{LAr}) + \dot{m}_{Ar} \lambda_{Ar} = 520.7 \text{ W} \quad (3.14)$$

The assumption previously made to treat this heat exchanger as a tube and shell model is crucial to adopt the logarithmic mean temperature difference (LMTD) method for the exchanged power calculation.

The thermal power of an heat exchanger can be determined with a relation similar to the Newton's convection law:

$$\dot{Q} = U A \Delta T_{med} \quad (3.15)$$

Where as in the previous section U is the overall heat transfer coefficient and A is the heat transfer area. The temperature difference between the hot and cold fluids varies along the exchange surface, therefore it is useful to consider a mean value of the temperature difference.

The most used mean value of the temperature difference in heat exchanger's analysis is the logarithmic mean temperature difference, expressed by the following equation:

$$\Delta T_{ml} = \frac{\Delta T_1 - \Delta T_2}{\ln \left(\frac{\Delta T_1}{\Delta T_2} \right)} \quad (3.16)$$

where ΔT_1 and ΔT_2 are the temperature differences between the two fluids at the inlet and outlet sections of the heat exchanger.

A condenser can be treated either as a concurrent or a countercurrent flow heat exchanger.

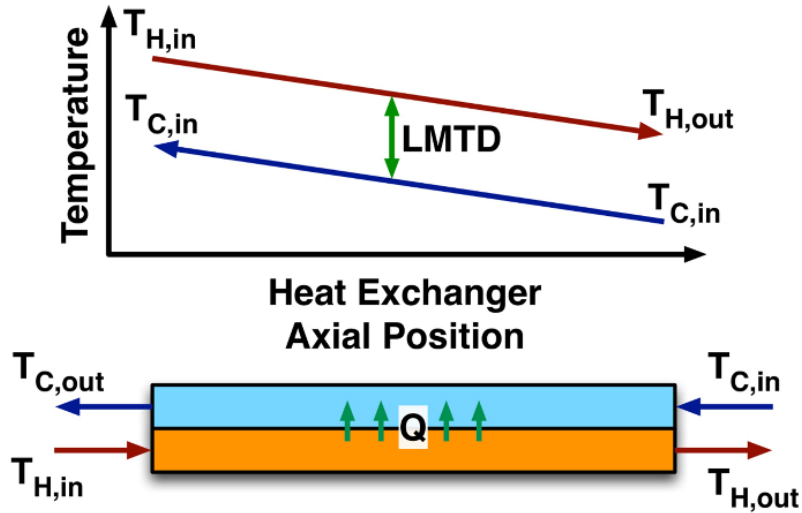


Figure 3.5: LMTD in counterflow heat exchanger

The previous equation is acceptable only for simple concurrent or countercurrent flow heat exchangers. For more complex heat exchangers, such as tube and shell models, a correction factor is needed:

$$\Delta T_{ml} = F \cdot \Delta T_{ml,cc} \quad (3.17)$$

The correction factor depends on the heat exchanger geometry and on its inlet and outlet fluids temperatures.

$\Delta T_{ml,cc}$ is the logarithmic mean temperature difference for a countercurrent flow heat exchanger with the same inlet and outlet conditions of the analyzed exchanger.

The correction factor for a condenser (phase change) is $F = 1$.

At this point it is possible to calculate the thermal power of the heat exchanger:

$$\dot{Q} = UA\Delta T_{ml} = 632 \text{ W} \quad (3.18)$$

That is more than the required power to liquefy out the desired Ar flow rate.

According to the previous calculation the time needed to liquefy the argon and fill all the 200 liters of the cryostat is of approximately 33.3 hours (1.39 days).

3.3 LN₂ CLOSED LOOP HYPOTHETICAL SETUP

An interesting exercise has been to analyze the case of a closed LN₂ loop of the Universal Condenser.

Basically the condenser would not receive a constant supply of liquid nitrogen from the external tank, but in the normal operation conditions, the evaporated nitrogen would be reintroduced into the LN₂ barrel where it would be liquefied thanks to a cryocooler.

In this analysis the Cryomech Gifford-McMahon AL600 Cryorefrigerator has been included (fig.3.6). This cryocooler can guarantee a cooling power up to 600 W.



Figure 3.6: Cryomech Gifford-McMahon AL600 cryocooler

In this scenario it is possible to calculate the maximum N₂ flow rate that the cryocooler can liquefy and it is possible to compare it with the previously calculated evaporation rate needed to liquefy the desired Ar flow rate.

$$\dot{m}_{N_2, \max} = \frac{\dot{Q}_{\text{Cryo}}}{\lambda_{N_2} + c_{p, N_2}(T_{N_2, i} - T_{N_2, o})} = 0.0024 \text{ kg/s} = 117 \text{ sl/m} \quad (3.19)$$

Where the inlet N₂ temperature $T_{N_2, i}$ is equal to the nitrogen temperature at the last plate heat exchanger.

To calculate the outlet temperature we can perform an energy balance limited to the nitrogen side of the heat exchanger, just like we did for the argon:

$$T_{N_2, o} = T_{N_2, i} + \frac{\dot{Q}}{\dot{m}_{N_2} c_{p, N_2}} = 122.4 \text{ K} \quad (3.20)$$

These results are reasonable, and a future upgrade of the system could be done. A system that does not require a constant refill of LN₂ would be much more efficient and cost-effective.

4

MECHANICAL ASSESSMENT OF THE UNIVERSAL CONDENSER

In this chapter we present the mechanical resistance verification of the Universal Condenser according to the CEN (Comité Européen de Normalisation) normative, and with the FEA Finite Element Analysis Software Ansys Mechanical.

This analysis was done following the EN 13445 and the EN 13458 standards.

EN 13445 is the European standard for the unfired pressure vessels, it provides rules for the design, fabrication, and inspection of pressure vessels with a maximum allowable pressure greater than 0,5 bar gauge but may be used for vessels operating at lower pressures, including vacuum.

EN 13458 standard is applicable to the design, fabrication, inspection and testing of static vacuum insulated cryogenic vessels designed for a maximum allowable pressure of more than 0,5 barg.

In this chapter only the EN 13445 standard is mentioned, due to the redundancy of some of the calculations required by the EN 13458 .

The EN 13445 standard concerning “Unfired pressure vessels” comprises the following Parts:

- **Part 1: General** - This part contains general information on the scope of the standard as well as terms, definitions, quantities, symbols and units which are applied throughout the standard.
- **Part 2: Materials** - This part deals with the general philosophy on materials, material grouping and low temperature behavior. It is limited to steel with sufficient ductility and, for components operating in the creep range, sufficient creep ductility. Part 2 also provides the general requirements for establishing technical delivery conditions and the requirements for marking the materials.
- **Part 3: Design** - This part of the standard gives the rules to be used for design and calculation under internal and/or external pressure (as applicable), local loads and actions other than pressure. The rules provided are both design by formulae (DBF), design by analysis (DBA) and design by experiment (DBE). The part also sets the requirements for fatigue analysis where needed and the rules to be followed when this is the case.
- **Part 4: Fabrication** - This part is based on existing good practice in previous national European Standards on manufacturing. It covers forming, welding procedures and welding qualification, production testing, and post weld heat treatment and repairs. Rules are also provided for material traceability and tolerances.
- **Part 5: Inspection and testing** - This part covers all those inspection and testing activities associated with the verification of the pressure vessel for

compliance with the standard, including design review by the manufacturer and supporting technical documentation, NDT and other inspection activities including document control, material traceability, joint preparation and welding. The level of testing is driven by the selection of the vessel testing group. Basically, the testing group determines the level of NDT and the joint coefficient used in the design.

- **Part 6: Requirements for the design and fabrication of pressure vessels and pressure parts constructed from spheroidal graphite cast iron** - This part contains special rules for material, design, fabrication, inspection, and testing of pressure vessels made from spheroidal graphite cast iron. In general the rules in parts 2–5 apply with additions and exceptions outlined in this part.
- **Part 7: Guidance on the use of conformity assessment procedures** - This part gives guidance on how to use the conformity assessment procedures in the Pressure Equipment Directive 97/23/EC. It is not a standard, but merely a CEN Technical Report.
- **Part 8: Additional requirements for pressure vessels of aluminium and aluminium alloys** - This part contains special rules for material, design, fabrication, inspection, and testing of pressure vessels made from aluminium and aluminium alloys. In general the rules in the relevant chapters of parts 2–5 apply with additions and exceptions outlined in this part.
- **Part 9: Compliance of EN 13445 series to ISO 16528** - This part details the conformance of the whole EN 13445 series to ISO 16528-1 "Boilers and pressure vessels — Part 1: Performance requirements". This is a CEN Technical Report.

In the following analysis, rules given in Part 3 - "Design" were applied.

4.1 UNIVERSAL CONDENSER DESIGN BY FORMULAE VERIFICATIONS BASED ON EN 13445

The Universal Condenser has been sub-divided, isolating its singular custom components. They have been individually analyzed in accordance with the code. The commercial components already certified by the producers, such as the Kaori K50 heat exchangers, have been ignored in the analysis.

The condenser's components that have been analyzed are:

- The N₂ barrel
- The heat exchanger shell
- The heat exchanger tubesheet and channels
- The external vessel
- The expansion bellow

The N₂ barrel and the the heat exchanger shell have been verified according to chapter 7 - "Shells under internal pressure" and chapter 10 - "Flat ends" rules.

The exchanger tubesheet and channels have been verified according to chapter 13 - "Heat Exchanger Tubesheets" rules.

The external vessel follows chapter 8 - "Shells under external pressure" regulations.

The expansion bellow has been verified according to chapter 14 - "Expansion bellows".

In chapter 5 the basic design criteria followed in the process are introduced, among which the following **classification of load cases** :

- **Normal operating load cases** - those acting on the pressure vessel during normal operation, including start-up and shutdown.
- **Exceptional load cases** - those corresponding to events of very low occurrence probability requiring the safe shutdown and inspection of the vessel or plant. Examples are pressure loading of secondary containment or internal explosion.
- **Testing load cases** - those corresponding to Testing load cases for final assessment related to tests after manufacture defined by EN 13445 – 5 : 2014 or Testing load cases in service related to repeated tests during the life time defined by the user.

For all the mentioned load cases the following calculation parameters are used:

- the calculation pressure P .
- the nominal design stresses f .
- the analysis thickness e_a
- the joint coefficient z

The calculation pressure P shall be based on the most severe condition of coincident differential pressure and temperature. It shall include the static and dynamic head where applicable, and shall be based on the maximum possible differential pressure in absolute value between the inside and outside of the vessel (or between the two adjacent chambers).

Vessels subject to external pressure shall be designed for the maximum differential pressure in absolute value to which the vessel may be subjected in service. Vessels subject to vacuum shall be designed for a full pressure of 0.1 MPa unless it can be shown that the amount of partial vacuum is limited, e.g. by a vacuum break valve or similar device, in which case a lower design pressure between 0.1 MPa and the set pressure of this safety device may be agreed.

The calculation temperature T shall not be less than the actual metal temperature expected in service or, where the through thickness temperature variation is known, the mean wall temperature. The calculation temperature shall include an adequate margin to cover uncertainties in temperature prediction. Where different metal temperatures can confidently be predicted for different parts of the vessel, the calculation temperature for any point in the vessel may be based on the predicted metal temperature.

Chapter 6 specifies maximum allowed values of the **nominal design stress** for pressure parts other than bolts and physical properties of steels.

For a specific component of a vessel, i.e. specific material, specific thickness, there are different values of the nominal design stress for the normal operating, testing, and exceptional load cases.

For exceptional load cases, a higher nominal design stress may be used. The manufacturer shall prescribe, in the instructions for use, an inspection of the vessel before returning it to service after occurrence of such an exceptional case.

The maximum values of the nominal design stress for normal operating and testing load cases shall be determined from the material properties with the appropriate safety factors as specified in clause 5.

For the tensile strength and the yield strength the values shall be those which apply to the materials in the final fabricated condition and shall conform to the minimum values of the technical documentation prepared in accordance with EN 13445 – 5 : 2014.

The Universal Condenser is entirely made of stainless steel AISI 304L. The EN 1.4306 is an austenitic stainless steel alloy with Chromium (Cr 18 – 20%), Nickel (Ni 10 – 12%) and a low Carbon content ($C \leq 0.030\%$). Its physical properties are specified in **Table 1** and its mechanical properties at the service temperature of 20°C are reported in **Table 2**.

The maximum allowed values of the nominal design stress for austenitic steels with a minimum rupture elongation from 35% is determined according to section 6.5.

For normal operating load cases the nominal design stress f shall not exceed f_d the greater of the two values:

- $f_d = \frac{R_{p1.0}}{1,5}$; or
- if a value of R_m is available, the smaller of two values:
 - the minimum tensile strength at calculation temperature, as given in the technical specification for the material, divided by the safety factor:

$$\left(f_d = \frac{R_m}{3} \right) \quad (4.1)$$

and

- the minimum 1% proof strength at calculation temperature, as given in the technical specification for the material divided by the safety factor:

$$\left(f_d = \frac{R_{p1.0}}{1,2} \right) \quad (4.2)$$

For testing load cases the nominal design stress f shall not exceed f_{test} the greater of the two values:

- $f_d = \frac{R_{p1.0}}{1,05}$; or
- $f_d = \frac{R_m}{2}$.

Because the condenser is not certified to operate at pressure values of more than 0.5 barg according to PED (Pressure Equipment Directive), the joint coefficient adopted was the least conservative: $z = 1$.

Density (g/cm ³)	7.9
Specific heat capacity (J/kg K)	500
Thermal conductivity (W/m K)	15

Table 2: AISI 304L physical properties at 20°C

Hardness (HB)	HB30	≤ 215
0,2% Yield strength (MPa)	R _{p0,2}	≥ 200
1,0% Yield strength (MPa)	R _{p1,0}	≥ 235
Tensile strength (MPa)	R _m	460 – 480
Elongation (%)	-	≥ 35 – 45
Young modulus (GPa)	E	200

Table 3: AISI 304L mechanical properties at 20°C

4.1.1 Shells Under Internal Pressure

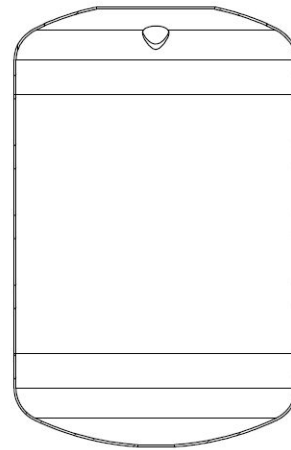
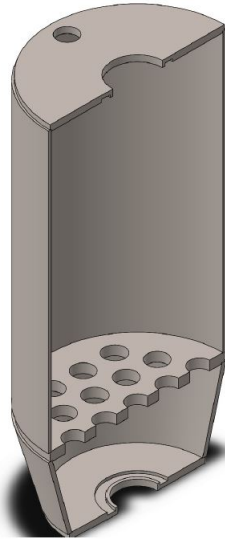
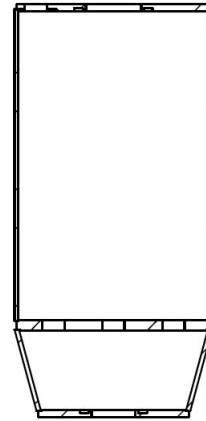
Chapter 7 provides the requirements for design against internal pressure of axisymmetric shells - cylinders, spheres, dished ends and cones.

The condenser components under internal pressure that have been analyzed according to chapter 7 are the N₂ **barrel** and the **heat exchanger** shell visible in Figure 4.1 .

For **cylindrical shells** the required thickness shall be calculated from one of the following equations:

$$e = \frac{P \cdot D_i}{2f \cdot z - P} \quad (4.3)$$

or

(a) *N₂ barrel 3D model*(b) *N₂ barrel CAD drawing*(c) *Heat exchanger shell 3D model*(d) *Heat exchanger shell CAD drawing***Figure 4.1:** N₂ barrel and heat exchanger shell

$$e = \frac{P \cdot D_e}{2f \cdot z + P} \quad (4.4)$$

For a given geometry:

$$P_{\max} = \frac{4f \cdot z \cdot e_a}{D_m} \quad (4.5)$$

Where e_a is the analysis thickness, f is the nominal design stress and D_i and D_e are the internal and external diameter.

The top and the bottom dished ends of the N₂ barrel are Kloepper type torispherical ends for which $R/D_e = 1.0$ and $r/D_e = 0.1$. Where R is the inside spherical radius of the central part of torispherical end and r is the inside radius of curvature of a knuckle.

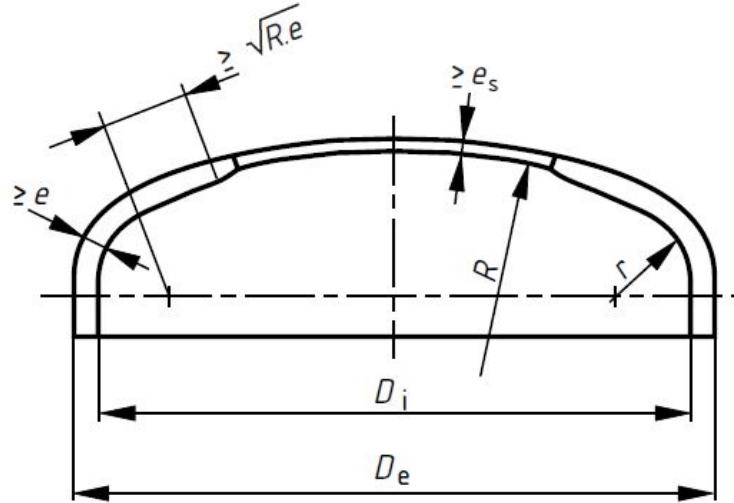


Figure 4.2: Geometry of torispherical end

For the **torispherical ends** the required thickness e shall be the greatest of:

$$e_s = \frac{P \cdot R}{2f \cdot z - 0.5P} \quad (4.6)$$

$$e_y = \frac{\beta \cdot P(0.75R + 0.2D_i)}{f} \quad (4.7)$$

$$e_b = (0.75R + 0.2D_i) \left[\frac{P}{111f_b} \left(\frac{D_i}{r} \right)^{0.825} \right] \left(\frac{1}{1.5} \right) \quad (4.8)$$

where β is found from figure 4.3 and $f_b = \frac{R_{p0.2}}{1.5}$

For a given geometry P_{\max} shall be the least of:

$$P_s = \frac{2f \cdot z \cdot e_a}{R + 0.5e_a} \quad (4.9)$$

$$P_y = \frac{f \cdot e_a}{\beta(0.75R + 0.2D_i)} \quad (4.10)$$

$$P_b = 111f_b \left(\frac{e_a}{0.75R + 0.2D_i} \right)^{1.5} \left(\frac{r}{D_i} \right)^{0.825} \quad (4.11)$$

where β is not the same parameter used in the thickness calculation, and can be found from figure 4.4.

For the cylindrical shell of the N_2 barrel $P_{\max} = 2.32$ MPa, while for the torispherical ends $P_{\max} = 1.65$ MPa. The maximum service pressure is set to 0.15 MPa by the safety relief valve. This value is far below the maximum allowable internal pressure obtained with the previous calculations.

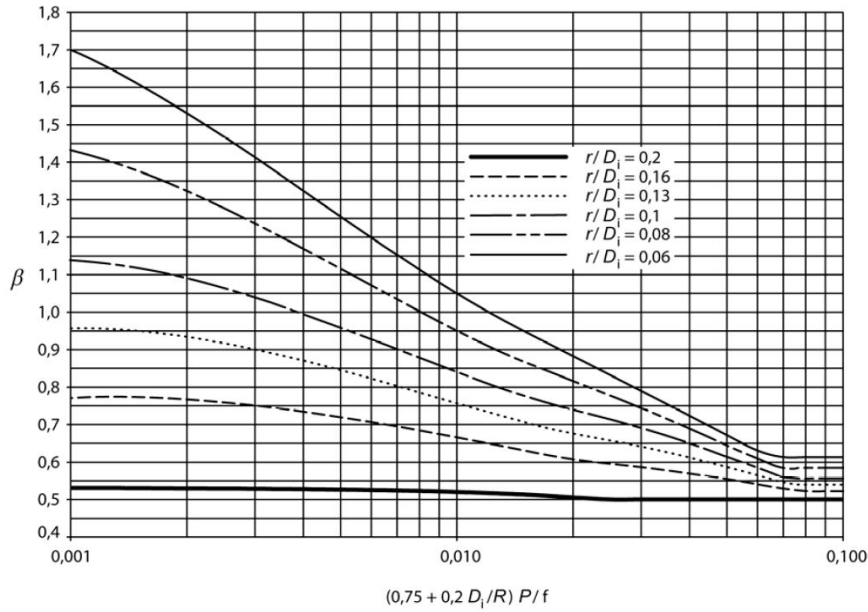


Figure 4.3: Parameter β for torispherical end - Design

Concerning the **heat exchanger shell**, the conical shell and the pierced flat ends have to be considered.

The required thickness at any point along the length of a cone shall be calculated from one of the following two equations:

$$e_{\text{con}} = \frac{P \cdot D_i}{2f \cdot z - P} \cdot \frac{1}{\cos(\alpha)} \quad (4.12)$$

or

$$e_{\text{con}} = \frac{P \cdot D_e}{2f \cdot z + P} \cdot \frac{1}{\cos(\alpha)} \quad (4.13)$$

For a given geometry:

$$P_{\text{max}} = \frac{2f \cdot z \cdot e_a \cdot \cos(\alpha)}{D_m} \quad (4.14)$$

D_i , D_e and D_m are the internal, external and mean diameter at the point under consideration, and α is the semi angle of cone at apex.

Chapter 10 of the code deals with the **pierced flat ends**. This clause specifies methods to determine the thickness of circular and non-circular unstayed flat ends under pressure.

The thickness of a pierced circular flat end welded to the shell shall not be less than:

$$e = \max \left\{ (Y_1 \cdot e_o); \left(C_1 \cdot Y_2 \cdot D_i \sqrt{\frac{P}{f}} \right) \right\} \quad (4.15)$$

where

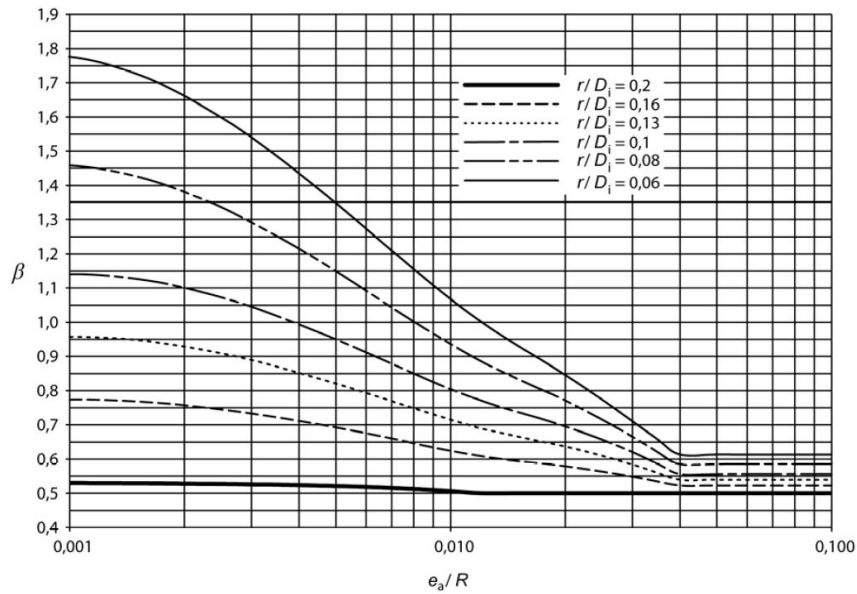


Figure 4.4: Parameter β for torispherical end - Rating

$$e_o = \max \left\{ \left(C_1 \cdot D_i \sqrt{\frac{P}{f}} \right); \left(C_2 \cdot D_i \sqrt{\frac{P}{f_{\min}}} \right) \right\} \quad (4.16)$$

is the required thickness of the unpierced flat end, C_1 and C_2 are the shape factors for calculation of circular flat ends, and Y_1 and Y_2 are the calculation coefficients for opening reinforcement.

For the **cylindrical shell** of the heat exchanger $P_{\max} = 5.58$ MPa, while for the conical shell $P_{\max} = 7.26$ MPa. Both the values are much higher with respect to the maximum service pressure.

The shell thickness value is much higher with respect to the minimum required thickness for **the pierced flat ends** of $e = 1.48$ mm for the top end and $e = 1.11$ mm for the bottom one.

4.1.2 Shells Under External Pressure

Chapter 8 provides requirements for the design of shells under external pressure loading. They apply to stiffened and unstiffened cylinders and cones, spheres and dished ends.

The only part of the universal condenser under an external pressure load is the external vessel. In figure 4.5 there is the external vessel 3D model and its section.

For shells made with austenitic steel, the nominal elastic limit shall be given by:

$$\sigma_e = \frac{R_{p0.2}}{1.25} \quad (4.17)$$

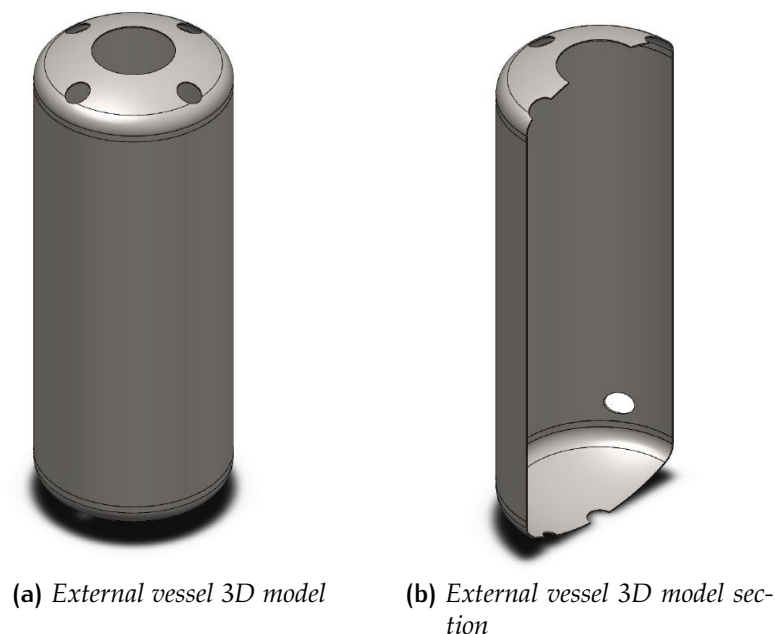


Figure 4.5: Universal condenser's external vessel

The nominal elastic limit value is $\sigma_e = 160$ MPa while the minimum safety factor which applies throughout this clause is $S = 1.5$ for design conditions and $S = 1.1$ for testing conditions.

The **cylindrical shell** part of the vessel falls into the category of the unstiffened cylinders with heads. The Unsupported length $L = 749$ mm in figure 4.6 is given by:

$$L = L_{\text{cyl}} + 0.4h' + 0.4h'' \quad (4.18)$$

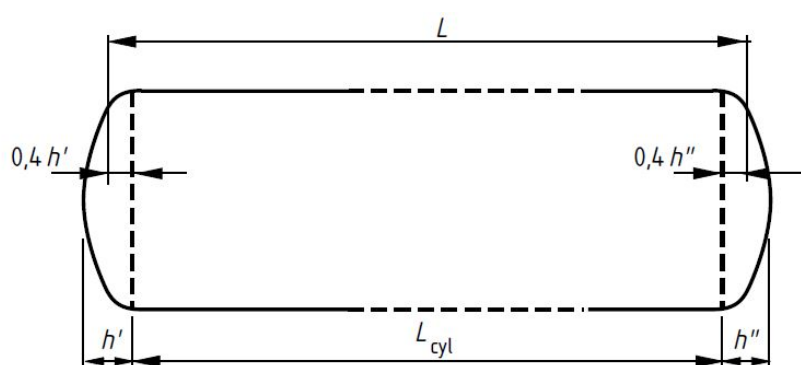


Figure 4.6: Cylinder with heads

The thickness of a cylinder shall not be less than that determined by the following procedure:

1. Select a value for e_a and calculate P_y as follows;

$$P_y = \frac{\sigma_e \cdot e_a}{R} \quad (4.19)$$

2. Calculate P_m from the following equation using the same assumed value for e_a :

$$P_m = \frac{E \cdot e_a \cdot \varepsilon}{R} \quad (4.20)$$

where E is the value of the modulus of elasticity at the calculation temperature, R is the mean radius of the cylindrical shell and ε is the mean elastic circumferential strain at collapse.

The parameter ε is obtained from figure 4.7 chart.

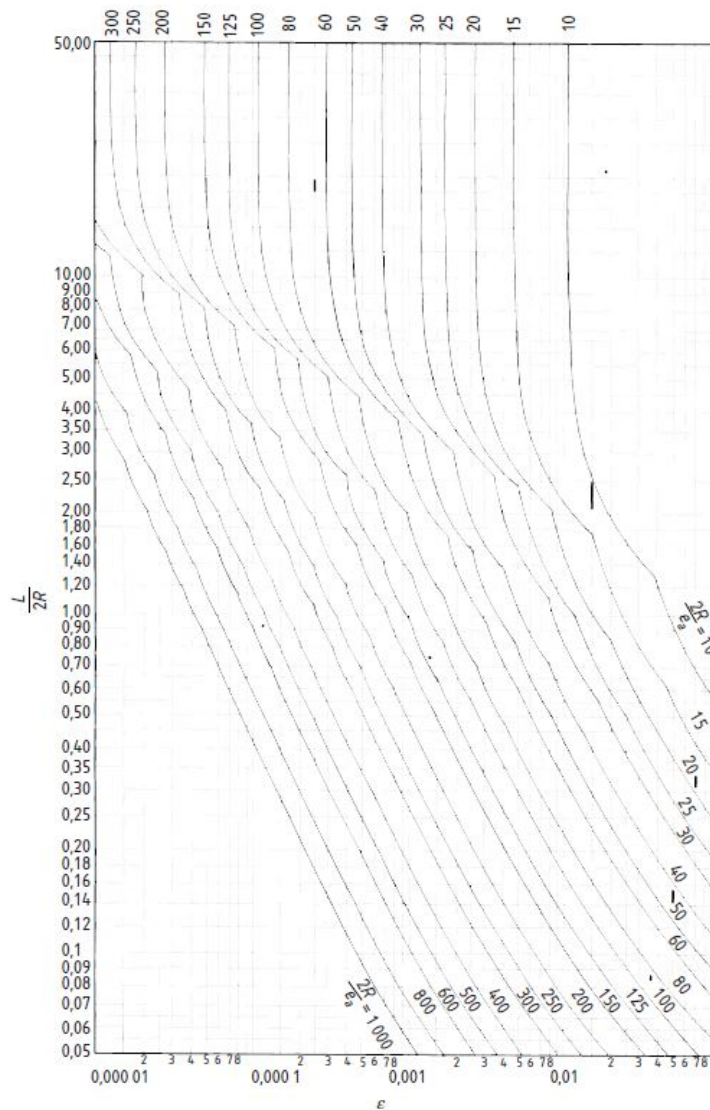


Figure 4.7: Values of ε

3. Calculate $\frac{P_m}{P_y}$ and determine $\frac{P_r}{P_y}$ from curve 1 in figure 4.8.

The following shall be satisfied:

$$P \leq P_r/S \quad (4.21)$$

Where P is the required external design pressure that in this case is equal to the atmospheric pressure, P_m is the theoretical elastic instability pressure for collapse of a perfect cylindrical shell, P_y is the pressure at which mean circumferential stress in a cylindrical shell reaches yield point, P_r is the calculated lower bound collapse pressure and S is the safety factor applied in this clause.

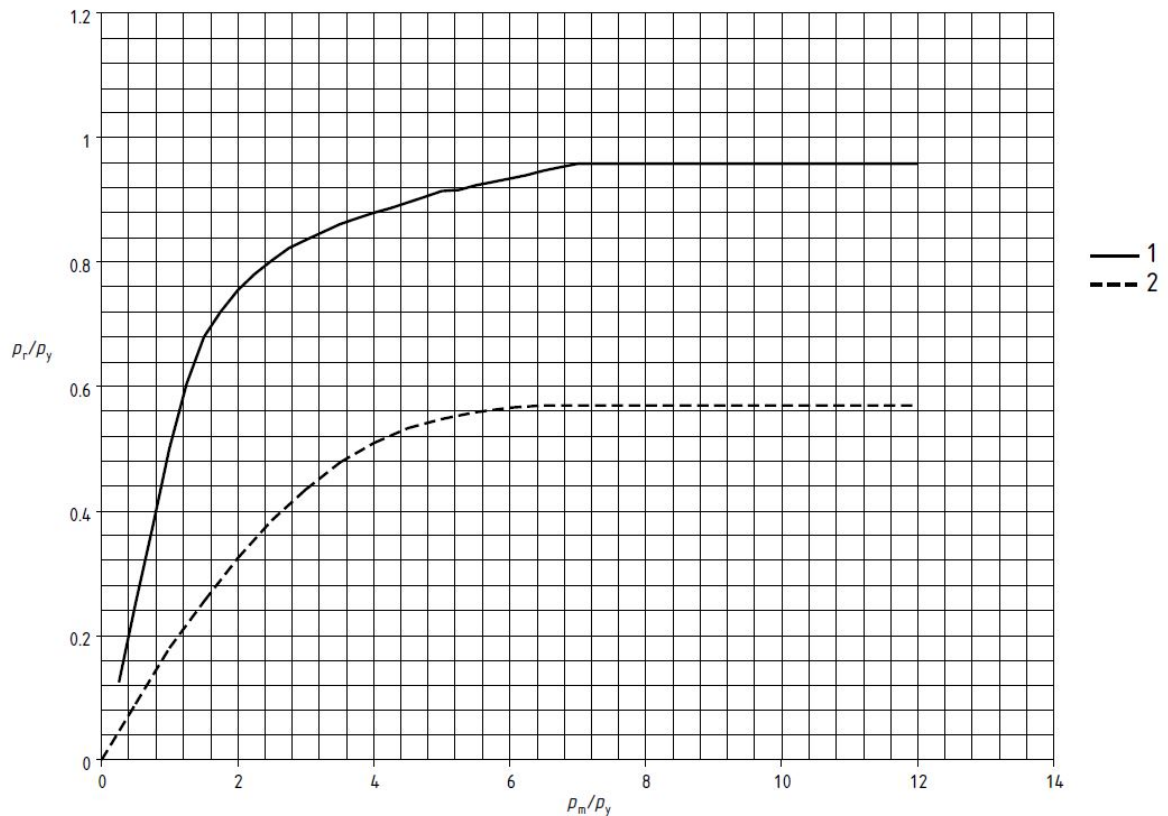


Figure 4.8: Values of $\frac{P_r}{P_y}$ versus $\frac{P_m}{P_y}$

In this case the actual thickness is more than the required thickness as proven by the value of $P_r/S = 0.27$ MPa that is higher than the external pressure loading $P_{atm} = 0.1$ MPa.

The vessel has two **torispherical ends**. Torispherical ends shall be designed as spherical shells of mean radius R equal to the external dishing or crown radius.

The design thickness shall be determined by the following procedure:

1. Assume a value for e_a and calculate:

$$P_y = \frac{2\sigma_e \cdot e_a}{R} \quad (4.22)$$

2. calculate P_m as follows:

$$P_m = \frac{1,21E \cdot e_a^2}{R^2} \quad (4.23)$$

3. Calculate $\frac{P_m}{P_y}$ and determine $\frac{P_r}{P_y}$ from curve 2 in figure 4.8.

$$P \leq P_r/S = 1.61 \text{ MPa} \quad (4.24)$$

That results verified.

4.1.3 Heat exchanger tubesheet and channels

Chapter 13 provides rules for tubesheet heat exchangers based on the classical elastic theory of thin shells. This clause foresees a distinction of tubesheet heat exchangers in the three following types:

- U-tube tubesheet heat exchangers;
- Fixed tubesheet heat exchangers;
- Floating tubesheet heat exchangers.

The Universal condenser tubesheet heat exchanger falls into the category of the U-tube tubesheet heat exchangers with a configuration where the tubesheet is integral with shell and channel.

This analysis has some conditions of applicability:

- The tubesheet shall be flat, circular and of uniform thickness;
- The tubesheet shall be uniformly perforated over a nominally circular area of diameter D_o , in either equilateral triangular or square pattern;
- The tubes shall be of uniform nominal thickness and diameter over their straight length, and same material;
- The tubes shall be rigidly attached to the tubesheet;
- Shell and channel shall be cylindrical at their junction to the tubesheet;
- Tube-side pressure P_t and shell-side pressure P_s are assumed to be uniform in each circuit;
- Other loadings, such as weight or pressure drop, are not considered.

It should be noted that the following calculations are made considering the two worst loading cases that can occur in service:

- **CASE A:** the tube-side (Ar side) pressure P_t is equal to the atmospheric pressure, while the shell-side (N_2 side) pressure value is $P_s = 1.5$ bar, the maximum allowed value.
- **CASE B:** the tube-side (Ar side) pressure is equal to the maximum allowed value $P_t = 1.5$ bar, while the shell-side (N_2 side) pressure value is $P_s = 1$ bar, atmospheric pressure.

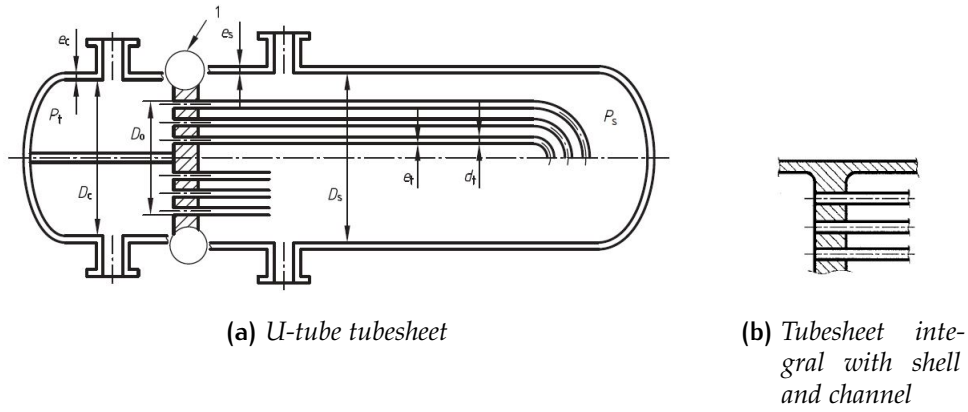


Figure 4.9: Typical U-tube tubesheet heat exchanger

The analysis procedure requires the determination of some intermediate coefficients:

1. The effective elastic constants of tubesheet: μ^* (the effective ligament efficiency), E^* (the effective elastic modulus), ν^* (the Poisson's ratio);
2. The moment M_{TS} due to pressures P_s and P_t acting on the unperforated tubesheet rim:

$$M_{TS} = \frac{D_o^2}{16} \left[(\rho_s - 1)(\rho_s^2 + 1)P_s - (\rho_c - 1)(\rho_c^2 + 1)P_t \right] \quad (4.25)$$

where ρ_s and ρ_c are the diameter ratios for shell and channel;

3. The integral shell and/or channel coefficients and moments M_{P_s} and/or M_{P_c} acting on the tubesheet, due to pressure in the integral shell and/or channel:

$$M_{P_s} = \rho_s k_s \beta_s (1 + e \beta_s) P'_s \quad (4.26)$$

$$M_{P_c} = \rho_c k_c \beta_c (1 + e \beta_c) P'_t \quad (4.27)$$

where k_s and k_c are the edge moments per unit length required to rotate respectively the shell and the channel edge through unit angle, and β_s and β_c are two coefficients based on the diameters, thickness and Poisson's ratios of the shell and channel.

4. The diameter ratio $K = \frac{A}{D_o}$ for tubesheet and coefficient

$$F = \frac{1 - \nu^*}{E^*} (\lambda_s + \lambda_c + E \ln K) \quad (4.28)$$

At this point it is possible to proceed with the analysis of the heat exchanger tubesheet, shell and channel.

The first step is the **evaluation of the maximum radial bending stress and shear stress in the tubesheet.**

The procedure in the first place involves the determination of the maximum bending moments in the **tubesheet**:

- Moment M^* acting on the unperforated tubesheet rim:

$$M^* = M_{TS} + M_{Pc} - M_{Ps} \quad (4.29)$$

- Moment M_p acting at periphery of tubesheet:

$$M_p = \frac{M^* - \frac{D_o^2}{32} F (P_s - P_t)}{1 + F} \quad (4.30)$$

- Moment M_0 acting at center of tubesheet:

$$M_0 = M_p + \frac{D_o^2}{64} (3 + \nu^*) (P_s - P_t) \quad (4.31)$$

Then we can obtain the **maximum bending moment acting on the tubesheet**:

$$M = \max (|M_p|; |M_0|) \quad (4.32)$$

All of these calculations lead to the evaluation of the **maximum radial bending stress in tubesheet**:

$$\sigma = \frac{6M}{\mu^* (e - h'_g)^2} \quad (4.33)$$

and of the **maximum shear stress in the tubesheet**:

$$\tau = \left(\frac{1}{4\mu} \right) \left(\frac{D_o}{e} \right) |P_s - P_t| \quad (4.34)$$

For each of the loading cases considered, the bending tubesheet stress σ shall not exceed $2f$, while the shear tubesheet stress τ shall not exceed $0.8f$. For the universal condenser this is true in both **CASE A** and **CASE B**:

CASE A

$$\sigma = 5.13 \text{MPa} \leq 2f = 313.33 \text{MPa} \quad (4.35)$$

$$\tau = 0.54 \text{MPa} \leq 0,8f = 125.33 \text{MPa} \quad (4.36)$$

CASE B

$$\sigma = 9.67 \text{MPa} \leq 2f = 313.33 \text{MPa} \quad (4.37)$$

$$\tau = -0.54 \text{MPa} \leq 0.8f = 125.33 \text{MPa} \quad (4.38)$$

The last step of the analysis is the **check of the shell and channel equivalent stresses**.

The equivalent stress in the **shell**, at its junction to the tubesheet, is given by:

$$\sigma_{s,eq} = \max [|\sigma_{s,m} - \sigma_{s,b} + P_s|; |\sigma_{s,m} + \sigma_{s,b}|] \quad (4.39)$$

where $\sigma_{s,m}$ is the axial membrane stress and is given by:

$$\sigma_{s,m} = \frac{D_s^2}{4e_s(D_s + e_s)} P_s \quad (4.40)$$

and $\sigma_{s,b}$ is the axial bending stress that is given by:

$$\sigma_{s,b} = \frac{6}{e_s^2} k_s \left[\beta_s P'_s + 3 \frac{1 - \nu^*}{E^*} \frac{D_o}{e^2} \left(\beta_s + \frac{2}{e} \right) \left(M_p + \frac{D_o^2}{32} (P_s - P_t) \right) \right] \quad (4.41)$$

For each of the normal operating loading cases the following statement must be true:

$$\sigma_{s,eq} \leq 1.5f_s \quad (4.42)$$

This is true for both **CASE A** and **CASE B**:

CASE A

$$\sigma_{s,eq} = 16.05 \text{MPa} \leq 1.5f_s = 235 \text{MPa} \quad (4.43)$$

CASE B

$$\sigma_{s,eq} = 10.95 \text{MPa} \leq 1.5f_s = 235 \text{MPa} \quad (4.44)$$

Finally the equivalent stress in the **channel**, at its junction to the tubesheet, is given by:

$$\sigma_{c,eq} = \max [|\sigma_{c,m} - \sigma_{c,b} + P_t|; |\sigma_{s,c} + \sigma_{c,b}|] \quad (4.45)$$

where $\sigma_{c,m}$ is the axial membrane stress and is given by:

$$\sigma_{c,m} = \frac{D_c^2}{4e_c(D_c + e_c)} P_t \quad (4.46)$$

and $\sigma_{c,b}$ is the axial bending stress that is given by:

$$\sigma_{c,b} = \frac{6}{e_c^2} k_c \left[\beta_c P'_t + 3 \frac{1 - \nu^*}{E^*} \frac{D_o}{e^2} \left(\beta_c + \frac{2}{e} \right) \left(M_p + \frac{D_o^2}{32} (P_s - P_t) \right) \right] \quad (4.47)$$

For each of the normal operating loading cases also this must be true:

$$\sigma_{c,eq} \leq 1.5f_c \quad (4.48)$$

For both **CASE A** and **CASE B** this happens to be true:

CASE A

$$\sigma_{c,eq} = 4.39 \text{MPa} \leq 1.5f_c = 235 \text{MPa} \quad (4.49)$$

CASE B

$$\sigma_{c,eq} = 6.55\text{MPa} \leq 1.5f_c = 235\text{MPa} \quad (4.50)$$

4.1.4 Expansion Bellow

This section is dedicated to the expansion bellow analysis. The chapter 14 of the EN 13445 – 3 : 2014 provides design rules for expansion bellows, consisting of a single or multiple convolutions, of three types:

- unreinforced U-shaped bellows
- reinforced U-shaped bellows
- toroidal bellows

subject to internal or external pressure and cyclic displacement.

On the universal condenser an unreinforced U-shaped bellow is installed (see figure 4.10), with the purpose of providing adequate flexibility for thermal expansion, whilst ensuring a safe design against internal pressure.

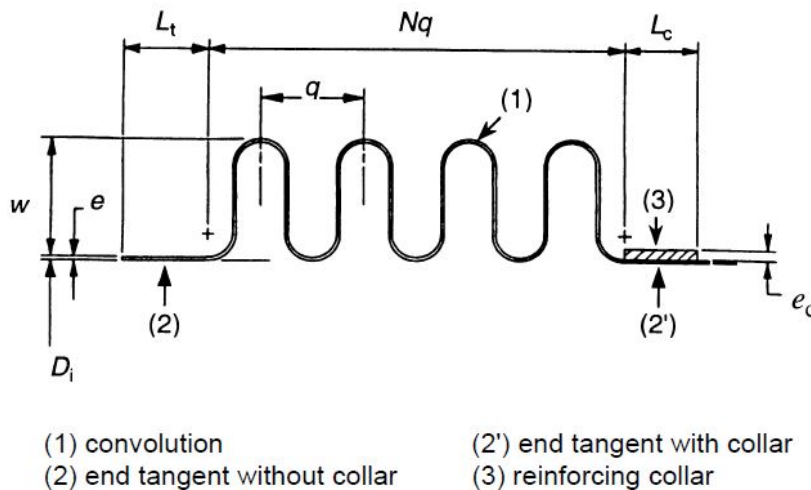


Figure 4.10: Unreinforced U-shaped bellow

An expansion bellows comprises one or more identical axisymmetric convolutions. Each convolution may have one or more plies of equal thickness and made of same material.

The bellow to analyze is subject to internal pressure only. The first step of the analysis is the **determination of strain caused by deformation**.

The maximum true strain caused by deformation for bellows is given by:

$$s_d = 1,04\sqrt{s_\theta^2 + s_b^2} \quad (4.51)$$

Where the circumferential true strain caused by deformation s_θ depends on the forming process. In this case the bellow is produced via an hydraulic forming process, and the following formula shall be used:

$$s_{\theta} = \ln \left(1 + 2 \frac{w}{D_i} \right) \quad (4.52)$$

while the bending component of the true strain caused by deformation s_b is independent of the forming process and given by:

$$s_b = \ln \left[1 + \frac{e_p}{2r_i + e_p} \right] \quad (4.53)$$

D_i is the inside diameter of bellows convolution and end tangents, e_p is the nominal thickness of one ply, r_i is the internal radius of torus at the crest and root of U-shaped convolutions and w is the convolution height.

Then it's possible to calculate the **stresses due to internal pressure** in the different sections of the bellow:

END TANGENT the circumferential membrane stress due to pressure is:

$$\sigma_{\theta,t}(P) = \frac{1}{2} \frac{(D_i + e)^2 \cdot L_t \cdot E_b \cdot k}{e \cdot (D_i + e) \cdot L_t \cdot E_b + e_c \cdot D_c \cdot L_c \cdot E_c \cdot k} \cdot P \quad (4.54)$$

where e is the bellows nominal thickness that for single ply bellows is equal to e_p , e_c is the collar thickness, D_c is the mean diameter of collar, L_c is the collar length, L_t is the end tangent length, E_b is the modulus of elasticity of bellows material at design temperature, E_c is the modulus of elasticity of collar material at design temperature, k is the factor considering the stiffening effect of the attachment weld and the end convolution on the pressure capacity of the end tangent and P is the calculation pressure.

According to the calculations the circumferential membrane stress due to pressure value is in the allowed range:

$$\sigma_{\theta,t}(P) = 1.31 \text{MPa} \leq f = 156.67 \text{MPa} \quad (4.55)$$

COLLAR the circumferential membrane stress due to pressure in this point is:

$$\sigma_{\theta,c}(P) = \frac{1}{2} \frac{D_c^2 \cdot L_t \cdot E_c \cdot k}{e \cdot (D_i + e) \cdot L_t \cdot E_b + e_c \cdot D_c \cdot L_c \cdot E_c \cdot k} \cdot P \quad (4.56)$$

Also this value results to be in the safe range:

$$\sigma_{\theta,c}(P) = 1.53 \text{MPa} \leq f = 156.67 \text{MPa} \quad (4.57)$$

BELLOWS CONVOLUTIONS for this part of the bellow there is more than one stress to evaluate:

- **The circumferential membrane stress due to pressure**

- For end convolutions:

$$\sigma_{\theta,E}(P) = \frac{1}{2} \cdot \frac{q \cdot D_m \cdot + L_t(D_i + e)}{A + e^* \cdot L_t} \cdot P \quad (4.58)$$

which shall comply with:

$$\sigma_{\theta,E}(P) = 1.73\text{MPa} \leq f = 156.67\text{MPa} \quad (4.59)$$

– For intermediate convolutions:

$$\sigma_{\theta,I}(P) = \frac{1}{2} \cdot \frac{q \cdot D_m}{A} \cdot P \quad (4.60)$$

that shall satisfy:

$$\sigma_{\theta,I}(P) = 0.72\text{MPa} \leq f = 156.67\text{MPa} \quad (4.61)$$

- **The meridional membrane stress due to pressure:**

$$\sigma_{m,m}(P) = \frac{w}{2e^*} \cdot P \quad (4.62)$$

- **The meridional bending stress due to pressure:**

$$\sigma_{m,b}(P) = \frac{1}{2n_p} \cdot \left(\frac{w}{e_p^*} \right) \cdot C_p \cdot P \quad (4.63)$$

These two have to fulfill:

$$\sigma_{m,m}(P) + \sigma_{m,b}(P) = 6,53\text{MPa} \leq K_f \cdot f = 470\text{MPa} \quad (4.64)$$

where $K_f = 3$ for as-formed bellows (with cold work).

Finally chapter 14 deals with the **column instability** and the **in-plane instability** due to internal pressure.

COLUMN INSTABILITY The allowable internal design pressure to avoid column instability, $P_{s,c}$, is given by:

$$P_{s,c} = 0.34 \frac{\pi K_b}{Nq} \quad (4.65)$$

where K_b is the bellows axial rigidity, N is the number of convolutions and q is the convolution pitch.

The internal pressure P shall not exceed $P_{s,c}$:

$$P = 0.15\text{MPa} \leq P_{s,c} = 6.72\text{MPa} \quad (4.66)$$

IN-PLANE INSTABILITY The allowable internal design pressure to avoid in-plane instability, $P_{s,i}$, is given by:

$$P_{s,i} = (\pi - 2) \frac{AR_e^*}{D_m q \sqrt{\alpha}} \quad (4.67)$$

where A is the cross sectional metal area of one convolution, α is the in-plane instability stress interaction factor and R_e^* effective proof stress at design temperature of bellows material.

Also in this case the internal pressure P shall not exceed $P_{s,i}$:

$$P = 0.15MPa \leq P_{s,i} = 10.54MPa \quad (4.68)$$

4.2 UNIVERSAL CONDENSER FEA ANALYSIS

This section is dedicated to the Finite Element Analysis (FEA) of the Universal condenser performed with Ansys Mechanical.

The Finite Element Analysis (FEA) is the simulation of any given physical phenomenon using the numerical technique called Finite Element Method (FEM).

FEM is a numerical method to solve a boundary value problem with a system of partial differential equations in two or three space variables that models the entire problem. These partial differential equations (PDEs) need to be solved in order to compute relevant quantities of a structure (like stresses, strains, etc.) and estimate the structural behavior under a given load.

Ansys Mechanical was the tool used for the Universal Condenser analysis. Ansys Mechanical software is a comprehensive FEA tool for structural analysis, including linear, nonlinear and dynamic studies.

The first step of this analysis was the creation of a simplified model of the Universal condenser using SpaceClaim, the Ansys's built-in 3D modeler.

The 3D model was imported from SolidWorks and then adjusted on SpaceClaim. As visible in figure 4.11 only the principal custom components were left, as in the previous normative analysis.

Then each element of the geometry was converted into a midsurface, and the material with its physical and mechanical properties was assigned to each of them. Creating a mid-surface shell model is possible thanks to the thin-walled geometry model starting point. Working with a mid-surface shell model creates fast running accurate simulations that pays off for the effort.

A crucial part of the preparation to the analysis is the connections definition and setting. Connections include contact regions, joints, springs, or beams. Contact conditions are formed where bodies meet. When an assembly is imported from a CAD system, contact between various parts is automatically detected. The differences in the contact settings determine how the contacting bodies can move relative to one another.

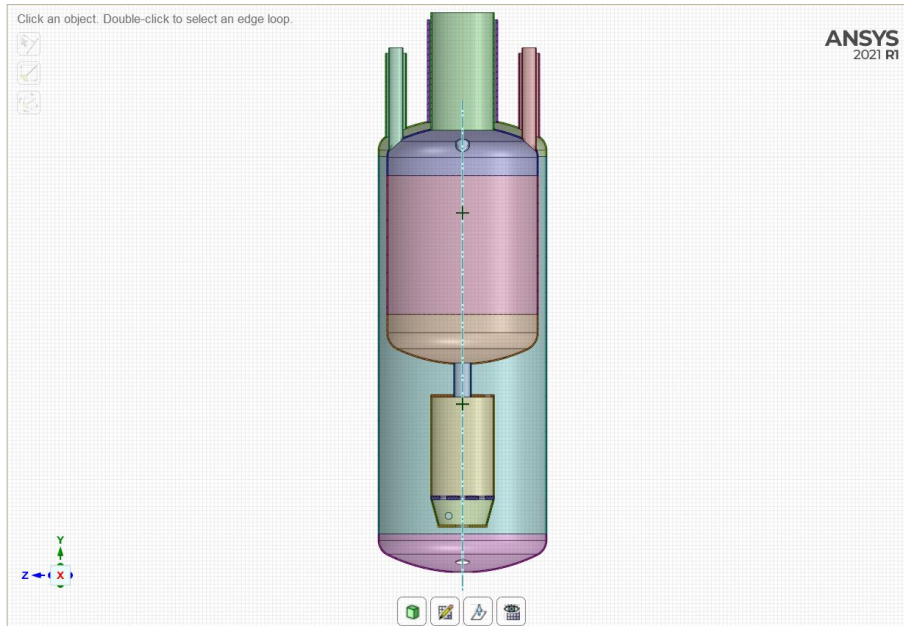


Figure 4.11: Simplified model of the Universal condenser on SpaceClaim

At this point the software produces a mesh of the components surfaces. A mesh is made up of elements which contain nodes (coordinate locations in space that can vary by element type) that represent the shape of the geometry. Creating the most appropriate mesh is the foundation of engineering simulations because the mesh influences the accuracy, convergence, and speed of the simulation. Mesh elements allow governing equations to be solved on predictably shaped and mathematically defined volumes.

In this analysis, after some tests, a reasonable balance between accuracy and computational expense was reached by using hexahedral (hex) elements with a size of 5 mm, producing 19147 nodes and 18948 elements (figure 4.12).

The next step is the definition of the boundary conditions and of the loads. A **Steady-state thermal analysis** was included in this simulation. The external vessel was set at room temperature (22°C), the N_2 barrel and the top chamber of the heat exchanger were set at the nitrogen liquefaction temperature (-196°C), while the bottom part was set at the argon liquefaction temperature (-186°C).

For the **Static structural analysis** first of all the fixed supports constraints were included to set the relative position of the internal components and of the external vessel. Then the standard earth gravity action was included along with the external atmospheric pressure, the internal pressure in each component and the hydrostatic pressure of the LN_2 and LAr . The Static structural analysis was connected to the Steady-state thermal analysis, therefore the results shown in the following figures (4.13; 4.14; 4.15; 4.16) are consequent to both the static and thermal loads. The deformation values and patterns are coherent with the loads and structure geometry.

The Equivalent stress according to the Von Mises hypothesis is consistent with the expectation. The most critical areas are the expected ones and the maximum value are acceptable according to the material's properties and to the geom-

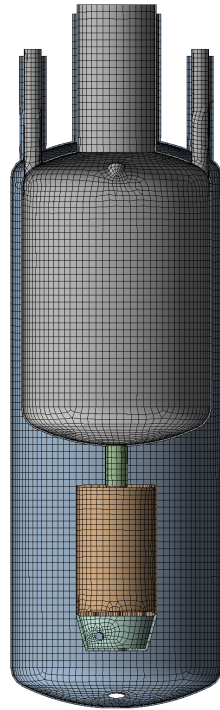


Figure 4.12: Universal condenser mesh

etry of the condenser (figure 4.17). However it should be noted that the stress peaks in the vicinity of the boundary conditions are numerical singularities since sensitivity studies have been performed by refining the mesh and obtaining an increase of the stress value.

Finally also a **linear eigenvalue buckling analysis** was performed. In structural engineering, buckling is the sudden deformation of a structural component under load. Even though the stresses that develop in the structure are below those needed to cause failure in the material of which the structure is composed, they can cause unpredictable deformations, possibly leading to complete loss of the member's load-carrying capacity.

Linear-buckling analysis calculates buckling load magnitudes that cause buckling and associated buckling modes. Ansys Mechanical provides calculations of a large number of buckling modes and the associated buckling-load factors (BLF). The BLF is expressed by a number which the applied load must be multiplied by to obtain the buckling-load magnitude.

Theoretically, it is possible to calculate as many buckling modes as the number of degrees of freedom in the FEA model. Most often, though, only the first positive buckling mode and its associated BLF need be found. This is because higher buckling modes have no chance of taking place — buckling most often causes catastrophic failure or renders the structure unusable.

See figure 4.18 for the solution. The load multiplier value of 9.19 is coherent with the results of the design by formulae of $P_m = 0.79\text{MPa}$ in the subsection 4.1.2.

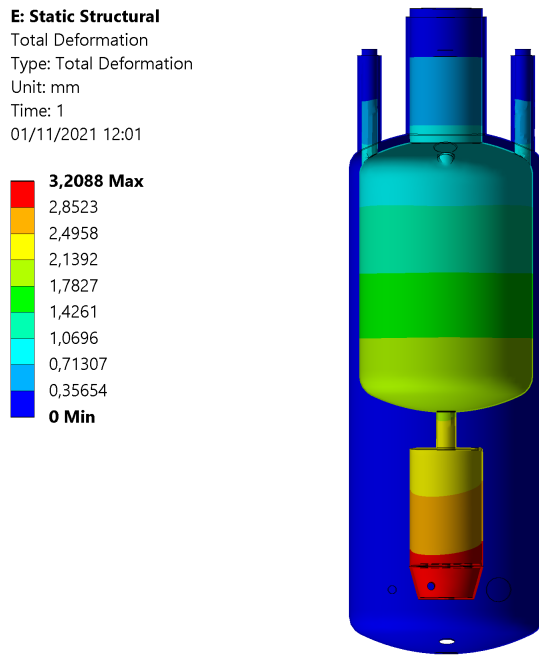


Figure 4.13: Total deformation

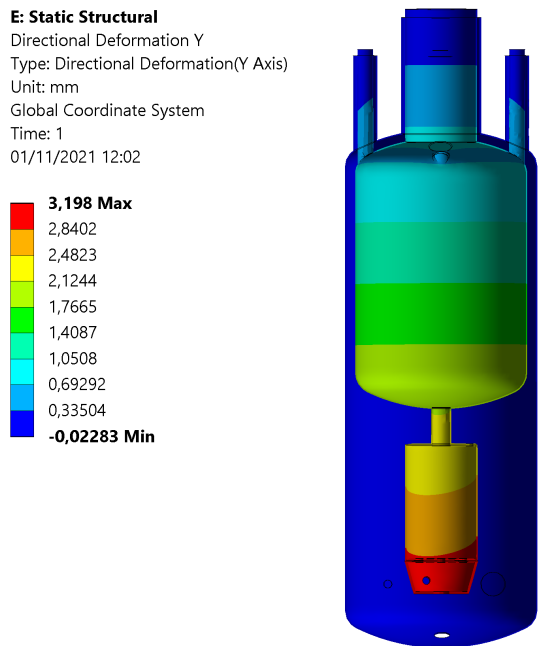


Figure 4.14: Deformation along Y axis

E: Static Structural
 Directional Deformation X
 Type: Directional Deformation(X Axis)
 Unit: mm
 Global Coordinate System
 Time: 1
 01/11/2021 12:03

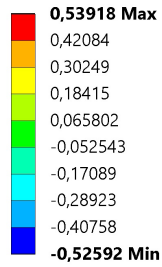


Figure 4.15: Deformation along X axis

E: Static Structural
 Directional Deformation Z
 Type: Directional Deformation(Z Axis)
 Unit: mm
 Global Coordinate System
 Time: 1
 01/11/2021 14:02

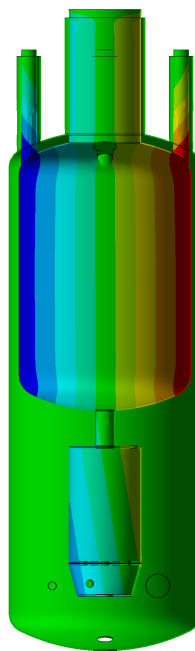
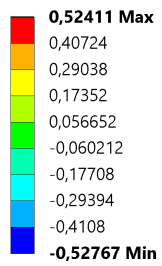
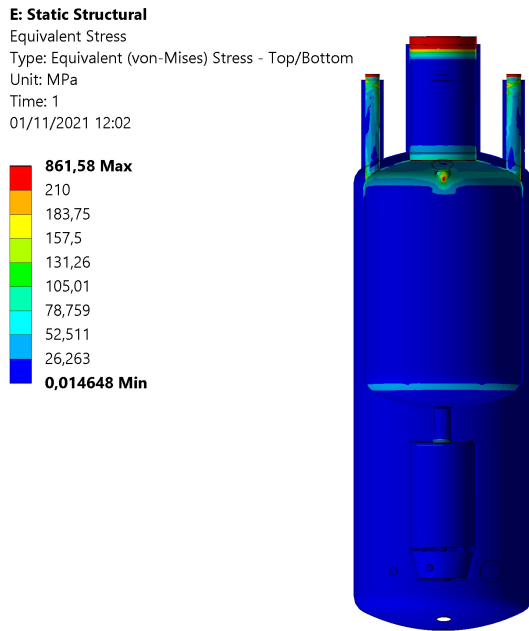
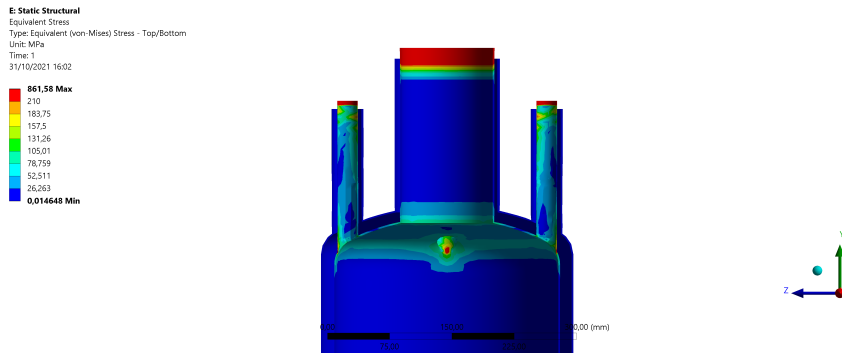


Figure 4.16: Deformation along Z axis



(a) Equivalent Von-Mises stress



(b) Equivalent stress in knuckle region

Figure 4.17: Equivalent Von-Mises stress result

F: Eigenvalue Buckling
Total Deformation
Type: Total Deformation
Load Multiplier (Linear): 9,197
Unit: mm
01/11/2021 12:04

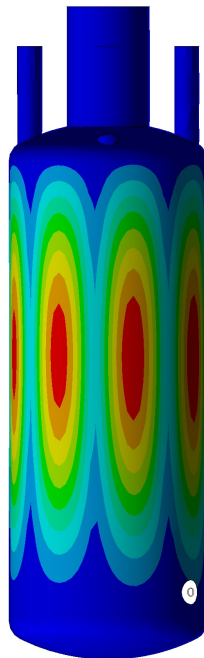
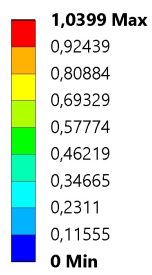


Figure 4.18: First positive buckling mode

5

ASSEMBLY AND COMMISSIONING

In the first section of this chapter we will describe the layout of Proto-0 in the Naples facility, with the assembly phase of the system and I will also mention the upgrades to the existing systems made to accommodate Proto-0.

In the following sections the first commissioning test of the cryogenic system and the preparation tests needed to ensure its proper functioning will be reported.

5.1 PROTO-0 ASSEMBLY

Proto-0's cryogenic system is composed of multiple elements that have different requirements. The component of the system have been deployed in two different areas.

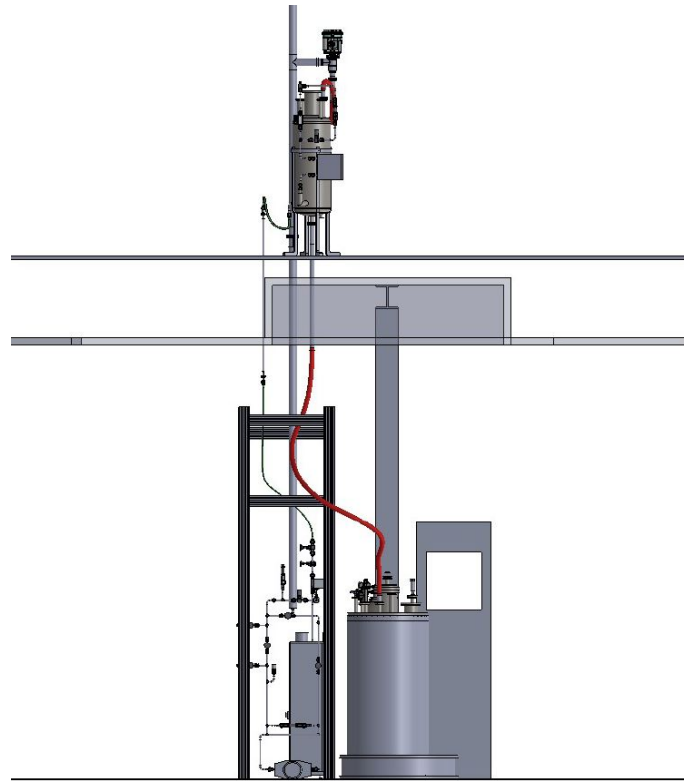


Figure 5.1: Proto-0 cryogenic system Solidworks model

Most of the system has been installed in the clean room, to be in the cleanest environment and to be easily accessible to the operators. The purification loop, the getter, the gas panel with the recirculation gas pump and the cryostat have been installed in the dedicated area of the clean room as shown in figure 5.2. All

these components were assembled around a Bosch aluminum profile structure in the middle of which is located the double wall vacuum insulated transfer line that comes from the external supply tank.



Figure 5.2: Proto-0 cryogenic system in the clean room

The cryostat and the gas panel have several sensors and elements that need to be connected to the cRIO slow control system. Therefore their position was chosen in relation to the position of the slow control rack cabinet. Another important factor that was considered is the accessibility of the valves of the gas panel and of the getter to the users. For safety and practical reasons, all the valves and switches have to be in an easily reachable position.

All the valves, the MFM and the inlet and outlet flexible lines are connected to the gas panel via VCR couplings. As mentioned in subsection 2.1.4 the VCR standard ensures leak-tight service if properly tightened.

The pressure sensor Wika S-20, the safety valves and the gas pump are connected via NPT fittings. NPT (National Pipe Tapered) is a U.S. standard for tapered threads. NPT threads have a 60° included angle and have a Sellers thread form (flattened peaks and valleys). Male and female tapered pipe threads wedge themselves together but need a sealant for a completely leak-free connection. Sealants fill any voids between the threads that could travel along the thread spiral. We used PTFE (Polytetrafluoroethylene) thread tape as sealant.

The PTFE, commercially known as Teflon, offers some useful properties: it is inert, it has a good temperature resistance and can perform at high and low tem-

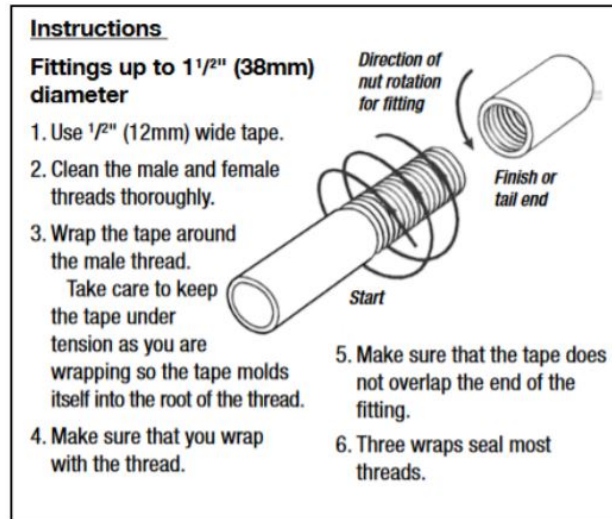


Figure 5.3: PTFE thread tape application procedure

peratures, and offers an extremely low friction. PTFE thread tape also provides suitable lubrication to prevent galling in stainless steel threads. Thread tape will only seal efficiently if it is correctly applied, and the fitting is correctly tightened.

Once the RTD sensors of the level indicator have been installed under the top flange of the cryostat, it has been possible to close the dewar. The top flange is connected to the dewar with 40 M10 stainless steel bolts. To ensure no leaks we applied a pure indium wire seal (fig.5.4).



(a) Pure indium wire spool



(b) Indium wire deployment

Figure 5.4: Indium wire sealing of the cryostat

The rest of the system was installed outside of the clean room. The Universal Condenser is in the "2nd level room", a room located on the top of the laboratory, exactly on top of the clean room's Proto-0 dedicated area (fig.5.5). The condenser, once installed, has no need to be in a temperature and purity controlled environment, but has to be above the cryostat to allow the liquefied nitrogen to flow through the vacuum insulated flexible transferline into the dewar only due to the gravitational force.



Figure 5.5: Proto-0 cryogenic system in 2nd level room

A critical operation performed during the assembly phase was the safety valves calibration (fig. 5.6).

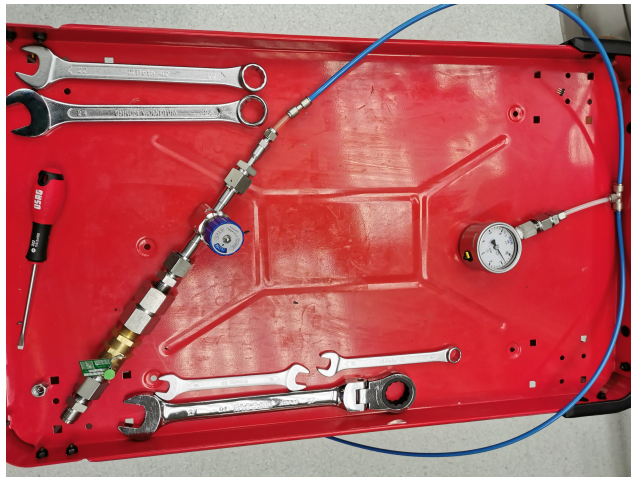


Figure 5.6: Safety valves calibration set-up

The safety valves installed on the system are Generant VRV1-750B-B-10 . Generant Series VRVI (Inline Vent Relief Valves) are supplied already assembled, preset and factory tested for leakage. We had to calibrate the gas pump by-pass safety valve to a different pressure to accommodate the gas pump outlet pres-

sure required by the purification getter. To calibrate the valve it is possible to adjust the tension of the spring that allows the opening. The spring tension can be adjusted by screwing or unscrewing the bolt connected to it, until the valve opens at the desired pressure value.

The major upgrades to the facility have been done to allow the installation of the condenser in the 2nd level room. The universal condenser is set to operate with a constant liquid nitrogen supply from the external tank. Therefore a tee line was installed on the double wall vacuum insulated line coming from the supply tank. The proportional pneumatic valve (PV10) has been installed directly onto this branch of the line, with the purpose of regulating the inlet LN₂ flux in the condenser (fig.5.7).

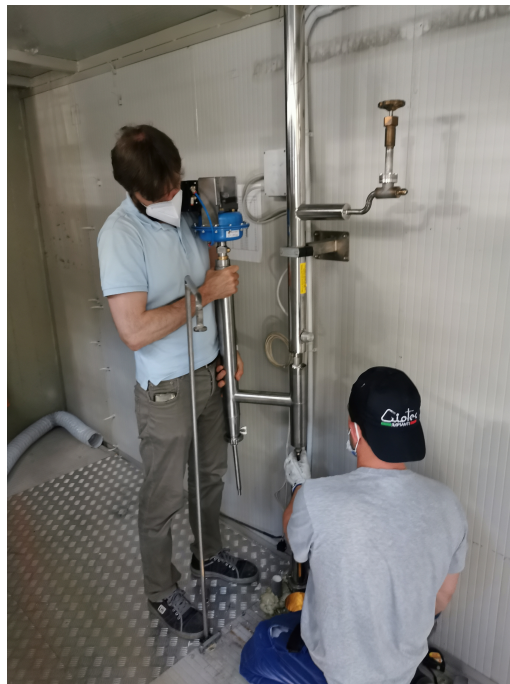


Figure 5.7: Proportional valve installation

Another crucial work was the installation of the flexible transfer line that delivers the liquefied Ar from the condenser to the cryostat. This line is composed by a rigid section that is installed through the floor of the 2nd level room and the ceiling of the clean room, and the flexible section that allows the easy connection to the cryostat and a certain range of acceptable positions for the cryostat around the transfer line source point. This works were all done by Criotec Impianti S.p.A., one of the main suppliers of the Naples facility, and of many other institutes and research centers (CERN, FZK, CEA, ENEA, Gran Sasso Laboratories). The specific skills in the cryogenic and vacuum sector along with Internationally certified plants, workers and procedures (plants: UNI EN ISO 9001 Quality System, UNI EN ISO 3834 – 2; welders: EN ISO 9606, procedures: UNI EN ISO 15614 and ASME BPVC) makes it one of the best options in the cryogenic and vacuum business. Also the flexible vacuum insulated transfer lines from the proportional valve to the condenser, from the condenser to the cryostat, the single wall flexible lines from the cryostat to the gas panel and from the gas panel to

the condenser along with the gas panel itself were produced by Criotec Impianti following our project.

Along with this works, also some electrical upgrades have been done. To connect all the sensors, the valves and the heat sink installed on the condenser to the slow control cRIO system located in the clean room, several cable connections for the signals and for the power supply had to be layed. Two switching boxes complete with DIN rail terminal blocks were installed, one in the clean room and one in the 2nd level room. Both were connected to the main electrical panel for power supply.

5.2 LEAK TESTS

Before commissioning the system, we performed a crucial preliminary test: the leak test.

This verification test is essential in this kind of systems, that have to manage fluids under pressure and have to preserve a given level of vacuum insulation. Therefore a perfect sealing is mandatory.

Leak testing is a non destructive examination method which is used for detection and localization of leaks and for measurement of leakage in systems or objects under vacuum or pressure.

In the leakage detection tests a pressure difference between the outer and the inner side of the object to be examined is produced. Then the amount of fluid which is passing through a leak is measured.

We have utilized both the "vacuum" and "overpressure" method for the leak tests. With the vacuum method the component to be examined for leaks is evacuated and sprayed from the outside with a search gas, in this case Helium. With the overpressure method the object to be examined for leaks is filled with a search gas under slight overpressure. The search gas escapes through any leaks present to the outside and is detected by a leak detector.

Helium is one of the smallest gas molecules and is inert. Being inert, helium is relatively safe to use (rather than hydrogen) as it will not react with any of the materials within the part to be tested. In most helium leak testing applications, a special vacuum pump equipped with a mass spectrometer is used to detect helium.

In helium leak testing, it is important to detect the background concentration of helium. As helium makes up 5.2 parts per million by volume of atmospheric air, a range higher than this indicates a source of helium close by.

For our tests we were testing with an acceptable leak test threshold below 8×10^{-9} mbarl/s. When testing at this low level, some additional precautions are needed to complete a viable test. For example, the atmospheric helium can cling to various surfaces and affect the test results. To prevent this, is possible to foresee some "pump and purge" cycles. The "cleaning" sequence must be:

1. Evacuate both the part and chamber,
2. Back fill the test volume with certified clean dry nitrogen,

3. Re-evacuate,
4. Fill the part with the test gas.

We performed two leak tests:

- On the Universal Condenser;
- On the assembled system.

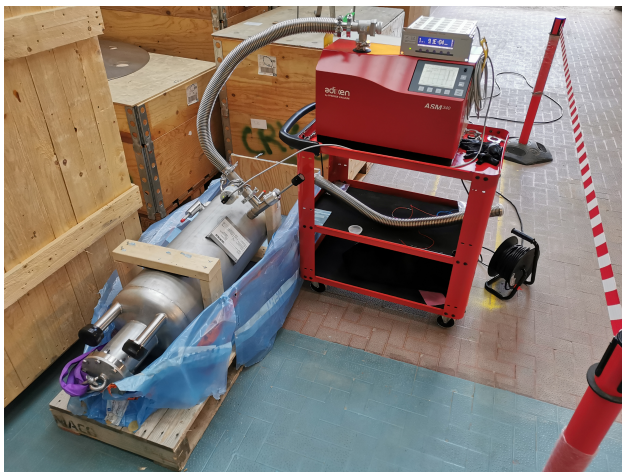
The other singular components were already tested by the producers (i.e. the gas panel was tested by Criotec).

5.2.1 Universal condenser leak test

Also the condenser had been leak tested by Demaco, but after the delivery, to a preliminary visual check it appeared that the inlet Ar line was bent of approximately 20° compared to the vertical design position. Therefore we had to verify the proper functioning of the component.

We performed two leak tests with two different methods.

The first test was done with the vacuum tracer probe test method. We connected the leak detector to the vacuum jacket port of the condenser. We evacuated the jacket volume until a vacuum level of 1×10^{-5} mbar. Then a spray gun was used to spray a fine jet of helium search gas on suspected of leaking areas (i.e. the weld seams of the bended Ar inlet line). The helium enters through leaks present on the evacuated test object and the detector connected to it. The detector indicates if a leak is present in the area the helium search gas is exposed to. This method can be really tricky, and is crucial preventing the possible leaks in the connection of the leak detector to the tested object.



(a) Condenser set-up



(b) Spray gun

Figure 5.8: Condenser leak test with vacuum method

The second test was performed with the overpressure method. The leak detector was still connected to the vacuum jacket, achieving a vacuum level of 1×10^{-5} mbar. This time we filled the internal components of the condenser with helium. An auxiliary pump was used to first get a vacuum level of 1×10^{-2}

mbar inside the internal components. Then we "broke" the vacuum filling them with helium gas. At this point we waited to see if the detector indicated the presence of helium in the vacuum jacket.

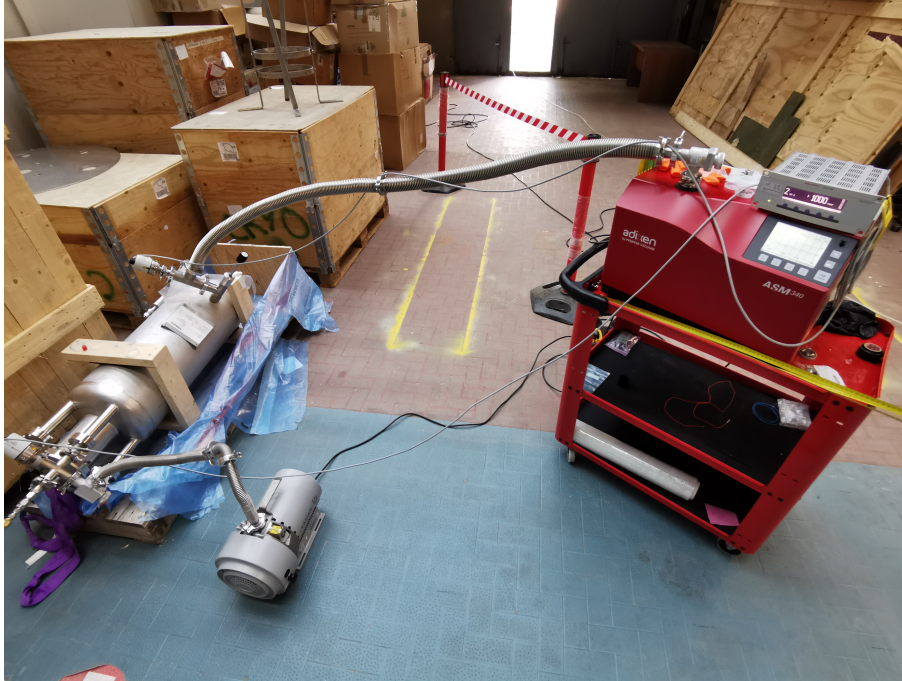


Figure 5.9: Condenser leak test with overpressure method

The tests were performed multiple times to avoid biased results. In all the tests the helium level detected by the mass spectrometer was below 7×10^{-9} mbarl/s, therefore we could assume that the damage didn't preclude the correct functioning of the component.

5.2.2 Assembled system leak test

At the end of the assembly phase, we performed a leak test of the Ar side of the system, to ensure that all the components were correctly connected.

The leak detector was connected to the gas panel together with an auxiliary pump and a vacuum sensor, via a VCR 1/2" to KF40 adapter.

We evacuated the entire Ar side volume until a pressure level of 7×10^{-3} mbar was reached, and we sprayed a fine jet of helium search gas at the connection areas.

Also this test was performed multiple times to avoid biased results.

The helium level detected by the mass spectrometer was below 7×10^{-9} mbarl/s, and that can be considered acceptable.



Figure 5.10: Assembled system leak test

5.3 COMMISSIONING

The goal of the commissioning test was to ensure that the cryogenic system could operate according to the simulations and calculations. The commissioning test was performed with a slightly different layout of the system.

Inside the cryostat there was no TPC, only the pt100 sensors of the level indicator was installed. Therefore on the top flange not all the feedthroughs were needed. We exploited two of the unused spots to install two windows in order to see the LAr build up in the cryostat. The purification getter was left in the by-pass mode and wasn't activated for this first test.

Regarding the condenser, we installed an additional vent line on one of the CF40 flanges to manually expel the nitrogen gas during the filling phase of the N₂ side of the condenser. The main purpose of this line was to prevent the constant activation of the relief safety valve in this phase, that could freeze and remain open.

Before the test, we performed three cycles of "pump and purge" to clean the system from the possible contaminating particles. This operation involves the pumping of the system till a pressure value of 2×10^{-2} mbar followed by the insertion of Ar gas.



Figure 5.11: Manual vent line for the nitrogen in the N₂ barrel

Then we could pump the Ar side of the system up to 4×10^{-4} mbar and insert the Ar at 1.4 bar.

At this point it was possible to start the test. The first step was to verify the status of the by-pass line (HW07) to connect the LN₂ tank to the double wall vacuum insulated line of the condenser. To feed the condenser with the liquid nitrogen the electric valve EV04 has to be open. These operations allow the LN₂ flux to arrive at the proportional valve PV10 that will regulate its inlet flow in the condenser. As explained in section 2.1.2, the proportional valve is designed to have a PID control based on the level indicator (LT1) and on the pressure sensor (PT1) installed on the condenser LN₂ barrel. During this test we controlled the opening rate of the PV10 and of the MFC manually from the slow control panel, to understand the system responses in the different phases (fig. 5.12).

At **9:28 a.m.** we started the condenser filling with LN₂ coming from the external supply tank. We opened the proportional valve (PV10) gradually up to 60%.

The initial conditions on the Ar side of the system were:

- **PT2**= 1.4 bar (pressure in the cryostat)
- **RTD**=293 K (temperature of the pt100 in the cryostat)

We switched on the gas pump and started the recirculation of gas argon in the system, keeping the Getter excluded in by-pass mode.

At **10:04 a.m.** with a liquid nitrogen level in the N₂ barrel of 68% (equal to approximately 13.6 liters) we gradually opened the MFC to allow the liquid nitrogen flow in the heat exchangers and begin the heat exchange with the Ar gas. The Ar gas flow rate reported by the MFM was 80 sL/m.

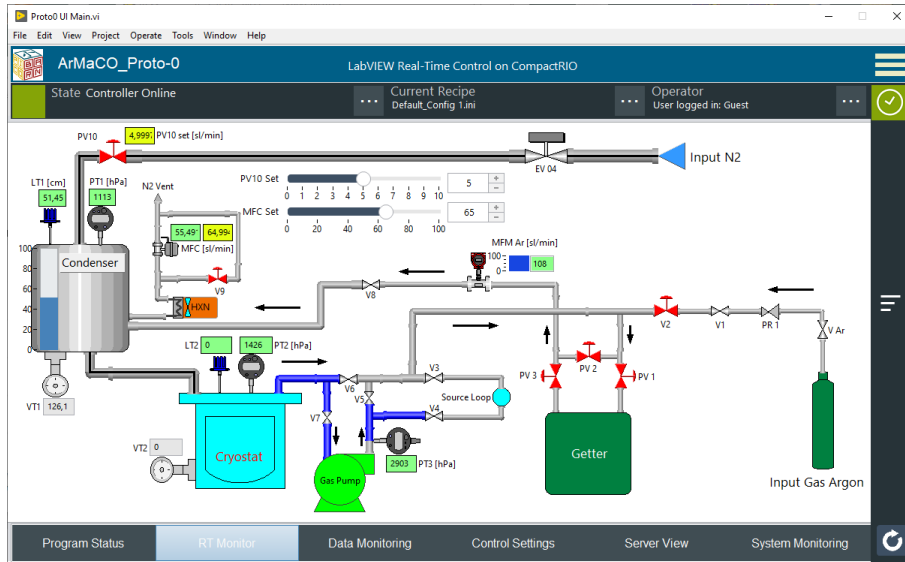


Figure 5.12: Proto-0 control panel - slow control

From this moment on we regulated the PV10 to only replace the N₂ used by the condenser, maintaining a constant level (between 50% and 60%) in the N₂ barrel.

During the argon liquefaction, we refilled the system with Ar gas coming from a pressurized bottle, in order to maintain a pressure in the condenser of 1.4 bar. Regulating the condenser argon inlet valve V8 and the opening of the Ar bottle, we were able to adjust the Ar gas flow rate coming into the condenser (up to 118 sL/m).

At **12:00 p.m.** we reached a temperature below 200K with all the pt100 in the dewar. During the Ar liquefaction we were able to reach a stable condition and to evaluate a liquefaction rate of 5 sL/m of Ar gas while the MFC was allowing a N₂ flow of 50 sL/m and the MFM was reading an Ar gas flow of 107 sL/m.

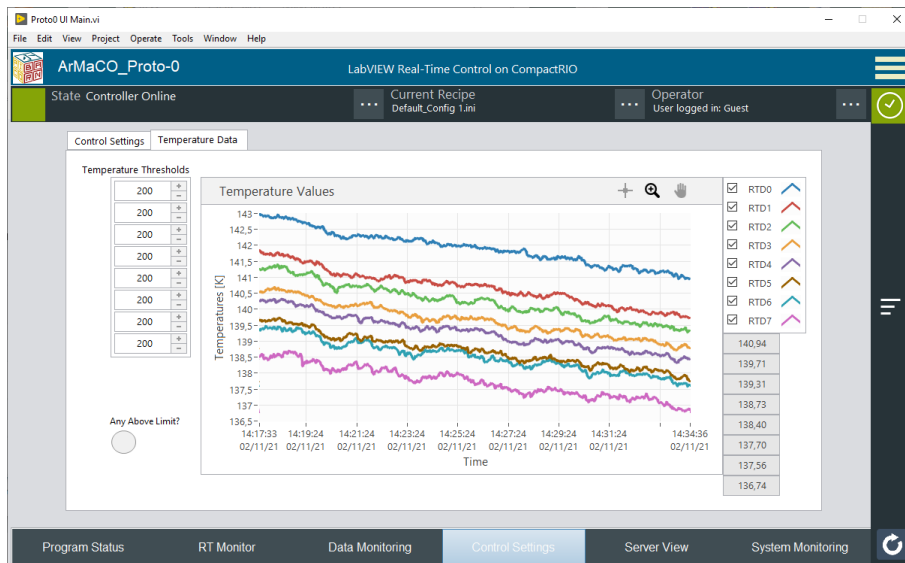


Figure 5.13: Temperature levels in the filling phase

At 15:30 p.m. we concluded the test with a pt100 temperature of 132 K and a LAr level slightly below the lowest pt100. The following graphic (fig.5.14) shows the correlation of the cryostat filling time versus the MFM Ar gas flow.

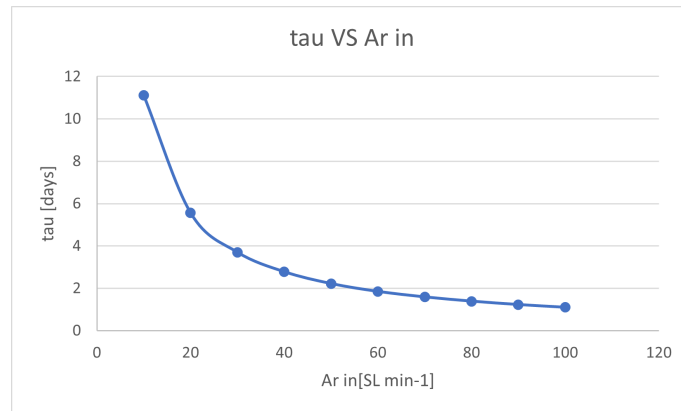


Figure 5.14: tau vs. Ar gas inlet flow (MFM)

During the test we noticed that to have a N₂ flow at the MFC higher than 55 sL/m (and therefore have a higher cooling power) a pressure higher than 1.15 bar in the N₂ barrel (PT1) was needed.

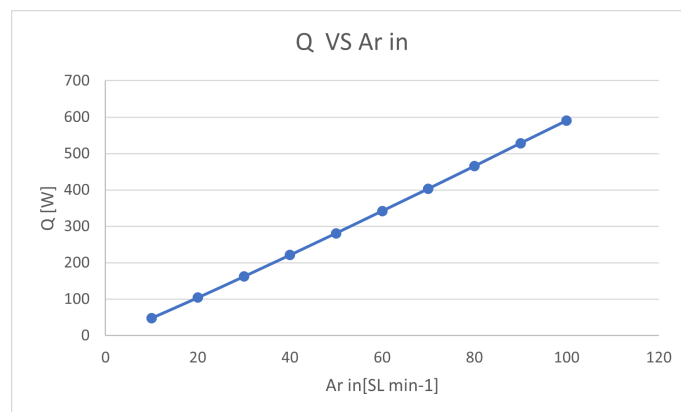


Figure 5.15: Condenser cooling power vs. Ar gas inlet flow (MFM)

The following figures show the correlation between the filling percentage of the nitrogen side of the tube and shell heat exchanger and the Ar gas inlet flow (5.16) or the evaporation rate of LN₂ (5.17) (corresponding to the N₂ flow rate at the MFC).

This first commissioning test is considered as a successful starting point for the calibration process of the system. The next step will be the set of the PID control parameters for the proportional valve and for the MFC. In this way the filling phase will be made almost entirely automatic.

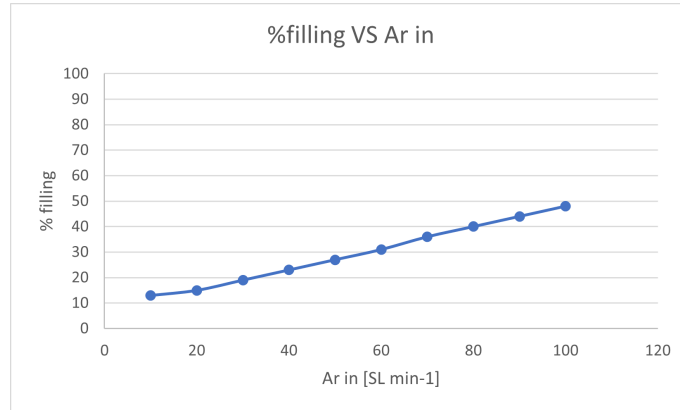


Figure 5.16: Condenser N₂ side filing % vs. Ar gas inlet flow (MFM)

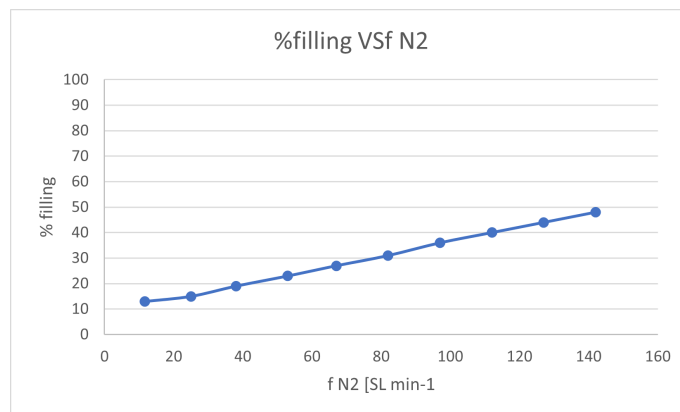


Figure 5.17: Condenser N₂ side filing % vs. N₂ outlet flow (MFC)

CONCLUSIONS

The Particles Physics research is closely linked to engineering due to the complex and innovative systems needed for its experiments. The engineering skills and expertise are crucial to achieve the technological progress that these experiments require.

The design of systems like the one I have been working on during my thesis experience, can lead to the development of ideas, methods and devices that can be deployed in different fields and applications.

I had to use many different skills from various engineering branches to deal with the different aspects of this project, and I've developed expertise in cryogenic and vacuum systems.

In my thesis work I followed the entire development process of a cryogenic system from its design to its assembly and start-up. I've done an extensive analysis of the key, custom designed, component. The mechanical and thermodynamic analyses of the Universal Condenser confirmed the quality of the design of this component. The commissioning test demonstrated the correct design and assembly of the entire system. With just minor adjustments it could be possible to install the TPC and begin the actual experiment.

Finally some possible upgrades have already been identified, and the evolution of this facility has just begun.

BIBLIOGRAPHY

- [1] The Global Argon Dark Matter Collaboration, *DarkSide-20k Technical Design Report*, April 2021
- [2] B.Bottino et al, *The DarkSide experiment*, IFAE 2016
- [3] Dr. D. A. Bauer, *Dark matter detection with cryogenic detectors*, 2008 J. Phys.: Conf. Ser. 120 042002
- [4] The Global Argon Dark Matter Collaboration, *Future Dark Matter Searches with Low-Radioactivity Argon*, Dec 2017
- [5] Michela Lai, *Dark matter search and neutrino physics in Liquid Argon*, Université de Paris, Università degli Studi di Cagliari, PhD degree thesis
- [6] CEN - COMITÉ EUROPÉEN DE NORMALISATION, *NF EN 13445 - Unfired pressure vessels*, Association Française de Normalisation (AFNOR — French standard institute), 12 December 2014
- [7] CEN - COMITÉ EUROPÉEN DE NORMALISATION, *(EN 13458 - Cryogenic vessels, Static vacuum-insulated vessels)*, November 2002
- [8] Yunus A. Cengel, *Introduction To Thermodynamics and heat transfer*, McGraw-Hill, 2009
- [9] Don Green, Marylee Z. Southard, *Perry's Chemical Engineers' Handbook*, McGraw-Hill, 2018
- [10] PROF. ING. GIULIANO CAMMARATA, *Trasmissione del calore*, Appunti, 12 Dic 2016
- [11] *Darkside*, <https://www.lngs.infn.it/it/darkside>
- [12] *Darkside-20k project*, <https://surfacetreatments.infn.it/projects/darkside-20k-project/>
- [13] *Darkside* - *Wikipedia*, https://en.wikipedia.org/wiki/Weakly_interacting_massive_particles
- [14] *Weakly interacting massive particles* - *Wikipedia*, <https://en.wikipedia.org/wiki/DarkSide>
- [15] *Vacuum insulated piping (VIP) - Demaco*, <https://demaco-cryogenics.com/vacuum-technology/>
- [16] *VENT RELIEF VALVE (VRV) - Generant*, <https://www.generant.com/product/vent-relief-valve/>

- [17] *Valves and actuators - Siemens*, <https://new.siemens.com/us/en/products/buildingtechnologies/hvac/valves-actuators.html>
- [18] *Guide to the Fundamentals of Helium Leak Testing*, <https://www.tqc.co.uk/our-services/leak-testing/helium/guide-to-helium-leak-testing/>
- [19] Helle H. Rasmussen, Leif Jeppesen, *Industrial applications of Helium Leak Test*, 7th European Conference on Non-destructive Testing, 1998
- [20] *VCR Metal Gasket Face Seal Fittings*, Manual, Swagelok
- [21] *Bellows-Sealed Valves*, Manual, Swagelok
- [22] *Brazed Plate Heat Exchanger*, Manual, Kaori
- [23] *Smartrack Series 100, Mass Flow Meters and Controllers Instruction Manual*, Sierra Instruments Instruction Manual, Sierra
- [24] *Mono Torr High Flow PS4-MT50-R Rare Gas Purifier*, Operation Manual, SAES Pure Gas, Inc.
- [25] *Metal Bellows Vacuum Pumps And Compressors*, Manual, Senior Aerospace Metal Bellows
- [26] *Buckling Analysis with FEA*, Paul M. Kurowski, <https://www.machinedesign.com/3d-printing-cad/fea-and-simulation/article/21831716/buckling-analysis-with-fea>